Nationwide deadwood mapping reveals rising mountain forests vulnerability

Luca Ferrari[1,2,*], Lars T. Waser[3], Achilleas Psomas[3], Clemens Mosig[4], Teja Kattenborn[5], Christian Ginzler[3], Verena C. Griess[1], Mirela Beloiu[1,2**]

[1] *Department of Environmental System Sciences, Institute of Terrestrial Ecosystems, ETH Zürich, 8092 Zurich, Switzerland.*
[2] *Ecosystem Ecology Group, Swiss Federal Research Institute WSL, Zürcherstrasse 111, 8902 Birmensdorf, Switzerland.*
[3] *Remote Sensing Group, Swiss Federal Research Institute WSL, Zürcherstrasse 111, 8902 Birmensdorf, Switzerland.*
[4] *Institute for Earth System Science and Remote Sensing, Leipzig University.*
[5] *Department of Sensor-based Geoinformatics, University of Freiburg.*

Corresponding authors:
** Luca Ferrari, luca.ferrari@usys.ethz.ch,*
*** Mirela Beloiu, mirela.beloiu@usys.ethz.ch*

This is a preprint manuscript submitted to EarthArXiv and has not been peer reviewed.

Highlights

- We mapped deadwood in Switzerland between 2018 and 2023 at high resolution.
- Deadwood increased up to 43% in every region covered by repeated aerial surveys.
- Deadwood was increasingly accumulated at mid to high elevations, peaking at 1,550 m.
- High temperatures and conifer dominated forests were the main deadwood drivers.

Abstract

Forest mortality is increasing globally under climate change, making detailed, large-scale monitoring essential for understanding ecosystem responses and guiding adaptive forest management. Here, we present a spatio-temporal assessment of standing deadwood in Switzerland from 2018 to 2023, derived from centimeter-scale high-resolution aerial imagery. We reveal a consistent upslope concentration of standing deadwood, with highest shares occurring around mid to high elevations (~1,500 m), despite declining forest cover, and relative increases of up to 43% in overlapping survey areas following the 2018 drought. Maximum temperature anomalies and conifer dominance were the strongest predictors of standing deadwood. The consistent accumulation of standing deadwood at higher elevations suggests increasing vulnerability of mountain forests, with implications for carbon storage, biodiversity, and disturbance susceptibility under ongoing climate change. These patterns highlight the need to address rising forest mortality as a key component of climate-adaptive forest management. Furthermore, our results demonstrate the potential of high-resolution remote sensing for large-scale forest mortality monitoring. Our methods offer a reproducible and transferable

framework for identifying vulnerability hotspots and supporting climate-adapted forest management.

Keywords

Forest mortality, forest monitoring, aerial imagery, tree mortality, drought, canopy mortality, temperature anomalies.

1. Introduction

The increase in frequency and intensity of heatwaves (IPCC, 2023a) and droughts (Vicente-Serrano et al., 2020; Chen et al., 2025; Hao et al., 2018) is leading to an acceleration in global trends of forest mortality (Allen et al., 2015; Hartmann et al., 2022). In Europe alone, drought caused an estimated 500,000 ha of excess forest mortality in recent years (Senf et al., 2020). The extreme drought of 2018 had particularly severe impacts, affecting approximately 11,200 km^2 of forested area across Europe (Schuldt et al., 2020). Mortality impacts forest ecosystem functions, e.g., habitat provision, carbon storage, and water cycling, and thus also disrupts the wide range of ecosystem services that provide economic, ecological, cultural, and social benefits. Such services include timber production, carbon sequestration (Thürig and Kaufmann, 2010; Jandl et al., 2013), water provisioning (Winter et al., 2025), recreational and cultural value (de Groot et al., 2002; Häyhä et al., 2015), as well as considerable potential for climate change mitigation and adaptation (IPCC, 2023b, 2023c). As climate extremes intensify, addressing forest mortality will be critical for sustaining ecosystem functions and the services they provide.

While our understanding of the drivers of tree mortality is still limited (Schweingruber and Wirth, 2009; Ammer et al., 2018), forest mortality often results from the interaction of multiple contributors, rather than from a single stressor (Franklin et al., 1987). Climatic stressors such as drought, elevated temperatures, and increased variability in precipitation have been associated with increased forest mortality rates (Hammond et al., 2022; Jääskeläinen et al., 2025; Neumann et al., 2017; Senf et al., 2020). Furthermore, these climatic stressors can also predispose tree species to other mortality agents such as bark beetle infestations (Hlásny et al., 2021; Schwarz et al., 2025). Forest composition modulates mortality responses, with drought- and heat-related mortality affecting both coniferous (e.g. Norway spruce, Scots pine) and deciduous forests (e.g. European beech), depending on species traits and disturbance interactions (Beloiu et al., 2022; Schuldt et al., 2020). However, studies investigating the physiology of tree mortality often cover limited sample sizes of tree species and environmental conditions (Mitchell et al., 2013). Switzerland provides a fitting example, with mortality tracked in 197 plots across Switzerland over 60 years (Hülsmann et al., 2018), and in 276 Swiss plots for more than a century (Etzold et al., 2019). While these assessments can provide a valuable understanding of physiology and forest dynamics, the data are scarce and have coarse resolution. Studies over larger areas are usually based on standardized inventory data such as the ICP Forests network (Eichhorn and Roskams, 2013), which provides long-term but coarse and low-resolution data. Such existing monitoring networks are not suited to detect damage

over continuous areas (Schuldt et al., 2020), and can lead to an underestimation of forest mortality (Cheng et al., 2024; Schiefer et al., 2024).

To improve our understanding of mortality patterns and processes, we need spatially extensive mortality observations. However, systematic assessments and databases of forest health are scarce and challenging to obtain (Trumbore et al., 2015), especially spatially explicit data of observed mortality at the national level at high spatiotemporal resolution. In recent years, the adoption of remote sensing techniques in the field of ecology has accelerated, thanks to the increasing availability of data, artificial intelligence methods, and open-source, efficient software (Senf, 2022). The increasing availability of pre-processed, analysis-ready data (Dwyer et al., 2018; Frantz, 2019)allows for performing analysis over large areas with increasing temporal resolution. Large-scale assessments of forest mortality can be carried out with satellite images (Campbell et al., 2020; Senf and Seidl, 2021); however, they often rely on medium or coarse spatial resolution data, such as Sentinel-2 (10 m), Landsat (30 m), or MODIS (250 m). This does not enable the identification of mortality at the scale of individual trees, and can compromise the inferences on the underlying physiological processes (Hartmann et al., 2018). Recent studies highlight the potential of combining high-resolution remote sensing data, such as airborne and UAV imagery, with supervised deep learning to map standing deadwood (Cheng et al., 2024; Mosig et al., 2026; Schiefer et al., 2023). However, despite the growing number of studies, spatially continuous assessments of forest mortality are lacking in most countries, including Switzerland. Improving the understanding of tree mortality requires large amounts of wall-to-wall data, covering wide gradients of climatic and environmental conditions, to allow the attribution of forest declines to human, climatic, and biotic drivers (Trumbore et al., 2015).

In this study, we utilize a globally calibrated semantic segmentation model (Möhring et al., 2025) to identify standing deadwood in high-resolution aerial images (10 – 25 cm) throughout Switzerland and evaluate the biotic and abiotic factors contributing to tree mortality. Based on wall-to-wall aerial images from 2018 to 2023, we produced multi-year maps depicting standing deadwood, computed yearly percentages of deadwood in forested areas, and pinpointed spatial hotspots of tree mortality. Across the main Swiss forest ecoregions, standing deadwood accounted for 0.20 – 0.83% of forest cover, corresponding to 107 – 1,389 ha. Analyses within forest reserves further revealed how climatic, biotic, and abiotic conditions shape mortality in unmanaged forests. Together, these results provide the first nationwide, spatially explicit assessment of standing deadwood in Switzerland, demonstrating how high-resolution aerial imagery can be leveraged to track forest mortality and its drivers under ongoing climate change.

2. Methods

The overall workflow of the study is illustrated in Figure 1 and consists of three main steps. Step I involves the data processing and cleaning. Step II focuses on the deadwood assessment. Step III covers the analysis of deadwood drivers. The study was carried out over the entire Switzerland. Within the study area, the elevation ranges from 193 to 4,628 m a.s.l., and the climate is temperate at low elevations, with areas in the cold and polar Köppen-Geiger climate classes at the highest elevations (Beck et al., 2018). Forests cover about 32 percent of

Switzerland's land area, and canopy composition is dominated by Norway spruce (*Picea abies*, ~38%), European beech (*Fagus sylvatica*, ~18%), and silver fir (*Abies alba*, ~12%), which together contribute roughly 70 % of canopy cover (NFI, n.d.).

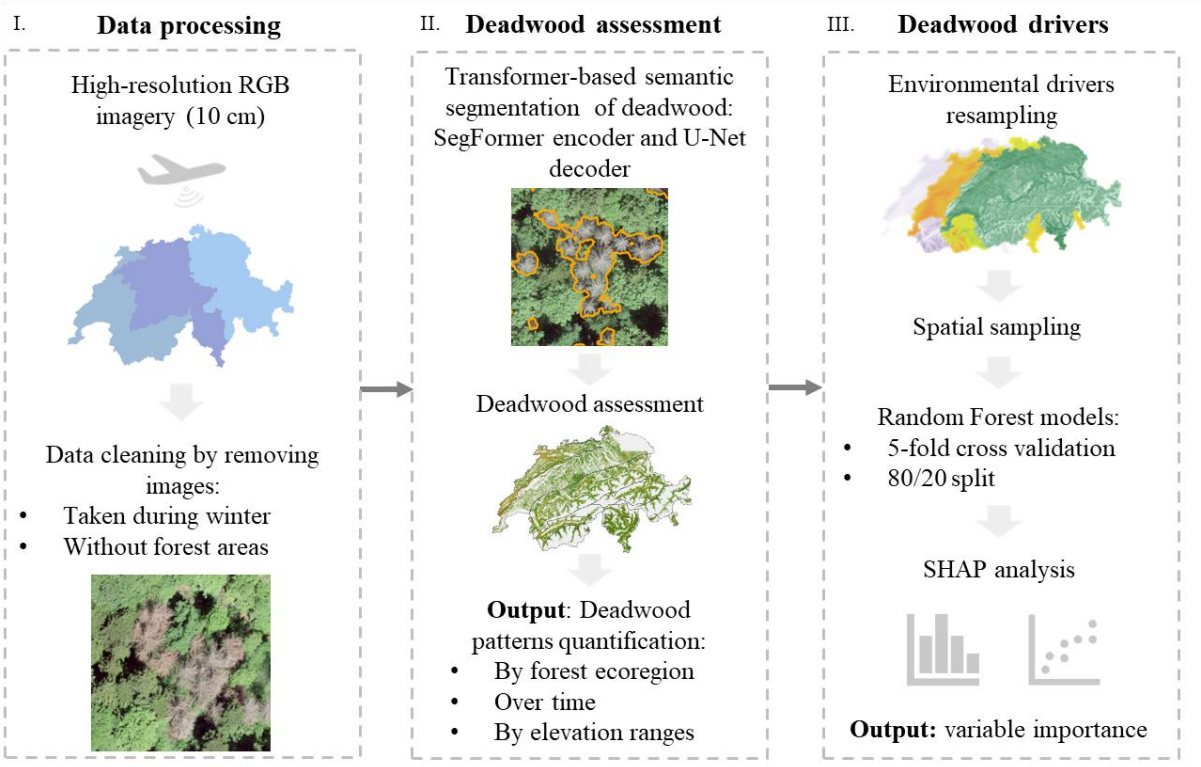

Figure 1: Workflow depicting the steps of data processing, deadwood assessment, and deadwood drivers' quantification.

2.1. Data

The aerial image dataset consists of RGB orthophotos from the SWISSIMAGE product, covering all of Switzerland with a ground resolution of 10 cm over plain areas and 25 cm over the Alps, provided by the Federal Office of Topography swisstopo(© swisstopo, n.d.). The dataset is updated on a 3-year cycle, with yearly flights covering approximately one third of Switzerland (Figure S1a). In this study, we used 86,774 images acquired between 2018 and 2023, to have two full cycles that allowed us to cover the entire Switzerland. Each orthophoto can be easily identified by the year and 8-digit ID included in the filename and based on the coordinates of the bottom left corner of the image. Because the orthophotos themselves do not have an explicit acquisition date, we determined the date of each image by checking its spatial overlap with the corresponding digital image strip footprints(© swisstopo, n.d.). Each footprint represents the area covered by the acquisition flight and the corresponding date.

Forested areas in Switzerland have been determined based on the Forest Type NFI 2018 dataset (Waser and Ginzler, 2021), at a 10 m spatial resolution and canopy height > 5 m (Waser et al., 2017). The dataset represents the probability of broadleaf forest (0-100%). In this study, we used this dataset primarily to establish a baseline of vegetation areas taller than 5 m. Subsequently, we removed woodland patches smaller than 0.5 ha (FAO, 2020) to further refine

our forest mask using ArcGIS. We grouped contiguous forest pixels and filtering patches by area by applying the functions “Region Group” and “Zonal Geometry”. The final forest mask includes all vegetation areas with canopy height > 5 m and areas > 0.5 ha.

The swissALTI3D digital terrain model (DTM) from swisstopo(© swisstopo, n.d.) was used to determine the altitude of the RGB orthophotos in data cleaning. The DTM uses 0.5 m spatial resolution LiDAR data for areas below 2000 m a.s.l. and stereo-image-correlation for higher altitudes, with a spatial resolution of 2 m.

Orthophotos are acquired between March and November and thus show both leaf-on and leaf-off conditions. To distinguish standing dead trees from leafless deciduous trees, we defined the leaf-on period as April 1st to September 30th annually. We selected images based on strip footprint dates, forest presence by the forest mask, and visual checks. We excluded images not intersecting with the forest mask or overlapping leaf-off period strips. Images overlapping leaf-on period strips were kept. We flagged images overlapping strips with conflicting dates (leaf-on and leaf-off) as their exact acquisition date was indeterminable. Additionally, images from April to May were assessed due to delayed leaf-out in mountainous deciduous trees, affecting canopy coverage early in the season. Overall, we assessed 15,704 images across the six years to compose the dataset. Table S1 shows the number of images removed during data cleaning and the reasons for their removal. The data cleaning process resulted in a total of 44,129 orthophotos between the years 2018-2023 (Figure S1b-c).

2.2. The semantic segmentation model

In this study, we applied a transformer-based semantic segmentation model to detect standing deadwood from aerial images across a wide range of resolutions (Möhring et al., 2025). The model was trained on 434 drones images of varying spatial resolutions obtained from the deadtrees.earth (Mosig et al., 2026). The model architecture consists of a SegFormer encoder and a U-Net decoder. As input, it takes RGB image tiles and outputs masks, converted to a probability distribution by applying a sigmoid layer. To obtain binary masks of presence/absence of standing deadwood, pixels with probability $p > 0.5$ were classified as standing deadwood. We assessed standing deadwood in Switzerland by applying the segmentation model to the entirely cleaned aerial orthophoto dataset and filtered the results with our forest mask to retain predictions within forested areas.

For the testing of the semantic segmentation model, we used tree mortality datasets comprising 48,368 geolocated trees with delineated tree crowns (Berger, 2024). Their crowns were primarily identified using RGB orthophotos and subsequently matched to corresponding RGBI images acquired simultaneously during the same aerial flights. The trees in the dataset are categorized into four health classes. For our purposes, we extracted the 15,587 trees classified as dead. Since the validation process requires fully labeled images for a reliable calculation of performance metrics, we complemented this dataset by manually delineating 837 additional dead trees. Finally, we selected a subset of 1,626 dead trees for model validation. These trees appear in four aerial 10 cm orthophotos (reference year 2022) that cover 4 km² of fully labeled forest area in the Canton of Grisons, Switzerland.

We validated our approach by applying the segmentation model to selected subsets of aerial orthophotos, which resulted in the generation of relevant segmentation masks. Subsequently, we utilized the tree mortality reference data to generate equivalent binary masks. We then applied the forest mask to both the model outputs and the reference masks to ensure that performance metrics were assessed exclusively within forested areas. Although the model identifies standing deadwood throughout the entire orthophotos, the reference labels are restricted to forest areas. Consequently, this masking step was essential for calculating comparable performance metrics. In the end, we assessed the filtered masks by computing Precision, Recall, and F1-score (Table S2).

2.3. Swiss Forest Ecoregions and forest reserves

We assessed standing deadwood in seven main Swiss forest ecoregions, dividing Switzerland into units based on climate, forest vegetation, and altitude (Frehner et al., 2005). Lowland and low mountain environments are represented by the Swiss Central Plateau (mean elevation 572 m a.s.l., ranging from 244 m to 1,548 m a.s.l.) and the Jura (803 m a.s.l., from 266 to 1,679 m a.s.l.), while the remaining regions span the Alps from montane to alpine conditions, including the Southern Pre-Alps (1,124 m a.s.l., from 193 m to 2,951 m a.s.l.), the Northern Intermediate Alps (1,755 m a.s.l., from 435 m to 3,929 m a.s.l.), the Southern Intermediate Alps (1,936 m a.s.l., from 311 m to 3,898 m a.s.l.), and the Continental Alps (2,426 m a.s.l., from 992 m to 4,628 m a.s.l.), capturing strong climatic and forest structural gradients across the country. The Northern Intermediate Alps, initially divided by beech presence, were merged and renamed. Similarly, the Southern Pre-Alps categories were combined into "Southern Alps". Lastly, Mendrisiotto was merged into the Southern Pre-Alps due to its small size and limited data, only available from 2018 swisstopo orthophotos.

For the identification of the main predictors of standing deadwood in Switzerland in forest reserves and unmanaged areas, we used the forest reserves dataset (BAFU, 2022). These 2,564 units cover 7.3% of the Swiss forests and identify areas where no management takes place, as well as areas where targeted action is taken to promote endangered species. The spatial distribution of the forest ecoregions and the location of the forest reserves is shown in Figure S2.

2.4. Deadwood drivers

To identify the main drivers of deadwood we fitted random forest regression models (Breiman, 2001) using the shares of standing deadwood per pixel in the previously described forest reserves areas as a response variable. Since standing deadwood was originally segmented at 10 cm on the image orthophotos, we aggregated the data to a 10 m grid to match the resolution of the forest mask applied to filter standing deadwood within forested areas. For each available forest reserve, we extracted the corresponding deadwood pixels for every available year between 2018 and 2023. Due to repeated aerial surveys in swisstopo's 3-year cycle, standing deadwood in several forest reserves was quantified twice with a 3-year interval. To prevent duplication and ensure unique representation per pixel, only the first deadwood occurrence for each reserve was retained, focusing on post-drought conditions of 2018.

As predictor variables we considered both abiotic and biotic factors. Detailed information on their spatial resolution is available in Table S3. Elevation, from the swissALTI3D DEM, was included to represent site topographic conditions. To represent edaphic site conditions, we included the Topographic Wetness Index (Sørensen et al., 2006), available water content (Meusburger et al., 2022), as well as the proportions of sand, clay, and organic carbon (Baltensweiler et al., 2021). Biotic variables include the probability of broadleaf, (Forest Type NFI 2018), canopy height, (vegetation height model NFI (Ginzler, 2021)), and basal area (unpublished Swiss NFI data based on the vegetation height model NFI). For consistency, the environmental predictors were also resampled to the same 10 m grid, ensuring that all variables were aligned to a common spatial framework.

Additionally, we included precipitation, mean, minimum, and maximum temperature (Table S4), provided by the Land Change Science Group, WSL. Daily observations from all available weather stations of the Federal Office of Meteorology and Climatology MeteoSwiss have been interpolated (Thornton et al., 1997) at 100 m spatial resolution. Furthermore, we used precipitation, minimum, mean, and maximum temperature to calculate the corresponding climatic water balance (George H. Hargreaves and Zohrab A. Samani, 1985). From these data, we derived yearly standardized anomalies of minimum and maximum temperature, as well as precipitation and climatic water balance, relative to the norm of 1981 – 2010:

$$Standardized\ anomaly_i = \frac{X_i - \mu_{1981-2010}}{SD_{1981-2010}}$$

Where i is the reference year, X_i the mean for the reference year, and $\mu_{1981-2010}$ and $SD_{1981-2010}$ the mean and standard deviation for the 1981-2010 period, respectively.

For each deadwood pixel, anomalies were computed for the year of deadwood occurrence, as well as the preceding five years, as climate extremes can show delayed effects on tree mortality (Klap et al., 2000; Knapp et al., 2024b). Anomalies are reported in Figure 4a, and from Figure S3 to Figure S6. To avoid multicollinearity among the predictors, we excluded the variables with Pearson correlation higher than 0.8 (Table S5).

We first quantified spatial dependence in the response variable to obtain a minimum deadwood sampling distance to avoid spatial autocorrelation by computing an empirical variogram of standing deadwood with the Matheron estimator (Matheron, 1962), and fitting a Gaussian (Chilès and Delfiner, 2012) theoretical variogram model, whose characteristic inflection and steeper rise near the origin capture the expected short-range continuity within forest reserves and the rapid loss of similarity across larger gaps between different forest reserves. The model estimated deadwood values become uncorrelated beyond a spatial range shown in Figure S7. Both empirical and fitted variograms indicated 95% of the sill was reached at 50 m. The operation was conducted in Python using the SciKit GStat package (Mälicke et al., 2021).

However, to ensure spatial independence between sampled observations relative to the 100 m climate grid, we set a range of 142 m (the diagonal of a 100 m squared cell) to ensure that no more than one sampled pixel fell within a single grid cell of the climatic predictors. We then sampled pixels from ten mortality strata to preserve the overall distribution. Pixels were drawn within each stratum using a Generalized Random Tessellation Stratified (Stevens Jr. and Olsen,

2004). If a stratum's tessellation failed, we used a random sampling as a fallback. Last, we applied an iterative filter using a KD-tree algorithm (Maneewongvatana and Mount, 1999) that enforces a minimum spacing of 142 m while prioritizing points from higher mortality strata, resulting in a final dataset of 24,133 pixels. The resulting sampled deadwood distribution at the 10 m scale is shown in Figure S8, which reports the full dataset and the dataset split by forest ecoregion. The distribution of the other environmental predictors is presented in the same format in the subsequent figures, from Figure S9 to Figure S17.

2.5. The random forest models

We fitted eight random forest regression models: one on the full dataset, and one for each Swiss forest ecoregion. We applied an 80/20 train-test split of each dataset, and we optimized the hyperparameters of each random forest through a 5-fold cross validated grid search on the training dataset. The grid search found the optimal number of trees (100, 300 600, 1000) and the minimum leaf size (1, 3, 5, 10) to minimize the minimum squared error.

Upon identification of the optimal parameters, each random forest model has been fitted on each corresponding full training dataset with a minimum squared error criterion. Since the deadwood distribution is heavily right-skewed (Figure S8), for each ecoregion we applied a train-test split based on an adaptive stratification. We binned the response variables into up to 10 quantile-based bins, defined to guarantee that each bin contained at least two data points, one for the training and one for the test dataset.

We determined the main environmental drivers of standing deadwood by computing SHAP (SHapley Additive exPlanations) (Lundberg and Lee, 2017) values for each random forest model. SHAP values quantify the marginal contribution of each predictor to the model's output for individual observations, allowing an interpretation of each predictor's influence. For robustness, we additionally calculated permutation importance for each model. This quantifies error increase after permuting a single variable expressed as the change in root mean squared error (ΔRMSE). Each variable was permuted 100 times per model, and the permutation importance was averaged. Both permutation importance and SHAP values were calculated for random forest regressions with an R^2 value higher than 0.1. The random forest models and the computation of the permutation importance values were implemented in Python, using the Scikit-learn package (Pedregosa et al., 2011), while the SHAP values were computed using the SHAP package (Lundberg et al., 2020).

3. Results

3.1. Uneven distribution of standing deadwood across Swiss forests

We mapped a cumulative total of 4,434 ha (0.47%) of standing deadwood out of 940,131 ha of monitored forested area across Switzerland. The quantification was based on the most recent annual observation available for each location, providing a spatially continuous assessment of standing deadwood despite differences in acquisition year across regions (Figure S1f). The highest standing deadwood was identified in the northern and central parts of Switzerland, while the lowest was in the southern part. The Jura region, characterized by low mountains

(803 m mean elevation), contained the highest amount (1,389 ha; 0.83% of forest area), followed by the Northern Pre-Alps (1,048 ha; 0.43%), while the Continental Alps record the lowest values (107 ha; 0.20%) (Figure 2a-b, Table S6).

Cumulative deadwood also varied across Swiss cantons (Figure 2c). The highest proportions were found in the Jura (1.21%), Vaud (0.86%), and Schaffhausen (0.79%), while the lowest proportions were observed in Zug (0.3%), Uri, and Nidwalden (both at 0.29%). The amount of standing deadwood detected in each ecoregion and canton is strongly constrained by the extent of forest captured in the available leaf-on aerial images. Coverage varies across years and regions (Figure S1f), ranging from only 0.2% of the forest in the Continental Alps (2018/2021) to 87% in the Southern Pre-Alps (2018) (Table S7, Table S8).

Yearly shares of standing deadwood per ecoregion ranged between 0.14 % and 1.13 % (Figure 2d, Table S7). The highest values were observed in the Jura, reaching 1.13% in 2020 and 1.03% in 2023, followed by the Swiss Central Plateau with 1.10% in 2020 and 0.51–0.58% in 2019 and 2022–2023. The Northern Pre-Alps showed rates from 0.24% in 2018 to 0.57% in 2023, while the Northern Intermediate Alps ranged from 0.20% in 2018 to 0.68% in 2020. When aggregating across all regions surveyed per year (Figure S1a-c), yearly totals of standing deadwood ranged from 751 to 1,313 ha between 2018 and 2023, corresponding to 0.25% to 0.65% of the mapped forest area (Table S9).

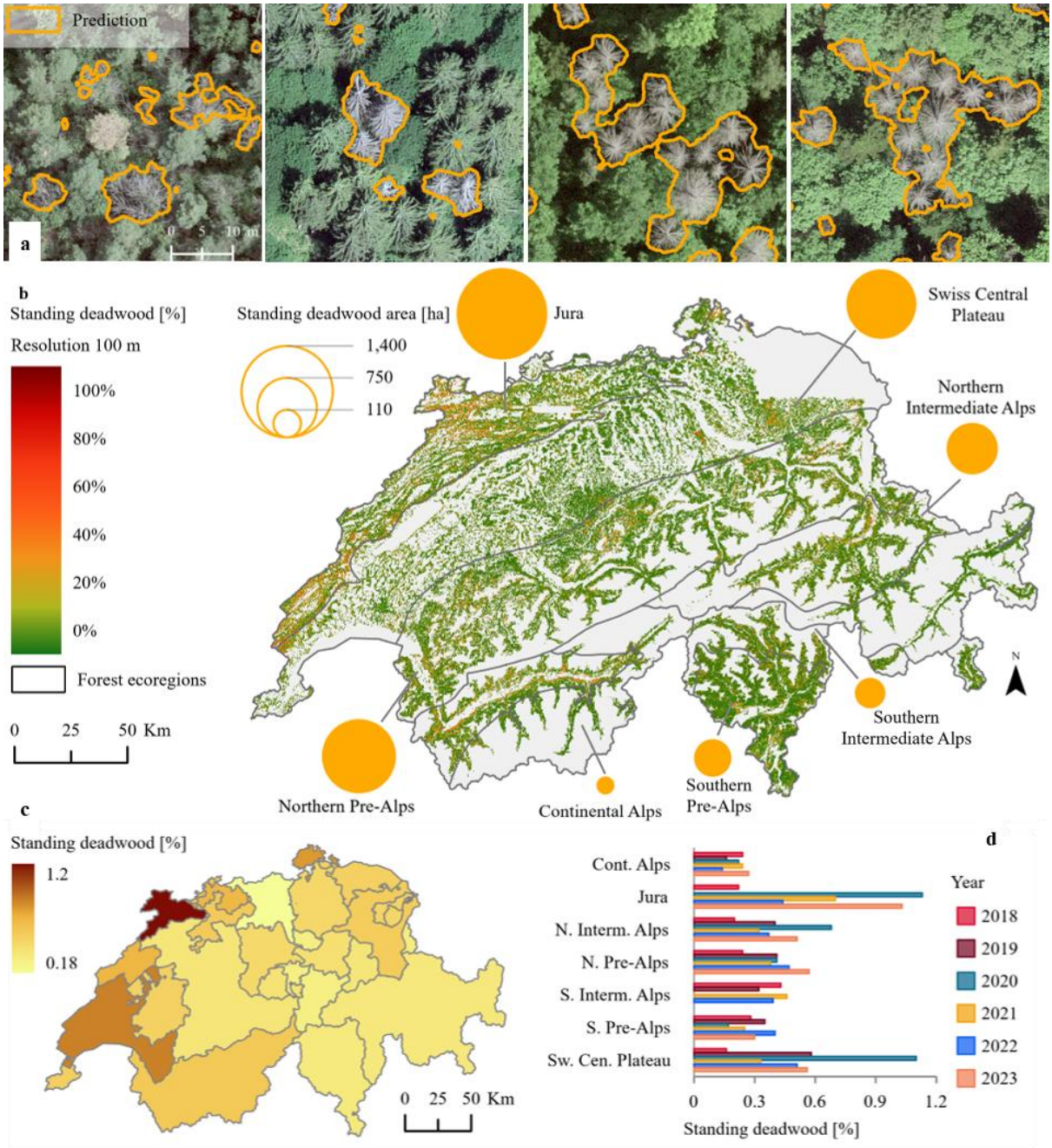

Figure 2: Standing deadwood segmentation, mapping, and summary statistics across Swiss forest ecoregions and Cantons (2018 – 2023). **a** Examples of dead trees segmentation. In each panel, the orange shapes represent the standing deadwood predictions of the segmentation model. **b** Composite map of standing deadwood from 2018 to 2023 for the main forest ecoregions in Switzerland. The segmentation outputs have been aggregated at 100 m spatial resolution for visualization purposes. The fraction of standing deadwood has been calculated as the ratio between the deadwood area, and the forest are in each pixel. For each location, the most recent annual share of deadwood is displayed, ensuring continuous spatial coverage despite regional differences in acquisition year. The orange circles denote the total area of standing deadwood per ecoregion from 2018 to 2023. **c** Share of cumulative deadwood at the cantonal level, relative to the cantonal forest area. **d** Histogram of share of standing deadwood in forested areas per ecoregion, per year.

3.2. Standing deadwood increases over time and peaks at higher elevations

Across the overlapping survey areas, deadwood was mapped independently in each set of high-resolution aerial images, yielding paired estimates for the first and second survey years within each observation cycle (Figure 3a, Table S10). Within these shared observation zones, the second survey consistently showed a larger deadwood extent than the first. For Switzerland as a whole, the mapped deadwood area was 514 and 733 ha in the 2018–2021 pair (+42.7%), 590 and 629 ha in the 2019–2022 pair (+6.5%), and 347 and 452 ha in the 2020–2023 pair (+30.4%). In protected areas, the corresponding paired values were 44 and 61 ha (+40.2%), 70 and 87 ha (+24.4%), and 20.9 and 21.3 ha (+1.8%).

Along the elevation gradient, deadwood percentage across the overlapping survey areas peaked at 1550 m a.s.l., despite declining forest area (Figure 3b). In these shared observation zones, largely located in the Alpine regions, deadwood area increased upslope and reached its maximum at 1400–1600 m a.s.l., whereas forest area peaked earlier (~1100–1300 m a.s.l.). The peak in deadwood percentage was dominated by the deadwood shares in 2023. In previous years the deadwood percentages peaked between 1450 and 1650 m a.s.l. across most survey years, with only a few years showing maximum at lower elevations (Figure S18a). Across the slope gradient, the deadwood peaked at 55°, after which it decreased. Deadwood and forest area showed largely similar distributions, both concentrated on mid-slopes of 35° (Figure 3c). All patterns refer to the cumulative deadwood for the exact spatial overlap of the six survey years (2018-2023).

Along the elevation gradient, standing deadwood share across the non-overlapping survey areas also peaked at ~1,550 m a.s.l., despite declining forest area at higher elevations (Figure 3b). Forest area consistently peaked at lower elevations (~550–1,150 m a.s.l.) and declined sharply above ~1,800 m, whereas deadwood share and area were systematically concentrated at higher elevations (Figure 3b-c, Figure S19c). As a result, deadwood area maxima was displaced 200–400 m upslope relative to forest area maxima. In contrast, deadwood share peaked at even higher elevations, indicating an increasing proportion of standing deadwood at higher elevation where overall forest cover is reduced.

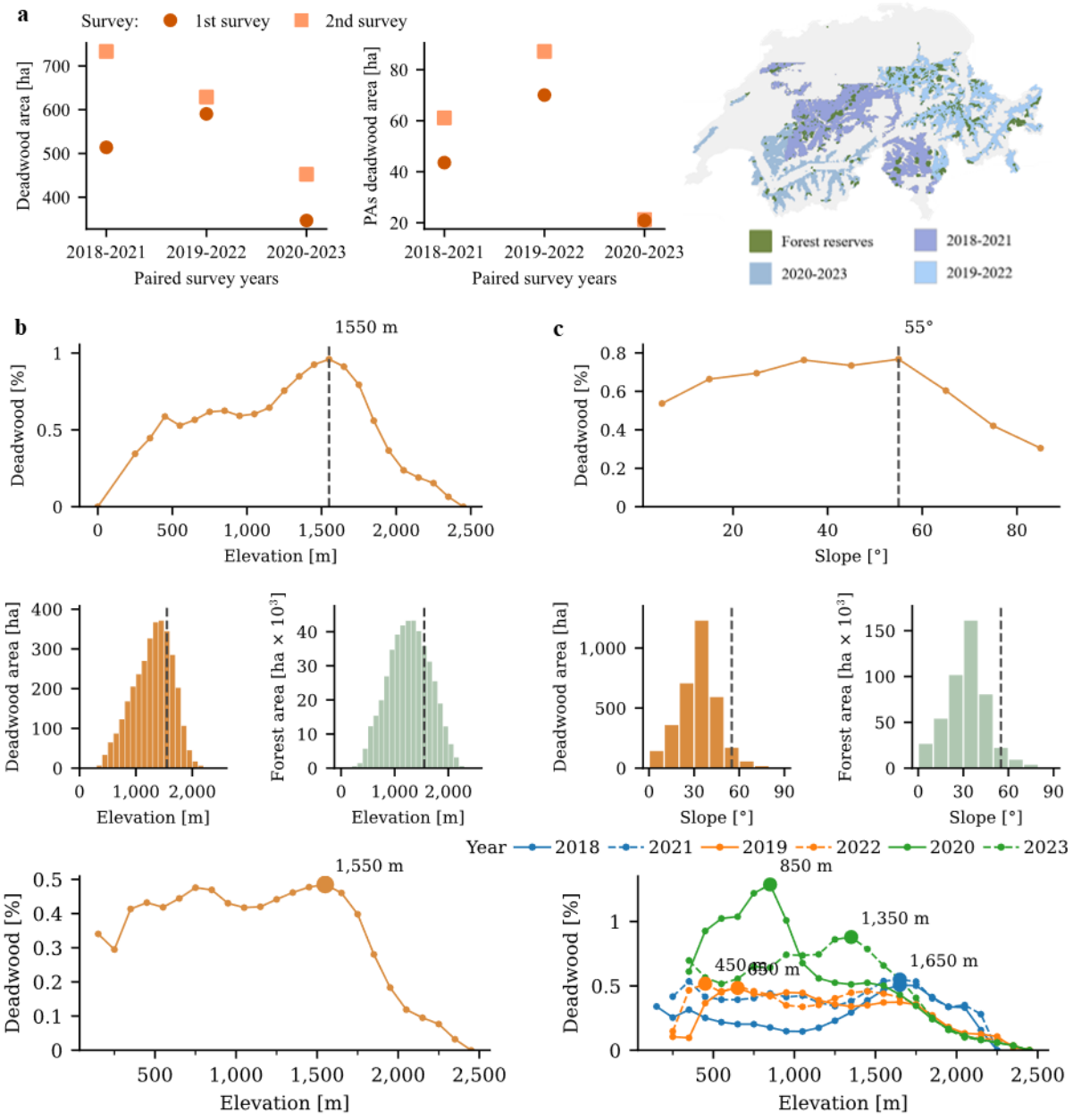

Figure 3: Standing deadwood patterns across repeated surveys and topographic gradients. **a** Standing deadwood mapped in paired survey years for the 2018–2021, 2019–2022, and 2020–2023 acquisition cycles for the overlapping forest areas and for protected areas, together with the map of the shared survey region. **b** Percentage of deadwood per elevation class for the overlapping forest areas, deadwood and forest area distributions along elevation gradients, and overall percentage of deadwood per elevation class aggregated across 2018–2023 over the entire study area. **c** Percentage of deadwood per slope class, deadwood and forest area distributions along slope gradients, and yearly percentage of deadwood per elevation class over the entire study area (solid lines: 2018–2020; dashed lines: 2021–2023, paired by color).

3.3. Temperature anomalies and forest composition shape deadwood patterns

Standing deadwood variability in Swiss forest reserves was partly explained by environmental and forest-related drivers, with the full model accounting for 17% of the observed variability

and ecoregion-specific models explaining between 4% and 21% (Table S11). Model performance was highest in the Northern Intermediate Alps (21%) and Swiss Central Plateau (18%) and lowest in the Southern Intermediate Alps (4%), with intermediate values in the Southern Pre-Alps (17%), Jura (16%), Continental Alps (15%), and Northern Pre-Alps (8%).

Across the full dataset, probability of broadleaf and lagged temperature anomalies were the most influential predictors, followed by canopy height, basal area, and soil properties (Figure 4b, Table S12-14). As probability of broadleaf represents the probability of broadleaf forest, its strong negative relationship with deadwood indicates higher standing deadwood in conifer-dominated forests (Figure 4d). Long-lag maximum temperature anomalies showed a consistently positive association with standing deadwood, whereas long-lag minimum temperature anomalies showed the opposite tendency, and short-lag anomalies contributed comparatively little. In particular, probability of broadleaf showed reduced importance in the Continental Alps and Northern Intermediate Alps, while long-lag maximum temperature anomalies contributed less in several ecoregion-specific models despite their high relevance in the full dataset, indicating region-dependent modulation of mortality drivers.

Ecoregion-specific analyses broadly mirrored the global patterns but revealed regional contrasts in the relative importance of drivers (Figure S20). Temperature anomalies dominated in both high-elevation regions such as the Continental Alps and lowland regions such as the Swiss Central Plateau whereas precipitation anomalies were most influential in mid-elevation mountain regions such as the Northern Intermediate Alps. Forest composition and structure, particularly probability of broadleaf, played a stronger role in lower mountain regions including the Jura and the Southern Pre-Alps. These results highlight a consistent role of forest structure and climate variability, with region-specific modulation of their relative contributions.

SHAP dependence plots revealed non-linear responses across climatic, structural, and site-related predictors (Figure 4d). Lagged temperature, precipitation, and climatic water balance effects were evident but generally weak (Figure S21 and 22), with precipitation anomalies and the 1-year lag climatic water balance showing slight positive trends at higher values, and minimum temperature anomalies associated with reduced deadwood shares at the lower end of their ranges (Figure S21f–k, 22b, d–h). Structural variables showed clearer contrasts, with basal area positively associated with standing deadwood and canopy height exhibiting elevated deadwood shares at intermediate values followed by declines in taller stands (Figure 4d). Soil and site-related variables, including clay content, soil carbon, and topographic wetness index, displayed non-monotonic responses with minimum deadwood shares at intermediate levels, while available water content showed a U-shaped relationship and elevation a consistent negative association (Figure S22c, i–j).

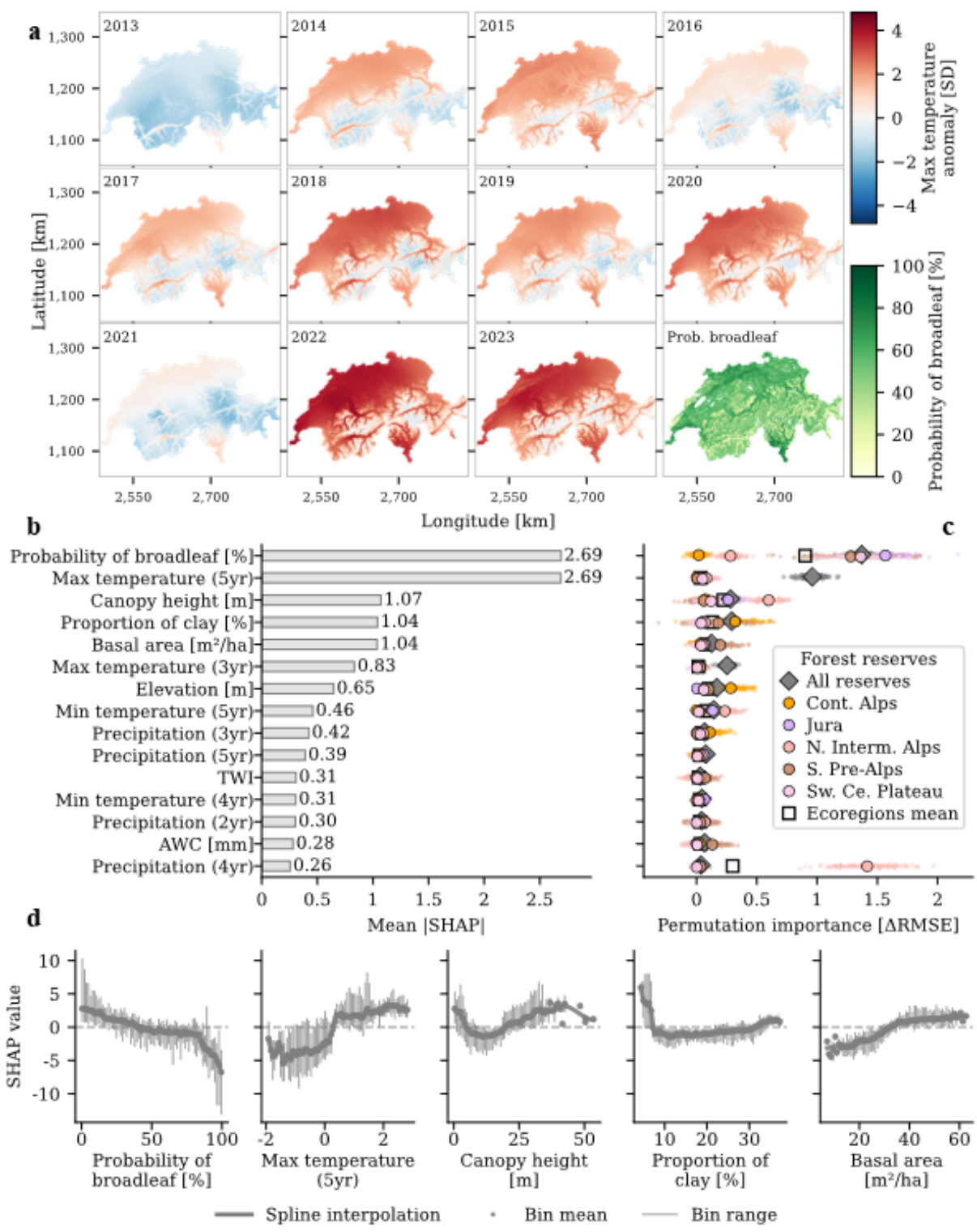

Figure 4: Maximum temperature anomalies, probability of broadleaf, SHAP values, permutation importance, and SHAP dependence plots of standing deadwood drivers derived from random forest models. **a** Yearly maximum temperature anomalies for 2013-2023 relative to the norm of 1981-2010, and country-level probability of broadleaf forest. Anomalies are calculated from the yearly mean maximum temperature and expressed as departures from the 1981-2010 mean in units of that baseline's standard deviation. **b** Absolute mean SHAP values of the fifteen most relevant variables from the random forest model fitted on the full dataset. SHAP values have been calculated on the entire test dataset. Abbreviations: TWI, Topographic

Wetness Index; AWC, Available Water Content. **c** variable permutation importance of the ten most relevant variables of the random forest models on the full and ecoregion-specific datasets, expressed as the change in RMSE when that feature is randomly permuted. Positive values indicate that shuffling the feature makes the model perform worse, and larger positive values correspond to higher importance. Jittered dots show all permutation repeats; diamond and larger circles with horizontal error bars mark the mean and standard deviation across repeats for the full dataset and ecoregion-specific datasets, respectively. Hollow black squares represent the average across ecoregions for each feature. **c** SHAP dependence plots for the full dataset model showing the marginal effects of the five most important predictors on standing deadwood. SHAP values for each predictor were binned in 70 bins, and a cubic spline was used to interpolate the average SHAP values for each bin. The solid grey lines show the spline interpolation, the grey dots indicate the mean SHAP value within each bin, and the vertical grey lines depict the range of SHAP values for each bin.

4. Discussion and conclusions

This study provided the first spatially explicit, nationwide assessment of standing deadwood dynamics, revealing systematic variation across elevation, forest composition, and climate gradients. Across forest ecoregions, standing deadwood shares ranged from 0.20 to 0.83% of forest area, with pronounced spatial heterogeneity. We showed that forest composition and climate jointly shape these patterns (up to 17%): standing deadwood was most strongly associated with conifer-dominated forests and positive temperature anomalies, whereas forest structural attributes showed secondary influence and edaphic factors contributed little explanatory power. Together, these results point to climate-sensitive forest composition as a primary determinant of contemporary standing deadwood distribution at the national scale.

The yearly deadwood rates across forest ecoregions (0.14 – 1.13%) of the leaf-on forest area were consistent with plot-based mortality estimates from Switzerland, i.e. 0.3 (Rigling et al., 2013) and 1.5% (Etzold et al., 2019) and for European forests, i.e. 0.5 and 2% (Idoate-Lacasia et al., 2025; Nagel et al., 2021; Woods et al., 2021). While comparable in magnitude, monitoring networks estimate mortality from discrete sample plots, whereas our analysis maps standing deadwood continuously across entire forest areas, enabling the identification of spatial patterns, gradients, and regional hotspots of forest mortality at the national scale.

Consistent with the widespread increase in forest mortality reported following the 2018 drought (Obladen et al., 2021; Schiefer et al., 2024; Thonfeld et al., 2022), including within Switzerland (Braun et al., 2021; Frei et al., 2022), standing deadwood increased systematically in areas covered by repeated aerial surveys. At the national scale, deadwood extent increased by 42.7%, 6.5%, and 30.4% between the 2018–2021, 2019–2022, and 2020–2023 survey pairs, respectively, with comparable increases observed within forest reserves (40.2%, 24.4%, and 1.8%). This increase was evident both at the national scale and within forest reserves, indicating a general rise in standing deadwood between successive survey years. However, because image coverage varied widely across years and regions (0.2–87% of forest area), temporal trends could only be assessed in areas surveyed more than once. Continuous, country-level acquisitions of high-resolution aerial imagery would therefore be required to enable consistent spatial and temporal assessments of changes in standing deadwood.

Standing deadwood accumulated disproportionately at higher elevations (~1,550 m) and on steeper slopes (55°), indicating that recent forest deadwood is structured by topographic gradients rather than forest availability alone (~550–1,150 m). The upslope displacement of deadwood share relative to forest area suggests increasing vulnerability of montane and subalpine forests, where warming temperatures reduce historical cold limitations while episodic drought and heat extremes impose novel stress combinations (Pepin et al., 2015). Similarly, elevated deadwood shares on steep slopes may reflect enhanced water limitation, shallow soils, and reduced buffering capacity against drought stress under warming climates (Anderegg et al., 2020; McDowell et al., 2008). Together, these patterns support the interpretation that climate change is reshaping spatial gradients of forest mortality, with topography modulating exposure and sensitivity to climatic extremes.

Our analysis identifies forest composition, climate anomalies, and stand structure as the primary determinants of standing deadwood patterns in Swiss forest reserves. Probability of broadleaf emerged as the strongest driver, with higher deadwood shares consistently associated with conifer-dominated stands, reflecting the heightened vulnerability of coniferous species, particularly Norway spruce, to drought and heat species (Idoate-Lacasia et al., 2025; Schiefer et al., 2024). Temperature anomalies, especially multi-year maximum temperature anomalies, further contributed to increased deadwood occurrence, consistent with lagged drought effects on tree mortality reported across Europe (Klap et al., 2000; Knapp et al., 2024a). Structural attributes modulated these climatic effects: deadwood shares increased with canopy height up to intermediate stand heights and with higher basal area, indicating the combined influence of stand development, competition, and exposure to climatic stress (Etzold et al., 2019; Ma et al., 2023). In contrast, edaphic factors played a secondary role, with lower deadwood shares on clay-rich soils, consistent with reduced drought sensitivity due to higher soil water-holding capacity (de Toledo et al., 2012, 2011).

Despite identifying ecologically meaningful drivers, the modest explanatory power of the models is consistent with other large-scale forest mortality studies (Ma et al., 2023; Trugman et al., 2021) and reflects the inherent complexity of mortality processes rather than methodological shortcomings. Tree mortality is stochastic and threshold-driven, shaped by interacting climatic stress, biotic agents, and disturbance events operating across multiple spatial and temporal scales, many of which are not captured by available predictors. Unobserved disturbances such as insect outbreaks, pathogens, windthrow, and legacy effects of past management, together with spatial aggregation of deadwood metrics, likely contribute substantially to unexplained variability and limit predictability from static environmental covariates alone. By focusing on forest reserves, where management interventions are absent or minimal, we reduced management-related biases, strengthening the interpretation of climate and structural drivers despite limited predictability.

Mapping standing deadwood using semantic segmentation of high-resolution aerial imagery enables spatially explicit, large-scale assessments, but several data-related constraints should be considered. The approach captures only mortality visible in the upper canopy and does not detect understory deadwood, leading to a likely underestimation of total standing deadwood. Detection accuracy depends on model performance (Möhring et al., 2025), and partial canopy

dieback may occasionally be misclassified as standing deadwood. Annual orthophoto acquisitions also vary in spatial coverage and represent single temporal snapshots, which may miss recent mortality or deadwood removal. Despite these limitations, the strong spatial consistency of deadwood patterns across independent survey years, overlapping and non-overlapping areas, and multiple analytical scales supports the robustness of the main conclusions and highlights the value of repeated high-resolution imagery for national-scale forest monitoring and climate-adaptive management.

The observed spatial concentration of standing deadwood at higher elevations suggests that montane and subalpine forests may represent emerging hotspots of climate-driven mortality, challenging the long-held assumption that these systems are buffered from drought and heat stress (Idoate-Lacasia et al., 2025; Klap et al., 2000; Schiefer et al., 2024). Increasing deadwood accumulation has important implications for carbon storage, habitat availability, and disturbance regimes, influencing biodiversity, fuel continuity, and the likelihood of secondary disturbances such as insect outbreaks and windthrow (Etzold et al., 2019; Ma et al., 2023).

By providing spatially explicit, wall-to-wall deadwood maps, this study moves beyond descriptive reporting and delivers actionable information that can support prioritization of monitoring efforts, identification of vulnerable forest areas, and evaluation of management strategies under changing climatic conditions. More broadly, the reproducible and transferable framework presented here demonstrates how high-resolution remote sensing can be integrated into climate-adaptive forest management, enabling consistent national-scale assessments and supporting proactive decision-making in forests increasingly exposed to climate extremes (Waser et al., 2025).

Funding information

This research was supported by the Upscale Project (Grant CRSII5_216562, Sinergia Call). C.M. thanks the European Space Agency for funding the “DeepFeatures” project via the AI4SCIENCE activity and the “FORTRACK” project.

CRediT authorship contribution statement

Luca Ferrari: Conceptualization, Methodology, Software, Formal Analysis, Data Curation, Writing – Original Draft, Visualization. **Lars T. Waser:** Methodology, Data Curation, Writing – Review & Editing. **Achilleas Psomas:** Methodology, Data Curation, Writing – Review & Editing. **Clemens Mosig:** Software, Writing – Review & Editing. **Teja Kattenborn:** Software, Writing – Review & Editing. **Christian Ginzler:** Methodology, Data Curation, Writing – Review & Editing. **Verena Griess:** Writing – Review & Editing, Supervision, Funding Acquisition. **Mirela Beloiu:** Conceptualization, Methodology, Formal Analysis, Data Curation, Writing – Original Draft, Visualization, Supervision.

Declaration of Interests

The authors declare no competing interests.

Acknowledgements

Luca Ferrari. and Mirela Beloiu warmly thank the Forest Resources Management group at ETH Zurich for the insightful discussions, as well as Normand Overney for the support in developing the code to download and process the data.

Data and code availability

Aerial orthophotos at 10 cm are freely available on the swisstopo website (https://www.swisstopo.admin.ch/en/orthoimage-swissimage-10). The standing deadwood segmentations and derived products, i.e., aggregations at 10 m and 100 m, deadwood shares for forest ecoregions and Swiss Cantons, will be made public after acceptance of the manuscript. The sources of the environmental variables are listed in Table S3. The Topographic Wetness Index and basal area data are available from Lars T. Waser. The climate data are available from Luca Ferrari. A visualization of the deadwood maps is available at: https://deadwood-480313.projects.earthengine.app/view/deadwood-visualization-ch.

The code for the aerial orthophotos downloading, data processing, deadwood assessment, and random forest modelling will be made public after acceptance of the manuscript. The code to run the semantic segmentation model is publicly available at https://github.com/cmosig/deadtreesmodels.

Declaration of generative AI and AI-assisted technologies in the manuscript preparation process.

During the preparation of this work, the authors used ChatGPT and Grammarly, both AI-assisted tools, to correct and improve the clarity of sentences, as well as ChatGPT and GitHub Copilot for programming assistance. After using this tool or service, the authors reviewed and edited the content as needed and take full responsibility for the content of the publication.

References

© swisstopo, n.d. Swisstopo SWISSIMAGE 10 cm [WWW Document]. URL https://www.swisstopo.admin.ch/en/orthoimage-swissimage-10 (accessed 5.23.24a).

© swisstopo, n.d. Digital Image Strips [WWW Document]. URL https://www.swisstopo.admin.ch/en/digital-image-strips (accessed 4.14.25b).

© swisstopo, n.d. swissALTI3D [WWW Document]. URL https://www.swisstopo.admin.ch/en/height-model-swissalti3d (accessed 4.14.25c).

Allen, C.D., Breshears, D.D., McDowell, N.G., 2015. On underestimation of global vulnerability to tree mortality and forest die-off from hotter drought in the Anthropocene. Ecosphere 6. https://doi.org/10.1890/ES15-00203.1

Ammer, C., Fichtner, A., Fischer, A., Gossner, M.M., Meyer, P., Seidl, R., Thomas, F.M., Annighöfer, P., Kreyling, J., Ohse, B., Berger, U., Feldmann, E., Häberle, K.-H., Heer, K., Heinrichs, S., Huth, F., Krämer-Klement, K., Mölder, A., Müller, J., Mund, M., Opgenoorth, L., Schall, P., Scherer-Lorenzen, M., Seidel, D., Vogt, J., Wagner, S., 2018. Key ecological research questions for Central European forests. Basic and Applied Ecology 32, 3–25. https://doi.org/10.1016/j.baae.2018.07.006

Anderegg, W.R.L., Trugman, A.T., Badgley, G., Anderson, C.M., Bartuska, A., Ciais, P., Cullenward, D., Field, C.B., Freeman, J., Goetz, S.J., Hicke, J.A., Huntzinger, D.,

Jackson, R.B., Nickerson, J., Pacala, S., Randerson, J.T., 2020. Climate-driven risks to the climate mitigation potential of forests. Science 368, eaaz7005. https://doi.org/10.1126/science.aaz7005

BAFU, B. für U.B.| O. fédéral de l'environnement O.| U. federale dell'ambiente, 2022. Forest Reserves.

Baltensweiler, A., Walthert, L., Hanewinkel, M., Zimmermann, S., Nussbaum, M., 2021. Machine learning based soil maps for a wide range of soil properties for the forested area of Switzerland. Geoderma Regional 27, e00437. https://doi.org/10.1016/j.geodrs.2021.e00437

Beck, H.E., Zimmermann, N.E., McVicar, T.R., Vergopolan, N., Berg, A., Wood, E.F., 2018. Present and future Köppen-Geiger climate classification maps at 1-km resolution. Sci Data 5, 180214. https://doi.org/10.1038/sdata.2018.214

Beloiu, M., Stahlmann, R., Beierkuhnlein, C., 2022. Drought impacts in forest canopy and deciduous tree saplings in Central European forests. Forest Ecology and Management 509, 120075. https://doi.org/10.1016/j.foreco.2022.120075

Berger, E., 2024. Detecting Single Tree Vitality and Mortality in Heterogeneous Temperate Forests Using Remote Sensing Data and Deep Learning (Master's Thesis). ETH Zurich.

Braun, S., Hopf, S.-E., Tresch, S., Remund, J., Schindler, C., 2021. 37 Years of Forest Monitoring in Switzerland: Drought Effects on Fagus sylvatica. Front. For. Glob. Change 4. https://doi.org/10.3389/ffgc.2021.765782

Breiman, L., 2001. Random Forests. Machine Learning 45, 5–32. https://doi.org/10.1023/A:1010933404324

Campbell, M.J., Dennison, P.E., Tune, J.W., Kannenberg, S.A., Kerr, K.L., Codding, B.F., Anderegg, W.R.L., 2020. A multi-sensor, multi-scale approach to mapping tree mortality in woodland ecosystems. Remote Sensing of Environment 245, 111853. https://doi.org/10.1016/j.rse.2020.111853

Chen, L., Brun, P., Buri, P., Fatichi, S., Gessler, A., McCarthy, M.J., Pellicciotti, F., Stocker, B., Karger, D.N., 2025. Global increase in the occurrence and impact of multiyear droughts. Science 387, 278–284. https://doi.org/10.1126/science.ado4245

Cheng, Y., Oehmcke, S., Brandt, M., Rosenthal, L., Das, A., Vrieling, A., Saatchi, S., Wagner, F., Mugabowindekwe, M., Verbruggen, W., Beier, C., Horion, S., 2024. Scattered tree death contributes to substantial forest loss in California. Nat Commun 15, 641. https://doi.org/10.1038/s41467-024-44991-z

Chilès, J., Delfiner, P., 2012. Geostatistics: Modeling Spatial Uncertainty, 1st ed. John Wiley & Sons, Ltd. https://doi.org/10.1002/9781118136188

de Groot, R.S., Wilson, M.A., Boumans, R.M.J., 2002. A typology for the classification, description and valuation of ecosystem functions, goods and services. Ecological Economics 41, 393–408. https://doi.org/10.1016/S0921-8009(02)00089-7

de Toledo, J.J., Magnusson, W.E., Castilho, C.V., Nascimento, H.E.M., 2012. Tree mode of death in Central Amazonia: Effects of soil and topography on tree mortality associated with storm disturbances. Forest Ecology and Management 263, 253–261. https://doi.org/10.1016/j.foreco.2011.09.017

de Toledo, J.J., Magnusson, W.E., Castilho, C.V., Nascimento, H.E.M., 2011. How much variation in tree mortality is predicted by soil and topography in Central Amazonia? Forest Ecology and Management 262, 331–338. https://doi.org/10.1016/j.foreco.2011.03.039

Dwyer, J.L., Roy, D.P., Sauer, B., Jenkerson, C.B., Zhang, H.K., Lymburner, L., 2018. Analysis Ready Data: Enabling Analysis of the Landsat Archive. Remote Sensing 10, 1363. https://doi.org/10.3390/rs10091363

Eichhorn, J., Roskams, P., 2013. Chapter 8 - Assessment of Tree Condition, in: Ferretti, M., Fischer, R. (Eds.), Forest Monitoring. Methods for Terrestrial Investigations in Europe with an Overview of North America and Asia, Forest Monitoring. Elsevier, pp. 139–167. https://doi.org/10.1016/B978-0-08-098222-9.00008-X

Etzold, S., Ziemińska, K., Rohner, B., Bottero, A., Bose, A.K., Ruehr, N.K., Zingg, A., Rigling, A., 2019. One Century of Forest Monitoring Data in Switzerland Reveals Species- and Site-Specific Trends of Climate-Induced Tree Mortality. Front. Plant Sci. 10. https://doi.org/10.3389/fpls.2019.00307

FAO, 2020. Global Forest Resources Assessment 2020. FAO. https://doi.org/10.4060/ca8753en

Franklin, J.F., Shugart, H.H., Harmon, M.E., 1987. Tree Death as an Ecological Process. BioScience Volume 37, 550–556. https://doi.org/10.2307/1310665

Frantz, D., 2019. FORCE—Landsat + Sentinel-2 Analysis Ready Data and Beyond. Remote Sensing 11, 1124. https://doi.org/10.3390/rs11091124

Frehner, M., Wasser, B., Schwitter, R., 2005. Nachhaltigkeit und Erfolgskontrolle im Schutzwald. Bundesamt für Umwelt, Wald und Landschaft (BUWAL), CH-3003 Bern.

Frei, E.R., Gossner, M.M., Vitasse, Y., Queloz, V., Dubach, V., Gessler, A., Ginzler, C., Hagedorn, F., Meusburger, K., Moor, M., Samblás Vives, E., Rigling, A., Uitentuis, I., von Arx, G., Wohlgemuth, T., 2022. European beech dieback after premature leaf senescence during the 2018 drought in northern Switzerland. Plant Biology 24, 1132–1145. https://doi.org/10.1111/plb.13467

George H. Hargreaves, Zohrab A. Samani, 1985. Reference Crop Evapotranspiration from Temperature. Applied Engineering in Agriculture 1, 96–99. https://doi.org/10.13031/2013.26773

Ginzler, C., 2021. Vegetation Height Model NFI.

Hammond, W.M., Williams, A.P., Abatzoglou, J.T., Adams, H.D., Klein, T., López, R., Sáenz-Romero, C., Hartmann, H., Breshears, D.D., Allen, C.D., 2022. Global field observations of tree die-off reveal hotter-drought fingerprint for Earth's forests. Nat Commun 13, 1761. https://doi.org/10.1038/s41467-022-29289-2

Hao, Z., Hao, F., Singh, V.P., Zhang, X., 2018. Changes in the severity of compound drought and hot extremes over global land areas. Environ. Res. Lett. 13, 124022. https://doi.org/10.1088/1748-9326/aaee96

Hartmann, H., Bastos, A., Das, A.J., Esquivel-Muelbert, A., Hammond, W.M., Martínez-Vilalta, J., McDowell, N.G., Powers, J.S., Pugh, T.A.M., Ruthrof, K.X., Allen, C.D., 2022. Climate Change Risks to Global Forest Health: Emergence of Unexpected Events of Elevated Tree Mortality Worldwide. Annual Review of Plant Biology 73, 673–702. https://doi.org/10.1146/annurev-arplant-102820-012804

Hartmann, H., Moura, C.F., Anderegg, W.R.L., Ruehr, N.K., Salmon, Y., Allen, C.D., Arndt, S.K., Breshears, D.D., Davi, H., Galbraith, D., Ruthrof, K.X., Wunder, J., Adams, H.D., Bloemen, J., Cailleret, M., Cobb, R., Gessler, A., Grams, T.E.E., Jansen, S., Kautz, M., Lloret, F., O'Brien, M., 2018. Research frontiers for improving our understanding of drought-induced tree and forest mortality. New Phytologist 218, 15–28. https://doi.org/10.1111/nph.15048

Häyhä, T., Franzese, P.P., Paletto, A., Fath, B.D., 2015. Assessing, valuing, and mapping ecosystem services in Alpine forests. Ecosystem Services 14, 12–23. https://doi.org/10.1016/j.ecoser.2015.03.001

Hlásny, T., Zimová, S., Merganičová, K., Štěpánek, P., Modlinger, R., Turčáni, M., 2021. Devastating outbreak of bark beetles in the Czech Republic: Drivers, impacts, and management implications. Forest Ecology and Management 490, 119075. https://doi.org/10.1016/j.foreco.2021.119075

Hülsmann, L., Bugmann, H., Cailleret, M., Brang, P., 2018. How to kill a tree: empirical mortality models for 18 species and their performance in a dynamic forest model. Ecological Applications 28, 522–540. https://doi.org/10.1002/eap.1668

Idoate-Lacasia, J., Stillhard, J., Portier, J., Bigler, C., Bugmann, H., Nagel, T.A., Casanelles-Abella, J., Käber, Y., Aakala, T., Blaschke, M., Brzeziecki, B., Carrer, M., Cateau, E., Frank, G., Fraver, S., Holik, J., Kucbel, S., Leyman, A., Meyer, P., Motta, R., Samonil, P., Seebach, L., Svoboda, M., Szwagrzyk, J., Vandekerkhove, K., Vostarek, O., Zlatanov, T., Hobi, M.L., 2025. Trends in background mortality in unmanaged forests across Europe over the last century. Journal of Ecology n/a. https://doi.org/10.1111/1365-2745.70135

IPCC, 2023a. Summary for Policymakers, in: Climate Change 2021 – The Physical Science Basis. Cambridge University Press, pp. 3–32. https://doi.org/10.1017/9781009157896.001

IPCC, 2023b. Agriculture, Forestry and Other Land Uses (AFOLU), in: Climate Change 2022 - Mitigation of Climate Change. Cambridge University Press, pp. 747–860. https://doi.org/10.1017/9781009157926.009

IPCC, 2023c. Climate Change 2022 – Impacts, Adaptation and Vulnerability: Working Group II Contribution to the Sixth Assessment Report of the Intergovernmental Panel on Climate Change, 1st ed. Cambridge University Press. https://doi.org/10.1017/9781009325844

Jääskeläinen, J., Junttila, S., O'Sullivan, H., Cheng, Y., Horion, S., Vastaranta, M., 2025. Quantifying the drivers of tree mortality: A case study from urban recreational boreal forest. Urban Forestry & Urban Greening 104, 128672. https://doi.org/10.1016/j.ufug.2025.128672

Jandl, R., Schüler, S., Schindlbacher, A., Tomiczek, C., 2013. Forests, Carbon Pool, and Timber Production, in: Lal, R., Lorenz, K., Hüttl, R.F., Schneider, B.U., von Braun, J. (Eds.), Ecosystem Services and Carbon Sequestration in the Biosphere. Springer Netherlands, Dordrecht, pp. 101–130. https://doi.org/10.1007/978-94-007-6455-2_6

Klap, J.M., Oude Voshaar, J.H., De Vries, W., Erisman, J.W., 2000. Effects of Environmental Stress on Forest Crown Condition in Europe. Part IV: Statistical Analysis of Relationships. Water, Air, & Soil Pollution 119, 387–420. https://doi.org/10.1023/A:1005157208701

Knapp, N., Wellbrock, N., Bielefeldt, J., Dühnelt, P., Hentschel, R., Bolte, A., 2024a. From single trees to country-wide maps: Modeling mortality rates in Germany based on the Crown Condition Survey. Forest Ecology and Management 568, 122081. https://doi.org/10.1016/j.foreco.2024.122081

Knapp, N., Wellbrock, N., Bielefeldt, J., Dühnelt, P., Hentschel, R., Bolte, A., 2024b. From single trees to country-wide maps: Modeling mortality rates in Germany based on the Crown Condition Survey. Forest Ecology and Management 568, 122081. https://doi.org/10.1016/j.foreco.2024.122081

Lundberg, S.M., Erion, G., Chen, H., DeGrave, A., Prutkin, J.M., Nair, B., Katz, R., Himmelfarb, J., Bansal, N., Lee, S.-I., 2020. From local explanations to global understanding with explainable AI for trees. Nat Mach Intell 2, 56–67. https://doi.org/10.1038/s42256-019-0138-9

Lundberg, S.M., Lee, S.-I., 2017. A unified approach to interpreting model predictions, in: Proceedings of the 31st International Conference on Neural Information Processing Systems, NIPS'17. Curran Associates Inc., Red Hook, NY, USA, pp. 4768–4777.

Ma, Q., Su, Y., Niu, C., Ma, Q., Hu, T., Luo, X., Tai, X., Qiu, T., Zhang, Y., Bales, R.C., Liu, L., Kelly, M., Guo, Q., 2023. Tree mortality during long-term droughts is lower in

structurally complex forest stands. Nat Commun 14, 7467. https://doi.org/10.1038/s41467-023-43083-8

Mälicke, M., Möller, E., Schneider, H.D., Müller, S., 2021. mmaelicke/scikit-gstat: A scipy flavoured geostatistical variogram analysis toolbox. https://doi.org/10.5281/zenodo.4835779

Maneewongvatana, S., Mount, D.M., 1999. Analysis of approximate nearest neighbor searching with clustered point sets. https://doi.org/10.48550/arXiv.cs/9901013

Matheron, G., 1962. Traité de géostatistique appliquée. Tome I. Paris : Technip, 1962.

McDowell, N.G., Pockman, W.T., Allen, C.D., Breshears, D.D., Cobb, N., Kolb, T., Plaut, J., Sperry, J., West, A., Williams, D.G., Yepez, E.A., 2008. Mechanisms of plant survival and mortality during drought: why do some plants survive while others succumb to drought? New Phytologist 178, 719–739. https://doi.org/10.1111/j.1469-8137.2008.02436.x

Meusburger, K., Trotsiuk, V., Schmidt-Walter, P., Baltensweiler, A., Brun, P., Bernhard, F., Gharun, M., Habel, R., Hagedorn, F., Köchli, R., Psomas, A., Puhlmann, H., Thimonier, A., Waldner, P., Zimmermann, S., Walthert, L., 2022. Soil–plant interactions modulated water availability of Swiss forests during the 2015 and 2018 droughts. Glob Chang Biol 28, 5928–5944. https://doi.org/10.1111/gcb.16332

Mitchell, P.J., O'Grady, A.P., Tissue, D.T., White, D.A., Ottenschlaeger, M.L., Pinkard, E.A., 2013. Drought response strategies define the relative contributions of hydraulic dysfunction and carbohydrate depletion during tree mortality. New Phytologist 197, 862–872. https://doi.org/10.1111/nph.12064

Möhring, J., Kattenborn, T., Mahecha, M.D., Cheng, Y., Beloiu Schwenke, M., Cloutier, M., Denter, M., Frey, J., Gassilloud, M., Göritz, A., Hempel, J., Horion, S., Jucker, T., Junttila, S., Khatri-Chhetri, P., Korznikov, K., Kruse, S., Laliberté, E., Maroschek, M., Neumeier, P., Pérez-Priego, O., Potts, A., Schiefer, F., Seidl, R., Vajna-Jehle, J., Zielewska-Büttner, K., Mosig, C., 2025. Global, multi-scale standing deadwood segmentation in centimeter-scale aerial images. ISPRS Open Journal of Photogrammetry and Remote Sensing 18, 100104. https://doi.org/10.1016/j.ophoto.2025.100104

Mosig, C., Vajna-Jehle, J., Mahecha, M.D., Cheng, Y., Hartmann, H., Montero, D., Junttila, S., Horion, S., Schwenke, M.B., Koontz, M.J., Maulud, K.N.A., Adu-Bredu, S., Al-Halbouni, D., Ali, M., Allen, M., Altman, J., Amorós, L., Angiolini, C., Astrup, R., Awada, H., Barrasso, C., Bartholomeus, H., Beck, P.S.A., Bozzini, A., Braun-Wimmer, J., Brede, B., Breunig, F.M., Brugnaro, S., Buras, A., Burchard-Levine, V., Camarero, J.J., Candotti, A., Capuder, L., Carrieri, E., Centritto, M., Chirici, G., Cloutier, M., Conciani, D., Cushman, K., Dalling, J.W., Dao, P.D., Dempewolf, J., Denter, M., Dogotari, M., Díaz-Delgado, R., Ecke, S., Eichel, J., Eltner, A., Fabbri, A., Fabi, M., Fassnacht, F., Ferreira, M.P., Fischer, F.J., Frey, J., Frick, A., Fuentes, J., Ganz, S., Garbarino, M., García, M., Gassilloud, M., Gazol, A., Gea-Izquierdo, G., Gerberding, K., Ghasemi, M., Giannetti, F., Gillan, J., Gonzalez, R., Gosper, C., Greene, T., Greinwald, K., Grieve, S., Große-Stoltenberg, A., Gutierrez, J.A., Göritz, A., Hajek, P., Hedding, D., Hempel, J., Heremans, S., Hernández, M., Heurich, M., Honkavaara, E., Höfle, B., Jackisch, R., Jucker, T., Kalwij, J.M., Kepfer-Rojas, S., Khatri-Chhetri, P., Kleinebecker, T., Klemmt, H.-J., Klouček, T., Koivumäki, N., Kolagani, N., Komárek, J., Korznikov, K., Kraszewski, B., Kruse, S., Krüger, R., Kuechly, H., Kwong, I.H.Y., Laliberté, E., Langan, L., Latifi, H., Leal-Medina, C., Lehmann, J.R.K., Li, L., Lines, E., Lisiewicz, M., Lopatin, J., Lucieer, A., Ludwig, A., Ludwig, M., Lyytikäinen-Saarenmaa, P., Ma, Q., Mansuy, N., Peña, J.M., Marino, G., Maroschek, M., Martín, M.P., Martín-Benito, D., Matham, P., Mazzoni, S., Meloni, F., Menzel, A., Meyer, H.,

Miraki, M., Moreno, G., Moreno-Fernández, D., Muller-Landau, H.C., Mälicke, M., Möhring, J., Müllerova, J., Naidu, S.S., Nardi, D., Neumeier, P., Nita, M.D., Näsi, R., Oppgenoorth, L., Orunbaev, S., Palmer, M., Paul, T., Pfenning, M., Potts, A., Prasanna, G.L., Prober, S., Puliti, S., Pérez-Luque, A.J., Pérez-Priego, O., Reudenbach, C., Revuelto, J., Rivas-Torres, G., Roberge, P., Roggero, P.P., Rossi, C., Ruehr, N.K., Ruiz-Benito, P., Runge, C.M., Satta, G.G.A., Scanu, B., Scherer-Lorenzen, M., Schiefer, F., Schiller, C., Schladebach, J., Schmehl, M.-T., Schmid, J., Schmidt, T.A., Schwarz, S., Seidl, R., Seifert, T., Barba, A.S., Shafeian, E., Shapiro, A., de Simone, L., Sohrabi, H., Soltani, S., Sotomayor, L., Sparrow, B., Steer, B.S.C., Stenson, M., Stöckigt, B., Su, Y., Suomalainen, J., Tamudo, E., Barbieri, M.J.T., Tomelleri, E., Torresani, M., Trepekli, K., Ullah, Saif, Ullah, Sami, Umlauft, J., Vargas-Ramírez, N., Vatandaslar, C., Visacki, V., Volpi, M., Vásquez, V., Wallis, C., Weinstein, B., Weiser, H., Wich, S., Ximena, T.C., Zarco-Tejada, P.J., Zdunic, K., Zielewska-Büttner, K., de Oliveira, R.A., van Wagtendonk, L., von Dosky, V., Kattenborn, T., 2026. deadtrees.earth — An open-access and interactive database for centimeter-scale aerial imagery to uncover global tree mortality dynamics. Remote Sensing of Environment 332, 115027. https://doi.org/10.1016/j.rse.2025.115027

Nagel, T.A., Firm, D., Rozman, A., 2021. Intermediate disturbances are a key driver of long-term tree demography across old-growth temperate forests. Ecology and Evolution 11, 16862–16873. https://doi.org/10.1002/ece3.8320

Neumann, M., Mues, V., Moreno, A., Hasenauer, H., Seidl, R., 2017. Climate variability drives recent tree mortality in Europe. Global Change Biology 23, 4788–4797. https://doi.org/10.1111/gcb.13724

NFI, n.d. NFI - The Swiss National Forest Inventory [WWW Document]. URL https://www.lfi.ch/en/about-the-nfi/purpose-and-aims (accessed 10.27.25).

Obladen, N., Dechering, P., Skiadaresis, G., Tegel, W., Keßler, J., Höllerl, S., Kaps, S., Hertel, M., Dulamsuren, C., Seifert, T., Hirsch, M., Seim, A., 2021. Tree mortality of European beech and Norway spruce induced by 2018-2019 hot droughts in central Germany. Agricultural and Forest Meteorology 307, 108482. https://doi.org/10.1016/J.AGRFORMET.2021.108482

Pedregosa, F., Varoquaux, G., Gramfort, A., Michel, V., Thirion, B., Grisel, O., Blondel, M., Prettenhofer, P., Weiss, R., Dubourg, V., Vanderplas, J., Passos, A., Cournapeau, D., Brucher, M., Perrot, M., Duchesnay, É., 2011. Scikit-learn: Machine Learning in Python. Journal of Machine Learning Research 12, 2825–2830.

Pepin, N., Bradley, R.S., Diaz, H.F., Baraer, M., Caceres, E.B., Forsythe, N., Fowler, H., Greenwood, G., Hashmi, M.Z., Liu, X.D., Miller, J.R., Ning, L., Ohmura, A., Palazzi, E., Rangwala, I., Schöner, W., Severskiy, I., Shahgedanova, M., Wang, M.B., Williamson, S.N., Yang, D.Q., Mountain Research Initiative EDW Working Group, 2015. Elevation-dependent warming in mountain regions of the world. Nature Clim Change 5, 424–430. https://doi.org/10.1038/nclimate2563

Rigling, A., Bigler, C., Eilmann, B., Feldmeyer-Christe, E., Gimmi, U., Ginzler, C., Graf, U., Mayer, P., Vacchiano, G., Weber, P., Wohlgemuth, T., Zweifel, R., Dobbertin, M., 2013. Driving factors of a vegetation shift from Scots pine to pubescent oak in dry Alpine forests. Global Change Biology 19, 229–240. https://doi.org/10.1111/gcb.12038

Schiefer, F., Schmidtlein, S., Frick, A., Frey, J., Klinke, R., Zielewska-Büttner, K., Junttila, S., Uhl, A., Kattenborn, T., 2023. UAV-based reference data for the prediction of fractional cover of standing deadwood from Sentinel time series. ISPRS Open Journal of Photogrammetry and Remote Sensing 8, 100034. https://doi.org/10.1016/j.ophoto.2023.100034

Schiefer, F., Schmidtlein, S., Hartmann, H., Schnabel, F., Kattenborn, T., 2024. Large-scale remote sensing reveals that tree mortality in Germany appears to be greater than previously expected. Forestry: An International Journal of Forest Research cpae062. https://doi.org/10.1093/forestry/cpae062

Schuldt, B., Buras, A., Arend, M., Vitasse, Y., Beierkuhnlein, C., Damm, A., Gharun, M., Grams, T.E.E., Hauck, M., Hajek, P., Hartmann, H., Hiltbrunner, E., Hoch, G., Holloway-Phillips, M., Körner, C., Larysch, E., Lübbe, T., Nelson, D.B., Rammig, A., Rigling, A., Rose, L., Ruehr, N.K., Schumann, K., Weiser, F., Werner, C., Wohlgemuth, T., Zang, C.S., Kahmen, A., 2020. A first assessment of the impact of the extreme 2018 summer drought on Central European forests. Basic and Applied Ecology 45, 86–103. https://doi.org/10.1016/J.BAAE.2020.04.003

Schwarz, S., Fassnacht, F.E., Hülsmann, L., Ruehr, N.K., 2025. Drivers of drought-induced canopy mortality in conifer and broadleaf forests across Luxembourg. EGUsphere 1–28. https://doi.org/10.5194/egusphere-2025-5021

Schweingruber, F.H., Wirth, C., 2009. Old Trees and the Meaning of 'Old,' in: Wirth, C., Gleixner, G., Heimann, M. (Eds.), Old-Growth Forests: Function, Fate and Value. Springer, Berlin, Heidelberg, pp. 35–54. https://doi.org/10.1007/978-3-540-92706-8_3

Senf, C., 2022. Seeing the System from Above: The Use and Potential of Remote Sensing for Studying Ecosystem Dynamics. Ecosystems 25, 1719–1737. https://doi.org/10.1007/s10021-022-00777-2

Senf, C., Buras, A., Zang, C.S., Rammig, A., Seidl, R., 2020. Excess forest mortality is consistently linked to drought across Europe. Nat Commun 11, 6200. https://doi.org/10.1038/s41467-020-19924-1

Senf, C., Seidl, R., 2021. Mapping the forest disturbance regimes of Europe. Nat Sustain 4, 63–70. https://doi.org/10.1038/s41893-020-00609-y

Sørensen, R., Zinko, U., Seibert, J., 2006. On the calculation of the topographic wetness index: evaluation of different methods based on field observations. Hydrology and Earth System Sciences 10, 101–112. https://doi.org/10.5194/hess-10-101-2006

Stevens Jr., D.L., Olsen, A.R., 2004. Spatially Balanced Sampling of Natural Resources. Journal of the American Statistical Association. https://doi.org/10.1198/016214504000000250

Thonfeld, F., Gessner, U., Holzwarth, S., Kriese, J., da Ponte, E., Huth, J., Kuenzer, C., 2022. A First Assessment of Canopy Cover Loss in Germany's Forests after the 2018–2020 Drought Years. Remote Sensing 14, 562. https://doi.org/10.3390/rs14030562

Thornton, P.E., Running, S.W., White, M.A., 1997. Generating surfaces of daily meteorological variables over large regions of complex terrain. Journal of Hydrology, Aggregate Description of Land-Atmosphere Interactions 190, 214–251. https://doi.org/10.1016/S0022-1694(96)03128-9

Thürig, E., Kaufmann, E., 2010. Increasing carbon sinks through forest management: a model-based comparison for Switzerland with its Eastern Plateau and Eastern Alps. Eur J Forest Res 129, 563–572. https://doi.org/10.1007/s10342-010-0354-7

Trugman, A.T., Anderegg, L.D.L., Anderegg, W.R.L., Das, A.J., Stephenson, N.L., 2021. Why is Tree Drought Mortality so Hard to Predict? Trends in Ecology & Evolution 36, 520–532. https://doi.org/10.1016/j.tree.2021.02.001

Trumbore, S., Brando, P., Hartmann, H., 2015. Forest health and global change. Science 349, 814–818. https://doi.org/10.1126/science.aac6759

Vicente-Serrano, S.M., Quiring, S.M., Peña-Gallardo, M., Yuan, S., Domínguez-Castro, F., 2020. A review of environmental droughts: Increased risk under global warming? Earth-Science Reviews 201, 102953. https://doi.org/10.1016/j.earscirev.2019.102953

Waser, L.T., Ginzler, C., 2021. Forest Type NFI 2018. National Forest Inventory (NFI).

Waser, L.T., Ginzler, C., Rehush, N., 2017. Wall-to-Wall Tree Type Mapping from Countrywide Airborne Remote Sensing Surveys. Remote Sensing 9, 766. https://doi.org/10.3390/rs9080766

Waser, L.T., Rehush, N., Horneber, H., Bienz, R., Stereńczak, K., Beloiu Schwenke, M., 2025. Toward a Collaborative Framework: Integrating Remote Sensing Research with Forestry Practice. The International Archives of the Photogrammetry, Remote Sensing and Spatial Information Sciences XLVIII-M-7–2025, 291–297. https://doi.org/10.5194/isprs-archives-XLVIII-M-7-2025-291-2025

Winter, C., Müller, S., Kattenborn, T., Stahl, K., Szillat, K., Weiler, M., Schnabel, F., 2025. Forest Dieback in Drinking Water Protection Areas—A Hidden Threat to Water Quality. Earth's Future 13, e2025EF006078. https://doi.org/10.1029/2025EF006078

Woods, K.D., Nagel, T.A., Brzeziecki, B., Cowell, C.M., Firm, D., Jaloviar, P., Kucbel, S., Lin, Y., Maciejewski, Z., Szwagrzyk, J., Vencurik, J., 2021. Multi-decade tree mortality in temperate old-growth forests of Europe and North America: Non-equilibrial dynamics and species-individualistic response to disturbance. Global Ecology and Biogeography 30, 1311–1333. https://doi.org/10.1111/geb.13291

5. Supplementary Information

5.1. Aerial imagery – spatial distribution for the leaf-on forest area.

These differences in yearly coverage determine the forest area available for deadwood mapping and are reported quantitatively in Figure 2. These differences in yearly coverage determine the forest area available for deadwood mapping and are reported quantitatively in Table S1.

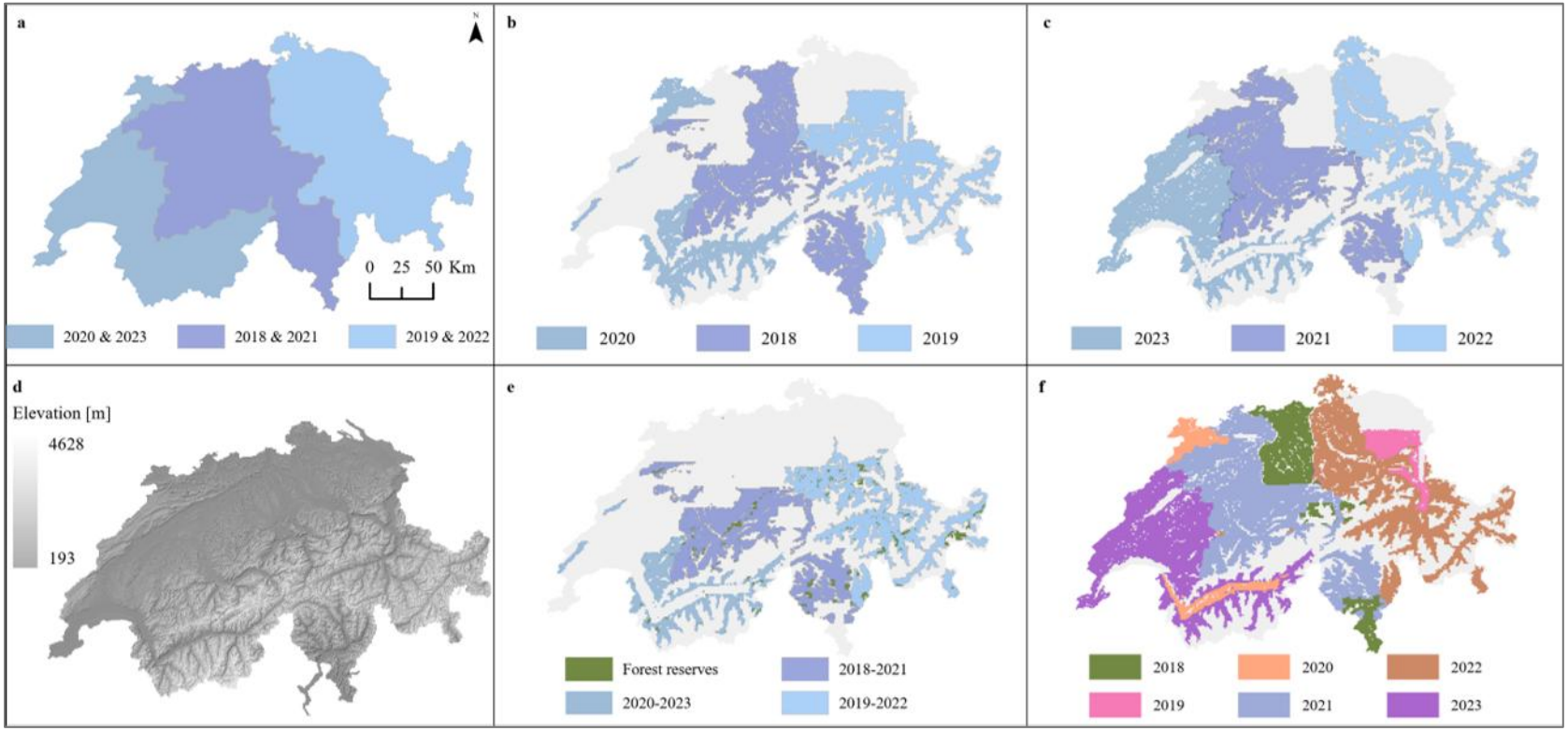

Figure S1: Spatial coverage of the aerial orthophotos dataset at 10 cm and digital elevation model of Switzerland. **a** Areas covered by the yearly aerial orthophotos at 10 cm dataset leaf-on/-off. Each year the flights cover approximately one third of Switzerland in a 3-year cycle, so the area covered in 2018 is covered again in 2021. **b,c** leaf-on orthophotos after the cleaning process. **d** digital elevation model swissALTI3D **e** map of the

overlapping areas between 2018–2021, 2019–2022, and 2020–2023 aerial orthophotos acquisition cycles, as well as forest reserves in the overlapping areas **f** composite map of the most recent areas surveyed by the aerial orthophotos.

5.2. Summary of aerial orthophotos at 10 cm dataset cleaning process

Table S1: Orthophotos cleaning summary, including the images removed because they included forested areas in leaf-off conditions, and images removed because they did not overlap with any forested area.

Year	Total images	Removed – leaf-off	Removed – no forest	Final images
2018	14,760	3,092	2,680	8,988
2019	15,322	4,100	4,443	6,789
2020	12,819	5,112	3,288	4,419
2021	15,592	4,177	2,379	9,036
2022	15,461	2,831	5,010	7,620
2023	12,820	1,851	3,692	7,277

5.3. Segmentation model validation

We tested the transformer-based semantic segmentation model on 1,626 dead trees, manually labelled over the forested area in four orthophotos covering 4 km² in the Canton of Grisons, Switzerland, for the reference year 2022. When comparing the model's predictions with the manual labels, we obtained an overall precision of 0.65, recall of 0.96, and an F1 score of 0.71. Table S2 reports the metrics calculated for each individual orthophotos, there listed by their year and coordinate ID. The individual results show minimal variation, with a precision ranging from 0.54 to 0.58, and a recall from 0.94 to 0.97.

Table S2: Average F1-score, Precision, and Recall across the test orthophotos; the orthophotos are listed by their year and coordinate ID.

Image	**F1-score**	**Precision**	**Recall**
2022_2743-1189	0.72	0.58	0.96
2022_2744-1189	0.72	0.58	0.94
2022_2768-1204	0.69	0.54	0.97
2022_2769-1204	0.73	0.58	0.97
Average	0.72	0.57	0.96

5.4. Swiss Forest Ecoregions and forest reserves

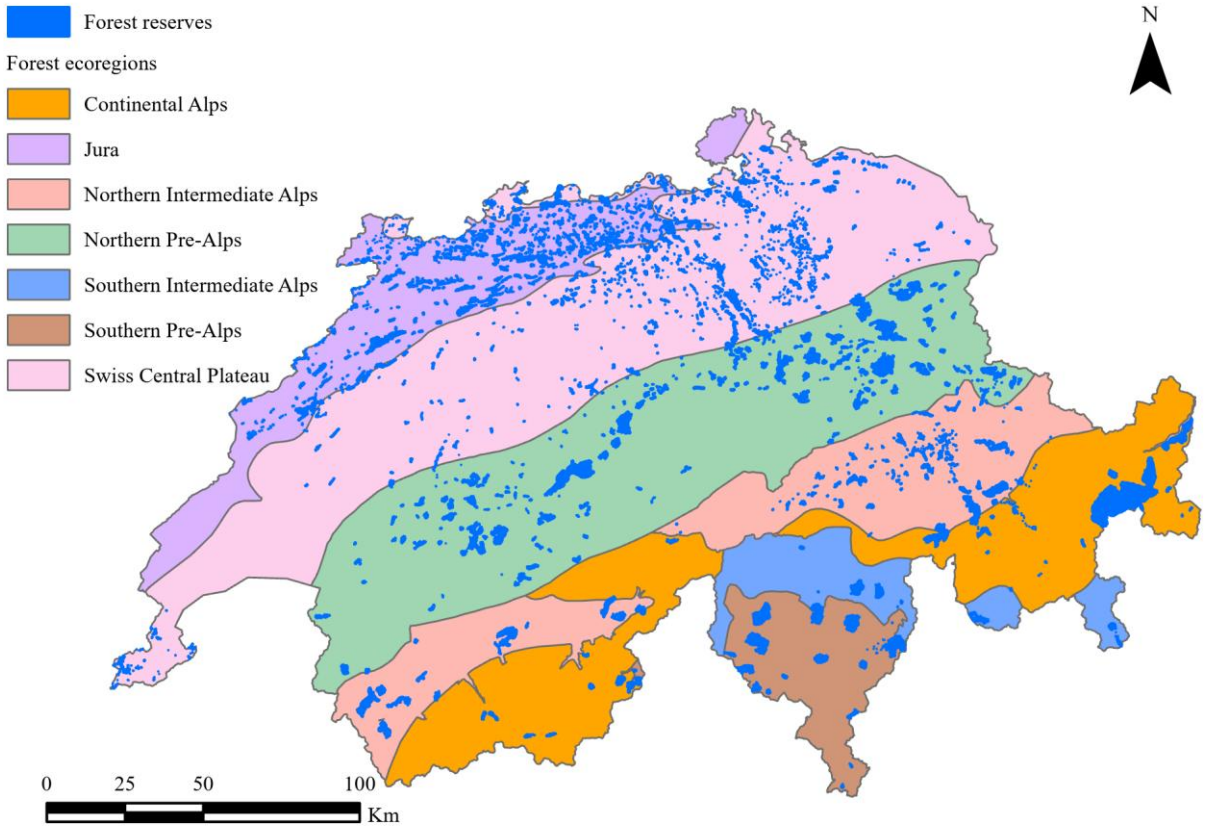

Figure S2: Spatial subdivision of Switzerland in forest ecoregion, and location of the Swiss forest reserves. The 2,564 forest reserves across Switzerland have a mean area of 47.8 ha, with a standard deviation of 372.6 ha.

5.5. Summary of the environmental and climate variables selected as standing deadwood predictors

Table S3: Summary information of the environmental variables.

Variable	Unit	Spatial resolution	Reference year	Source
Elevation	m a. s. l	2 m	2019-2023	swissALTI3D, Federal Office of Topography Swisstopo
Topographic Wetness Index	-	25 m		
Available Water Content at 2 m depth	mm	25 m	2022	(Meusburger et al., 2022)
Proportion sand/clay/organic carbon at 2 m depth	%	25 m	2021	(Baltensweiler et al., 2021)
Probability of broadleaf	%	10 m	2018	(Waser and Ginzler, 2021)
Canopy height	m	0.5 m	2021	(Ginzler, 2021)
Basal area	m^2/ha	25 m	2023	Unpublished dataset based on (Ginzler, 2021)

Table S4: Summary information of climate variables.

Variable	Spatial resolution	Temporal resolution	Period
Precipitation	100 m	Daily [mm/d], monthly [mm/month]	1930 - 2024
Minimum temperature	100 m	Daily [°C], monthly [°C]	1930 - 2024
Maximum temperature	100 m	Daily [°C], monthly [°C]	1930 - 2024
Mean temperature	100 m	Daily [°C], monthly [°C]	1930 - 2024

5.6. Climate anomalies calculation across Switzerland

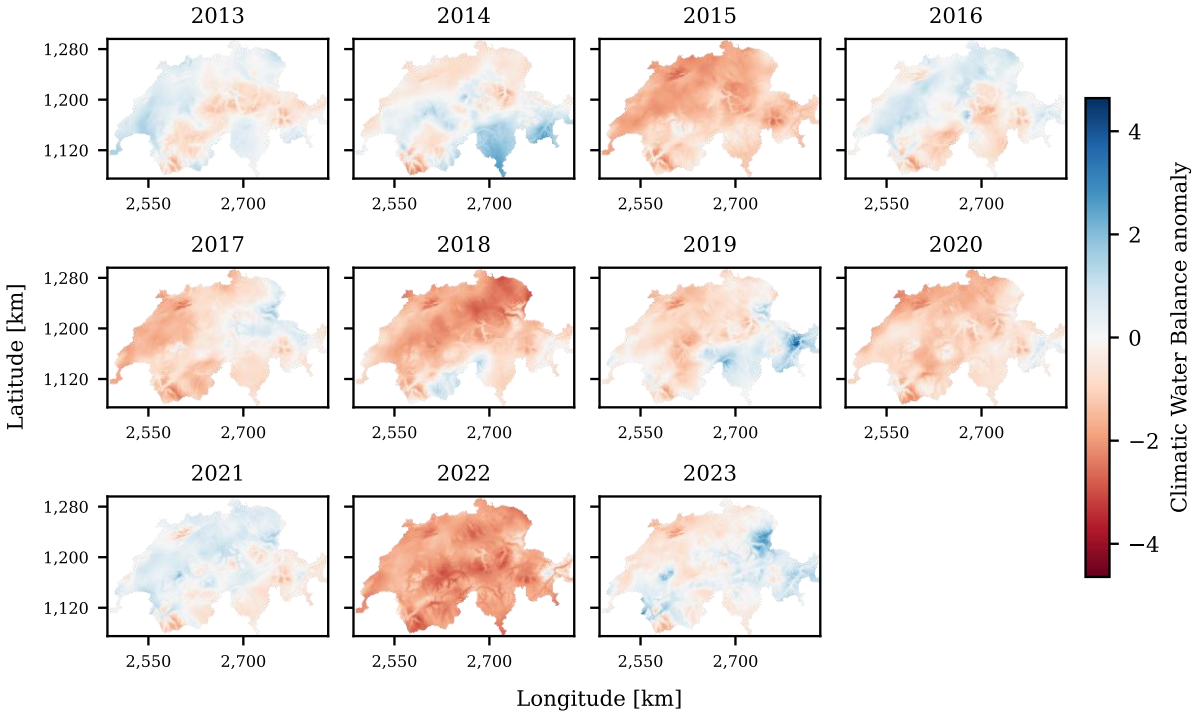

Figure S3: Yearly Climatic Water Balance anomalies for 2013-2023 relative to the norm of 1981-2010. Anomalies are calculated from the yearly cumulative climatic water balance and expressed as departures from the 1981-2010 mean in units of that baseline's standard deviation.

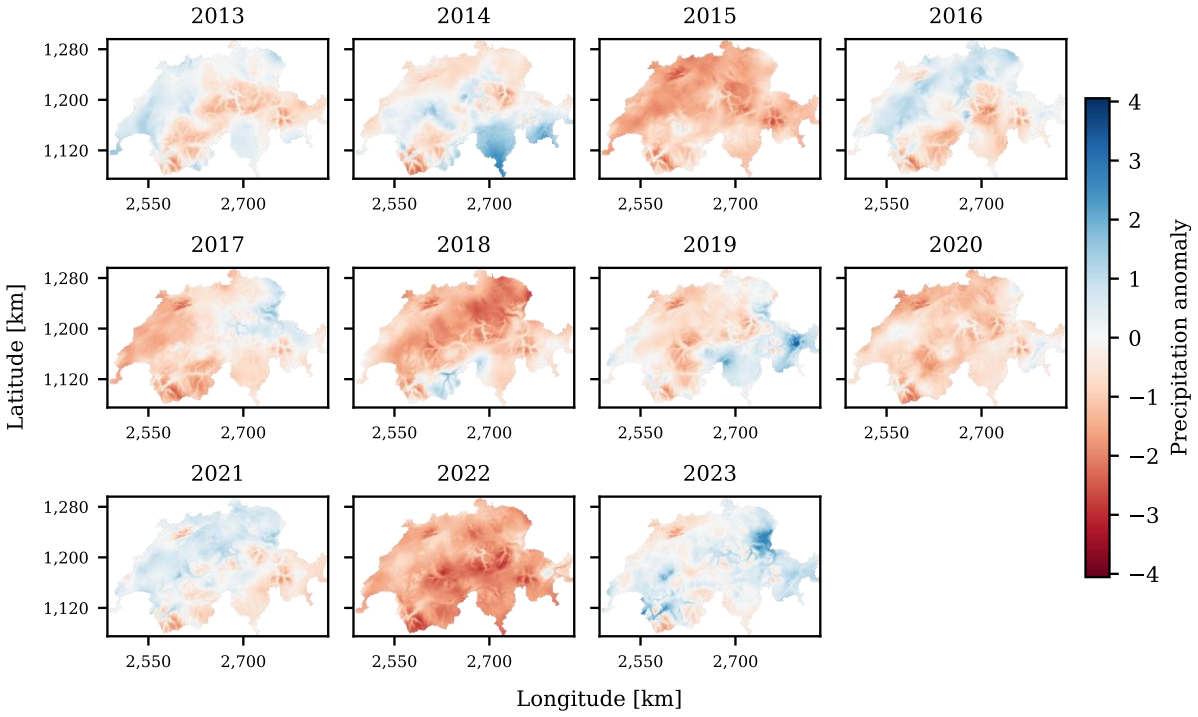

Figure S4: Yearly precipitation anomalies for 2013-2023 relative to the norm of 1981-2010. Anomalies are calculated from the yearly cumulative precipitation and expressed as departures from the 1981-2010 mean in units of that baseline's standard deviation.

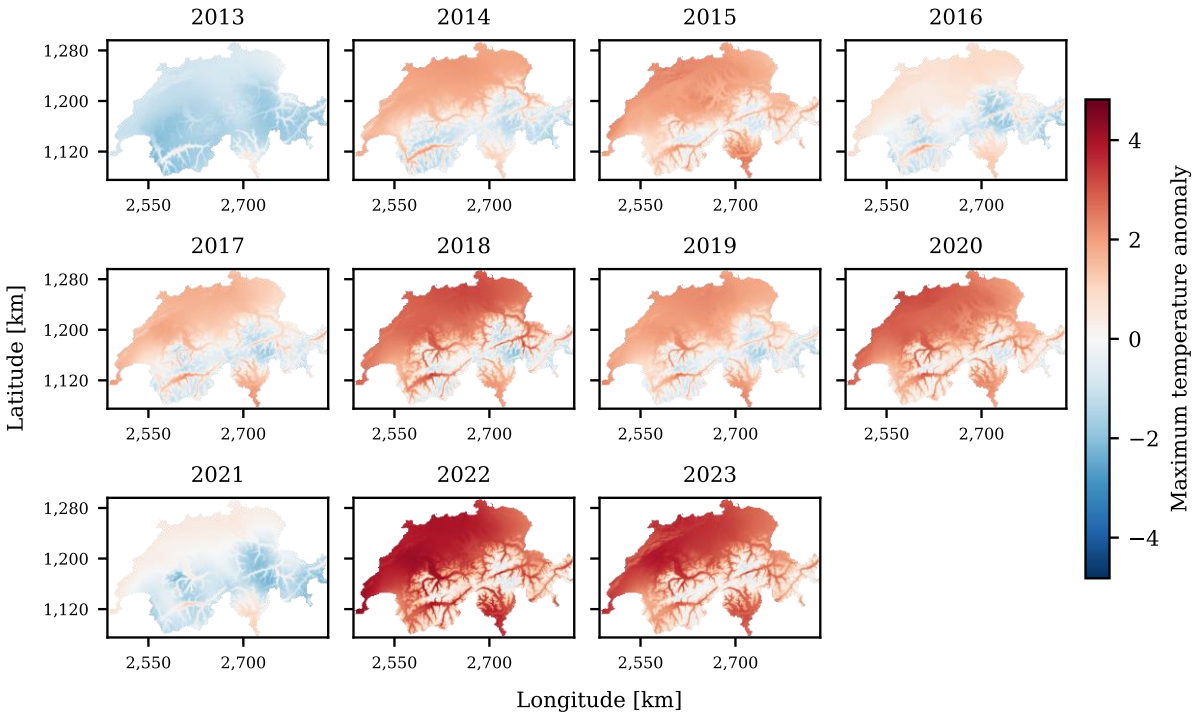

Figure S5: Yearly maximum temperature anomalies for 2013-2023 relative to the norm of 1981-2010. Anomalies are calculated from the yearly mean maximum temperature and expressed as departures from the 1981-2010 mean in units of that baseline's standard deviation.

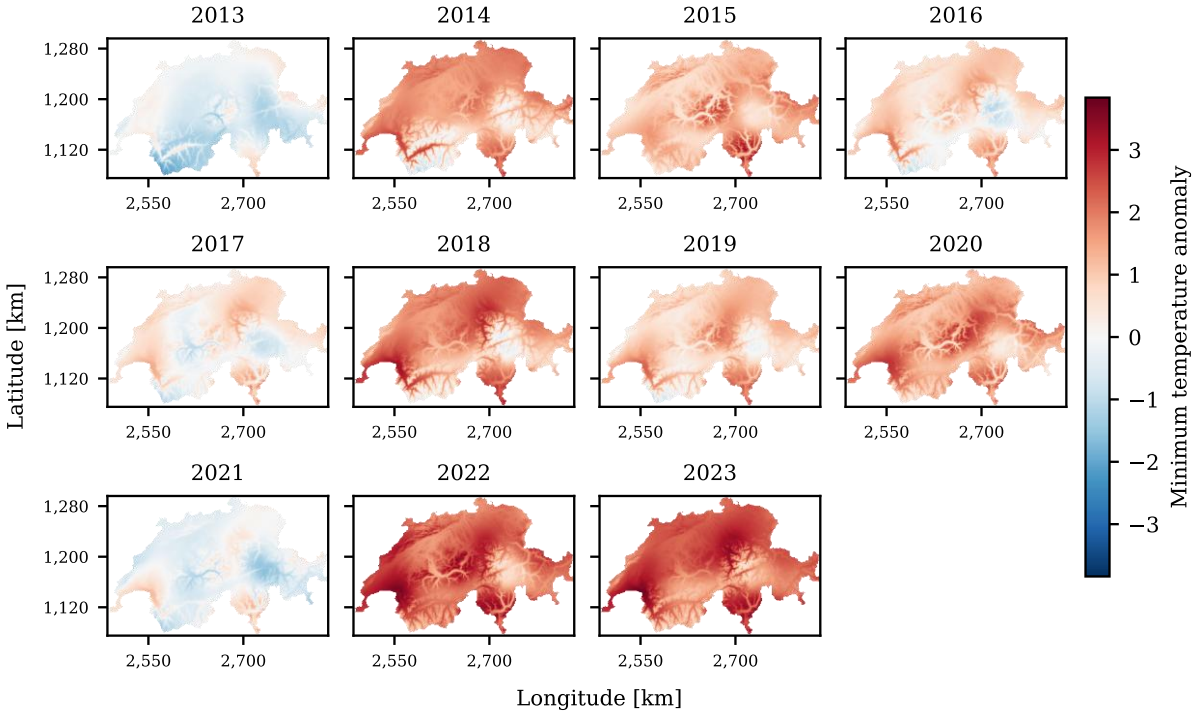

Figure S6: Yearly minimum temperature anomalies for 2013-2023 relative to the norm of 1981-2010. Anomalies are calculated from the yearly mean minimum temperature and expressed as departures from the 1981-2010 mean in units of that baseline's standard deviation.

5.7. Results of the correlation analysis

Table S5: Correlation coefficients between the selected variables. Variables with correlation coefficient higher than 0.8 were excluded from the analysis.

First variable	Second variable	Correlation
Precipitation anomaly (4 yr)	Climatic water balance anomaly (4 yr)	0.99
Precipitation anomaly (0 yr)	Climatic water balance anomaly (0 yr)	0.98
Precipitation anomaly (2 yr)	Climatic water balance anomaly (2 yr)	0.98
Precipitation anomaly (1 yr)	Climatic water balance anomaly (1 yr)	0.98
Precipitation anomaly (5 yr)	Climatic water balance anomaly (5 yr)	0.97
Precipitation anomaly (3 yr)	Climatic water balance anomaly (3 yr)	0.97
Sand content	Clay content	-0.94
Maximum temperature anomaly (5 yr)	Minimum temperature anomaly (5 yr)	0.75
Minimum temperature anomaly (5 yr)	Minimum temperature anomaly (1 yr)	0.74
Maximum temperature anomaly (2 yr)	Climatic water balance anomaly (2 yr)	-0.73
Maximum temperature anomaly (0 yr)	Minimum temperature anomaly (0 yr)	0.72
Maximum temperature anomaly (3 yr)	Minimum temperature anomaly (3 yr)	0.69
Minimum temperature anomaly (4 yr)	Minimum temperature anomaly (0 yr)	0.69
Elevation	Maximum temperature anomaly (3 yr)	-0.69
Maximum temperature anomaly (1 yr)	Climatic water balance anomaly (1 yr)	-0.67
Maximum temperature anomaly (0 yr)	Climatic water balance anomaly (0 yr)	-0.67
Maximum temperature anomaly (3 yr)	Climatic water balance anomaly (3 yr)	-0.67
Elevation	Maximum temperature anomaly (4 yr)	-0.66
Maximum temperature anomaly (1 yr)	Minimum temperature anomaly (1 yr)	0.66
Minimum temperature anomaly (1 yr)	Climatic water balance anomaly (1 yr)	-0.66
Probability of broadleaf	Elevation	-0.65
Precipitation anomaly (1 yr)	Minimum temperature anomaly (1 yr)	-0.64
Precipitation anomaly (2 yr)	Maximum temperature anomaly (2 yr)	-0.62
Maximum temperature anomaly (2 yr)	Minimum temperature anomaly (2 yr)	0.61
Elevation	Maximum temperature anomaly (2 yr)	-0.61
Elevation	Maximum temperature anomaly (0 yr)	-0.60
Basal area	Canopy height	0.59
Maximum temperature anomaly (4 yr)	Climatic water balance anomaly (4 yr)	-0.59
Organic carbon content	Available water content	-0.58
Maximum temperature anomaly (5 yr)	Climatic water balance anomaly (5 yr)	-0.55
Minimum temperature anomaly (1 yr)	Climatic water balance anomaly (0 yr)	0.55
Precipitation anomaly (0 yr)	Minimum temperature anomaly (1 yr)	0.54
Maximum temperature anomaly (3 yr)	Maximum temperature anomaly (1 yr)	0.54
Precipitation anomaly (0 yr)	Maximum temperature anomaly (0 yr)	-0.54
Precipitation anomaly (1 yr)	Maximum temperature anomaly (1 yr)	-0.53
Maximum temperature anomaly (5 yr)	Minimum temperature anomaly (1 yr)	0.53
Probability of broadleaf	Maximum temperature anomaly (3 yr)	0.53
Minimum temperature anomaly (0 yr)	Climatic water balance anomaly (0 yr)	-0.53
Maximum temperature anomaly (5 yr)	Maximum temperature anomaly (1 yr)	0.53
Maximum temperature anomaly (4 yr)	Maximum temperature anomaly (0 yr)	0.52
Maximum temperature anomaly (5 yr)	Maximum temperature anomaly (2 yr)	0.52
Minimum temperature anomaly (5 yr)	Climatic water balance anomaly (3 yr)	0.52
Precipitation anomaly (3 yr)	Minimum temperature anomaly (5 yr)	0.51

First variable	Second variable	Correlation
Precipitation anomaly (3 yr)	Maximum temperature anomaly (3 yr)	-0.51
Precipitation anomaly (4 yr)	Maximum temperature anomaly (4 yr)	-0.50
Maximum temperature anomaly (3 yr)	Maximum temperature anomaly (2 yr)	0.50
Elevation	Maximum temperature anomaly (1 yr)	-0.49
Minimum temperature anomaly (5 yr)	Climatic water balance anomaly (4 yr)	-0.48
Maximum temperature anomaly (1 yr)	Minimum temperature anomaly (4 yr)	-0.47
Precipitation anomaly (5 yr)	Precipitation anomaly (0 yr)	0.47
Precipitation anomaly (4 yr)	Minimum temperature anomaly (5 yr)	-0.47
Precipitation anomaly (0 yr)	Minimum temperature anomaly (0 yr)	-0.47
Climatic water balance anomaly (5 yr)	Climatic water balance anomaly (0 yr)	0.47
Maximum temperature anomaly (3 yr)	Maximum temperature anomaly (0 yr)	0.47
Precipitation anomaly (0 yr)	Minimum temperature anomaly (5 yr)	0.46
Precipitation anomaly (5 yr)	Climatic water balance anomaly (0 yr)	0.46
Minimum temperature anomaly (2 yr)	Climatic water balance anomaly (2 yr)	-0.46
Organic carbon content	Climatic water balance anomaly (4 yr)	0.46
Minimum temperature anomaly (0 yr)	Climatic water balance anomaly (1 yr)	0.46
Precipitation anomaly (0 yr)	Climatic water balance anomaly (5 yr)	0.45
Available water content	Elevation	-0.45
Precipitation anomaly (0 yr)	Minimum temperature anomaly (2 yr)	-0.45
Precipitation anomaly (2 yr)	Minimum temperature anomaly (2 yr)	-0.44
Maximum temperature anomaly (4 yr)	Maximum temperature anomaly (2 yr)	0.44
Minimum temperature anomaly (5 yr)	Climatic water balance anomaly (0 yr)	0.44
Organic carbon content	Precipitation anomaly (4 yr)	0.44
Precipitation anomaly (1 yr)	Minimum temperature anomaly (0 yr)	0.44
Climatic water balance anomaly (3 yr)	Climatic water balance anomaly (0 yr)	0.43
Sand content	Elevation	0.43
Precipitation anomaly (3 yr)	Precipitation anomaly (0 yr)	0.43
Probability of broadleaf	Maximum temperature anomaly (2 yr)	0.43
Maximum temperature anomaly (4 yr)	Maximum temperature anomaly (3 yr)	0.42
Minimum temperature anomaly (2 yr)	Climatic water balance anomaly (0 yr)	-0.42
Precipitation anomaly (0 yr)	Climatic water balance anomaly (3 yr)	0.42
Maximum temperature anomaly (5 yr)	Climatic water balance anomaly (4 yr)	-0.42
Elevation	Climatic water balance anomaly (3 yr)	0.41
Available water content	Maximum temperature anomaly (0 yr)	0.41
Available water content	Maximum temperature anomaly (4 yr)	0.41
Organic carbon content	Maximum temperature anomaly (4 yr)	-0.41
Precipitation anomaly (3 yr)	Climatic water balance anomaly (0 yr)	0.41
Minimum temperature anomaly (4 yr)	Climatic water balance anomaly (1 yr)	0.41
Maximum temperature anomaly (0 yr)	Climatic water balance anomaly (5 yr)	-0.41
Precipitation anomaly (1 yr)	Maximum temperature anomaly (0 yr)	0.41
Probability of broadleaf	Maximum temperature anomaly (4 yr)	0.40
Maximum temperature anomaly (5 yr)	Maximum temperature anomaly (4 yr)	0.39
Clay content	Climatic water balance anomaly (5 yr)	-0.39
Clay content	Elevation	-0.39
Precipitation anomaly (5 yr)	Maximum temperature anomaly (5 yr)	-0.38
Sand content	Maximum temperature anomaly (1 yr)	-0.38
Clay content	Precipitation anomaly (5 yr)	-0.38

First variable	Second variable	Correlation
Maximum temperature anomaly (4 yr)	Minimum temperature anomaly (4 yr)	0.38
Maximum temperature anomaly (0 yr)	Minimum temperature anomaly (4 yr)	0.38
Precipitation anomaly (4 yr)	Minimum temperature anomaly (3 yr)	0.37
Minimum temperature anomaly (2 yr)	Climatic water balance anomaly (1 yr)	0.37
Precipitation anomaly (0 yr)	Maximum temperature anomaly (1 yr)	0.36
Clay content	Maximum temperature anomaly (3 yr)	0.36
Maximum temperature anomaly (3 yr)	Minimum temperature anomaly (5 yr)	-0.36
Climatic water balance anomaly (1 yr)	Climatic water balance anomaly (0 yr)	-0.36
Minimum temperature anomaly (5 yr)	Climatic water balance anomaly (1 yr)	-0.36
Probability of broadleaf	Maximum temperature anomaly (1 yr)	0.36
Elevation	Maximum temperature anomaly (5 yr)	-0.36
Probability of broadleaf	Maximum temperature anomaly (0 yr)	0.36
Precipitation anomaly (2 yr)	Climatic water balance anomaly (3 yr)	0.35
Precipitation anomaly (4 yr)	Maximum temperature anomaly (5 yr)	-0.35
Precipitation anomaly (1 yr)	Climatic water balance anomaly (0 yr)	-0.35
Maximum temperature anomaly (1 yr)	Minimum temperature anomaly (5 yr)	0.35
Elevation	Canopy height	-0.35
Precipitation anomaly (1 yr)	Minimum temperature anomaly (5 yr)	-0.35
Sand content	Maximum temperature anomaly (3 yr)	-0.35
Clay content	Maximum temperature anomaly (1 yr)	0.35
Probability of broadleaf	Climatic water balance anomaly (3 yr)	-0.35
Sand content	Climatic water balance anomaly (5 yr)	0.34
Maximum temperature anomaly (4 yr)	Maximum temperature anomaly (1 yr)	0.34
Climatic water balance anomaly (3 yr)	Climatic water balance anomaly (2 yr)	0.34
Sand content	Climatic water balance anomaly (3 yr)	0.34
Maximum temperature anomaly (5 yr)	Maximum temperature anomaly (0 yr)	0.34
Precipitation anomaly (1 yr)	Minimum temperature anomaly (4 yr)	0.34
Maximum temperature anomaly (2 yr)	Maximum temperature anomaly (0 yr)	0.34
Elevation	Climatic water balance anomaly (0 yr)	0.34
Precipitation anomaly (0 yr)	Climatic water balance anomaly (1 yr)	-0.33
Maximum temperature anomaly (3 yr)	Climatic water balance anomaly (2 yr)	-0.33
Minimum temperature anomaly (2 yr)	Minimum temperature anomaly (0 yr)	0.33
Minimum temperature anomaly (4 yr)	Minimum temperature anomaly (2 yr)	0.33
Available water content	Minimum temperature anomaly (4 yr)	0.33
Precipitation anomaly (1 yr)	Minimum temperature anomaly (2 yr)	0.33
Maximum temperature anomaly (0 yr)	Climatic water balance anomaly (1 yr)	0.32
Sand content	Climatic water balance anomaly (1 yr)	0.32
Precipitation anomaly (3 yr)	Precipitation anomaly (2 yr)	0.32
Sand content	Precipitation anomaly (5 yr)	0.32
Clay content	Climatic water balance anomaly (1 yr)	-0.32
Clay content	Climatic water balance anomaly (3 yr)	-0.32
Available water content	Minimum temperature anomaly (0 yr)	0.32
Minimum temperature anomaly (3 yr)	Climatic water balance anomaly (4 yr)	0.31
Probability of broadleaf	Sand content	-0.31
Maximum temperature anomaly (3 yr)	Climatic water balance anomaly (0 yr)	-0.31
Clay content	Maximum temperature anomaly (4 yr)	0.31
Precipitation anomaly (2 yr)	Maximum temperature anomaly (3 yr)	-0.31

First variable	Second variable	Correlation
Sand content	Maximum temperature anomaly (4 yr)	-0.31
Sand content	Maximum temperature anomaly (2 yr)	-0.30
Minimum temperature anomaly (4 yr)	Climatic water balance anomaly (0 yr)	-0.30
Organic carbon content	Elevation	0.30
Organic carbon content	Minimum temperature anomaly (3 yr)	0.30
Precipitation anomaly (1 yr)	Precipitation anomaly (0 yr)	-0.30
Maximum temperature anomaly (2 yr)	Climatic water balance anomaly (4 yr)	-0.30
Maximum temperature anomaly (1 yr)	Minimum temperature anomaly (0 yr)	-0.30
Maximum temperature anomaly (1 yr)	Minimum temperature anomaly (3 yr)	0.30
Minimum temperature anomaly (4 yr)	Climatic water balance anomaly (3 yr)	0.30
Precipitation anomaly (5 yr)	Maximum temperature anomaly (0 yr)	-0.30
Minimum temperature anomaly (0 yr)	Climatic water balance anomaly (4 yr)	0.29
Clay content	Precipitation anomaly (1 yr)	-0.29
Precipitation anomaly (4 yr)	Minimum temperature anomaly (0 yr)	0.29
Maximum temperature anomaly (1 yr)	Climatic water balance anomaly (0 yr)	0.29
Precipitation anomaly (3 yr)	Maximum temperature anomaly (5 yr)	0.29
Minimum temperature anomaly (3 yr)	Climatic water balance anomaly (3 yr)	-0.29
Precipitation anomaly (0 yr)	Minimum temperature anomaly (4 yr)	-0.28
Maximum temperature anomaly (0 yr)	Minimum temperature anomaly (2 yr)	0.28
Precipitation anomaly (3 yr)	Climatic water balance anomaly (2 yr)	0.28
Maximum temperature anomaly (1 yr)	Climatic water balance anomaly (3 yr)	-0.28
Precipitation anomaly (2 yr)	Precipitation anomaly (0 yr)	0.28
Sand content	Climatic water balance anomaly (4 yr)	0.28
Maximum temperature anomaly (2 yr)	Climatic water balance anomaly (3 yr)	-0.28
Sand content	Precipitation anomaly (1 yr)	0.28
Probability of broadleaf	Clay content	0.28
Minimum temperature anomaly (3 yr)	Minimum temperature anomaly (2 yr)	0.28
Precipitation anomaly (2 yr)	Minimum temperature anomaly (3 yr)	-0.27
Probability of broadleaf	Minimum temperature anomaly (3 yr)	0.27
Minimum temperature anomaly (0 yr)	Climatic water balance anomaly (2 yr)	0.27
Maximum temperature anomaly (5 yr)	Climatic water balance anomaly (2 yr)	-0.27
Sand content	Precipitation anomaly (3 yr)	0.26
Minimum temperature anomaly (2 yr)	Climatic water balance anomaly (5 yr)	-0.26
Clay content	Climatic water balance anomaly (0 yr)	-0.26
Canopy height	Maximum temperature anomaly (3 yr)	0.26
Minimum temperature anomaly (0 yr)	Climatic water balance anomaly (5 yr)	-0.26
Clay content	Precipitation anomaly (0 yr)	-0.26
Available water content	Climatic water balance anomaly (0 yr)	-0.26
Sand content	Precipitation anomaly (4 yr)	0.26
Sand content	Maximum temperature anomaly (5 yr)	-0.26
Canopy height	Maximum temperature anomaly (4 yr)	0.26
Maximum temperature anomaly (2 yr)	Maximum temperature anomaly (1 yr)	0.26
Precipitation anomaly (4 yr)	Maximum temperature anomaly (3 yr)	0.25
Minimum temperature anomaly (5 yr)	Minimum temperature anomaly (3 yr)	-0.25
Clay content	Precipitation anomaly (3 yr)	-0.25
Clay content	Canopy height	0.25
Precipitation anomaly (3 yr)	Minimum temperature anomaly (4 yr)	0.25

First variable	Second variable	Correlation
Elevation	Precipitation anomaly (3 yr)	0.25
Canopy height	Maximum temperature anomaly (0 yr)	0.25
Clay content	Maximum temperature anomaly (2 yr)	0.25
Maximum temperature anomaly (2 yr)	Climatic water balance anomaly (0 yr)	-0.25
Minimum temperature anomaly (1 yr)	Climatic water balance anomaly (3 yr)	0.25
Precipitation anomaly (0 yr)	Climatic water balance anomaly (2 yr)	0.25
Organic carbon content	Maximum temperature anomaly (0 yr)	-0.24
Sand content	Canopy height	-0.24
Clay content	Maximum temperature anomaly (5 yr)	0.24
Precipitation anomaly (5 yr)	Minimum temperature anomaly (3 yr)	0.24
Precipitation anomaly (3 yr)	Minimum temperature anomaly (1 yr)	0.24
Probability of broadleaf	Precipitation anomaly (3 yr)	-0.24
Maximum temperature anomaly (2 yr)	Climatic water balance anomaly (5 yr)	-0.24
Maximum temperature anomaly (1 yr)	Minimum temperature anomaly (2 yr)	-0.24
Elevation	Minimum temperature anomaly (3 yr)	-0.24
Clay content	Climatic water balance anomaly (4 yr)	-0.24
Maximum temperature anomaly (5 yr)	Climatic water balance anomaly (1 yr)	-0.23
Precipitation anomaly (2 yr)	Climatic water balance anomaly (0 yr)	0.23
Available water content	Precipitation anomaly (1 yr)	0.23
Precipitation anomaly (0 yr)	Maximum temperature anomaly (3 yr)	-0.23
Maximum temperature anomaly (4 yr)	Minimum temperature anomaly (5 yr)	0.23
Precipitation anomaly (5 yr)	Minimum temperature anomaly (0 yr)	-0.23
Precipitation anomaly (4 yr)	Maximum temperature anomaly (2 yr)	-0.23
Maximum temperature anomaly (0 yr)	Climatic water balance anomaly (3 yr)	-0.23
Minimum temperature anomaly (5 yr)	Climatic water balance anomaly (5 yr)	-0.23
Precipitation anomaly (2 yr)	Minimum temperature anomaly (0 yr)	0.23
Precipitation anomaly (5 yr)	Minimum temperature anomaly (2 yr)	-0.22
Maximum temperature anomaly (0 yr)	Minimum temperature anomaly (1 yr)	-0.22
Maximum temperature anomaly (5 yr)	Minimum temperature anomaly (4 yr)	-0.22
Probability of broadleaf	Climatic water balance anomaly (2 yr)	-0.22
Climatic water balance anomaly (2 yr)	Climatic water balance anomaly (0 yr)	0.22
Precipitation anomaly (1 yr)	Maximum temperature anomaly (2 yr)	0.22
Sand content	Minimum temperature anomaly (4 yr)	0.22
Probability of broadleaf	Basal area	-0.22
Elevation	Climatic water balance anomaly (2 yr)	0.22
Elevation	Minimum temperature anomaly (2 yr)	-0.22
Clay content	Precipitation anomaly (4 yr)	-0.22
Elevation	Precipitation anomaly (0 yr)	0.22
Minimum temperature anomaly (2 yr)	Minimum temperature anomaly (1 yr)	-0.21
Canopy height	Maximum temperature anomaly (2 yr)	0.21
Minimum temperature anomaly (3 yr)	Climatic water balance anomaly (2 yr)	-0.21
Sand content	Minimum temperature anomaly (0 yr)	0.21
Precipitation anomaly (3 yr)	Minimum temperature anomaly (3 yr)	-0.21
Precipitation anomaly (2 yr)	Minimum temperature anomaly (1 yr)	0.21
Climatic water balance anomaly (4 yr)	Climatic water balance anomaly (2 yr)	0.21
Minimum temperature anomaly (4 yr)	Climatic water balance anomaly (2 yr)	0.21
Organic carbon content	Precipitation anomaly (1 yr)	-0.21

First variable	Second variable	Correlation
Basal area	Elevation	0.21
Probability of broadleaf	Canopy height	0.20
Available water content	Minimum temperature anomaly (1 yr)	-0.20
Minimum temperature anomaly (4 yr)	Minimum temperature anomaly (1 yr)	-0.20
Probability of broadleaf	Available water content	0.20
Probability of broadleaf	Maximum temperature anomaly (5 yr)	0.20
Minimum temperature anomaly (1 yr)	Climatic water balance anomaly (2 yr)	0.20
Topographic wetness index	Available water content	0.20
Sand content	Climatic water balance anomaly (0 yr)	0.20
Precipitation anomaly (0 yr)	Maximum temperature anomaly (2 yr)	-0.20
Clay content	Minimum temperature anomaly (3 yr)	0.20
Topographic wetness index	Organic carbon content	-0.20
Basal area	Maximum temperature anomaly (3 yr)	-0.19
Available water content	Climatic water balance anomaly (1 yr)	0.19
Minimum temperature anomaly (3 yr)	Climatic water balance anomaly (5 yr)	0.19
Maximum temperature anomaly (4 yr)	Minimum temperature anomaly (3 yr)	0.19
Basal area	Maximum temperature anomaly (2 yr)	-0.19
Topographic wetness index	Elevation	-0.19
Sand content	Precipitation anomaly (0 yr)	0.18
Available water content	Precipitation anomaly (0 yr)	-0.18
Available water content	Canopy height	0.18
Climatic water balance anomaly (5 yr)	Climatic water balance anomaly (2 yr)	0.18
Maximum temperature anomaly (5 yr)	Climatic water balance anomaly (3 yr)	0.18
Maximum temperature anomaly (2 yr)	Minimum temperature anomaly (3 yr)	0.18
Organic carbon content	Minimum temperature anomaly (1 yr)	0.18
Probability of broadleaf	Climatic water balance anomaly (0 yr)	-0.18
Maximum temperature anomaly (3 yr)	Minimum temperature anomaly (2 yr)	0.18
Precipitation anomaly (4 yr)	Climatic water balance anomaly (2 yr)	0.18
Clay content	Maximum temperature anomaly (0 yr)	0.18
Maximum temperature anomaly (4 yr)	Climatic water balance anomaly (0 yr)	-0.18
Minimum temperature anomaly (4 yr)	Minimum temperature anomaly (3 yr)	0.17
Probability of broadleaf	Precipitation anomaly (2 yr)	-0.17
Elevation	Climatic water balance anomaly (4 yr)	0.17
Precipitation anomaly (1 yr)	Maximum temperature anomaly (5 yr)	-0.17
Precipitation anomaly (3 yr)	Maximum temperature anomaly (1 yr)	-0.17
Precipitation anomaly (4 yr)	Precipitation anomaly (1 yr)	0.17
Precipitation anomaly (2 yr)	Minimum temperature anomaly (4 yr)	0.17
Available water content	Maximum temperature anomaly (3 yr)	0.17
Minimum temperature anomaly (3 yr)	Minimum temperature anomaly (1 yr)	0.17
Canopy height	Climatic water balance anomaly (0 yr)	-0.17
Precipitation anomaly (2 yr)	Maximum temperature anomaly (5 yr)	-0.17
Probability of broadleaf	Minimum temperature anomaly (2 yr)	0.17
Organic carbon content	Maximum temperature anomaly (2 yr)	-0.16
Maximum temperature anomaly (3 yr)	Climatic water balance anomaly (4 yr)	0.16
Organic carbon content	Maximum temperature anomaly (5 yr)	-0.16
Precipitation anomaly (2 yr)	Climatic water balance anomaly (5 yr)	0.16
Canopy height	Maximum temperature anomaly (1 yr)	0.16

First variable	Second variable	Correlation
Basal area	Precipitation anomaly (5 yr)	-0.16
Basal area	Precipitation anomaly (1 yr)	-0.16
Precipitation anomaly (5 yr)	Minimum temperature anomaly (5 yr)	-0.16
Probability of broadleaf	Organic carbon content	-0.16
Topographic wetness index	Maximum temperature anomaly (4 yr)	0.16
Canopy height	Climatic water balance anomaly (3 yr)	-0.16
Precipitation anomaly (3 yr)	Climatic water balance anomaly (4 yr)	-0.15
Precipitation anomaly (4 yr)	Climatic water balance anomaly (1 yr)	0.15
Maximum temperature anomaly (2 yr)	Climatic water balance anomaly (1 yr)	0.15
Maximum temperature anomaly (2 yr)	Minimum temperature anomaly (0 yr)	-0.15
Climatic water balance anomaly (4 yr)	Climatic water balance anomaly (1 yr)	0.15
Precipitation anomaly (1 yr)	Climatic water balance anomaly (4 yr)	0.15
Canopy height	Minimum temperature anomaly (3 yr)	0.15
Topographic wetness index	Maximum temperature anomaly (0 yr)	0.15
Sand content	Maximum temperature anomaly (0 yr)	-0.15
Maximum temperature anomaly (5 yr)	Minimum temperature anomaly (2 yr)	0.14
Available water content	Minimum temperature anomaly (2 yr)	0.14
Minimum temperature anomaly (1 yr)	Climatic water balance anomaly (4 yr)	-0.14
Precipitation anomaly (4 yr)	Climatic water balance anomaly (3 yr)	-0.14
Organic carbon content	Climatic water balance anomaly (1 yr)	-0.14
Basal area	Climatic water balance anomaly (3 yr)	0.14
Maximum temperature anomaly (4 yr)	Minimum temperature anomaly (0 yr)	0.14
Organic carbon content	Minimum temperature anomaly (5 yr)	-0.14
Precipitation anomaly (2 yr)	Climatic water balance anomaly (4 yr)	0.14
Basal area	Climatic water balance anomaly (2 yr)	0.14
Clay content	Minimum temperature anomaly (4 yr)	-0.14
Available water content	Precipitation anomaly (2 yr)	0.14
Precipitation anomaly (3 yr)	Maximum temperature anomaly (2 yr)	-0.14
Climatic water balance anomaly (5 yr)	Climatic water balance anomaly (4 yr)	0.14
Precipitation anomaly (4 yr)	Precipitation anomaly (3 yr)	-0.14
Maximum temperature anomaly (5 yr)	Maximum temperature anomaly (3 yr)	0.14
Precipitation anomaly (4 yr)	Climatic water balance anomaly (5 yr)	0.14
Minimum temperature anomaly (4 yr)	Climatic water balance anomaly (5 yr)	0.13
Canopy height	Maximum temperature anomaly (5 yr)	0.13
Precipitation anomaly (0 yr)	Maximum temperature anomaly (5 yr)	0.13
Canopy height	Precipitation anomaly (0 yr)	-0.13
Basal area	Clay content	0.13
Available water content	Climatic water balance anomaly (4 yr)	-0.13
Climatic water balance anomaly (4 yr)	Climatic water balance anomaly (3 yr)	-0.13
Minimum temperature anomaly (1 yr)	Minimum temperature anomaly (0 yr)	-0.13
Precipitation anomaly (3 yr)	Maximum temperature anomaly (0 yr)	-0.13
Maximum temperature anomaly (3 yr)	Minimum temperature anomaly (4 yr)	-0.13
Minimum temperature anomaly (2 yr)	Climatic water balance anomaly (4 yr)	0.13
Precipitation anomaly (3 yr)	Climatic water balance anomaly (1 yr)	0.13
Precipitation anomaly (4 yr)	Minimum temperature anomaly (1 yr)	-0.13
Precipitation anomaly (2 yr)	Climatic water balance anomaly (1 yr)	-0.13
Clay content	Minimum temperature anomaly (0 yr)	-0.13

First variable	Second variable	Correlation
Precipitation anomaly (4 yr)	Minimum temperature anomaly (2 yr)	0.13
Climatic water balance anomaly (2 yr)	Climatic water balance anomaly (1 yr)	-0.13
Elevation	Climatic water balance anomaly (5 yr)	0.13
Precipitation anomaly (5 yr)	Precipitation anomaly (4 yr)	0.12
Maximum temperature anomaly (2 yr)	Minimum temperature anomaly (1 yr)	-0.12
Organic carbon content	Precipitation anomaly (3 yr)	-0.12
Sand content	Climatic water balance anomaly (2 yr)	0.12
Precipitation anomaly (4 yr)	Precipitation anomaly (2 yr)	0.12
Clay content	Minimum temperature anomaly (1 yr)	0.12
Minimum temperature anomaly (0 yr)	Climatic water balance anomaly (3 yr)	0.12
Elevation	Precipitation anomaly (2 yr)	0.12
Canopy height	Minimum temperature anomaly (2 yr)	0.12
Precipitation anomaly (1 yr)	Climatic water balance anomaly (2 yr)	-0.12
Sand content	Minimum temperature anomaly (3 yr)	-0.12
Precipitation anomaly (1 yr)	Maximum temperature anomaly (3 yr)	0.12
Sand content	Organic carbon content	0.12
Available water content	Maximum temperature anomaly (2 yr)	0.12
Minimum temperature anomaly (2 yr)	Climatic water balance anomaly (3 yr)	-0.11
Organic carbon content	Precipitation anomaly (2 yr)	-0.11
Precipitation anomaly (3 yr)	Minimum temperature anomaly (0 yr)	0.11
Maximum temperature anomaly (2 yr)	Minimum temperature anomaly (5 yr)	0.11
Available water content	Climatic water balance anomaly (2 yr)	0.11
Clay content	Climatic water balance anomaly (2 yr)	-0.11
Maximum temperature anomaly (1 yr)	Maximum temperature anomaly (0 yr)	0.11
Canopy height	Precipitation anomaly (3 yr)	-0.11
Maximum temperature anomaly (2 yr)	Minimum temperature anomaly (4 yr)	-0.11
Probability of broadleaf	Precipitation anomaly (0 yr)	-0.11
Basal area	Maximum temperature anomaly (0 yr)	-0.11
Basal area	Topographic wetness index	-0.11
Clay content	Precipitation anomaly (2 yr)	-0.10
Basal area	Climatic water balance anomaly (1 yr)	-0.10
Basal area	Climatic water balance anomaly (5 yr)	-0.10
Maximum temperature anomaly (4 yr)	Minimum temperature anomaly (1 yr)	0.10
Precipitation anomaly (5 yr)	Precipitation anomaly (1 yr)	0.10
Climatic water balance anomaly (3 yr)	Climatic water balance anomaly (1 yr)	0.10
Precipitation anomaly (5 yr)	Minimum temperature anomaly (4 yr)	0.10
Sand content	Minimum temperature anomaly (1 yr)	-0.10
Maximum temperature anomaly (1 yr)	Climatic water balance anomaly (5 yr)	-0.10
Minimum temperature anomaly (3 yr)	Minimum temperature anomaly (0 yr)	0.10
Precipitation anomaly (5 yr)	Climatic water balance anomaly (4 yr)	0.10
Topographic wetness index	Precipitation anomaly (1 yr)	0.10
Organic carbon content	Climatic water balance anomaly (0 yr)	0.10
Precipitation anomaly (5 yr)	Precipitation anomaly (2 yr)	0.10
Clay content	Minimum temperature anomaly (2 yr)	0.10
Basal area	Precipitation anomaly (2 yr)	0.10
Available water content	Precipitation anomaly (4 yr)	-0.10
Precipitation anomaly (5 yr)	Climatic water balance anomaly (2 yr)	0.10

First variable	Second variable	Correlation
Maximum temperature anomaly (5 yr)	Minimum temperature anomaly (3 yr)	-0.10
Precipitation anomaly (2 yr)	Precipitation anomaly (1 yr)	-0.10
Precipitation anomaly (5 yr)	Maximum temperature anomaly (4 yr)	0.10
Basal area	Maximum temperature anomaly (1 yr)	-0.10
Precipitation anomaly (5 yr)	Maximum temperature anomaly (2 yr)	-0.10
Elevation	Minimum temperature anomaly (1 yr)	0.09
Basal area	Precipitation anomaly (3 yr)	0.09
Sand content	Precipitation anomaly (2 yr)	0.09
Precipitation anomaly (3 yr)	Precipitation anomaly (1 yr)	0.09
Elevation	Precipitation anomaly (1 yr)	-0.09
Probability of broadleaf	Minimum temperature anomaly (5 yr)	-0.09
Sand content	Minimum temperature anomaly (2 yr)	-0.09
Precipitation anomaly (2 yr)	Minimum temperature anomaly (5 yr)	0.09
Basal area	Minimum temperature anomaly (1 yr)	0.09
Canopy height	Climatic water balance anomaly (2 yr)	-0.08
Basal area	Sand content	-0.08
Maximum temperature anomaly (1 yr)	Climatic water balance anomaly (4 yr)	-0.08
Organic carbon content	Canopy height	-0.08
Precipitation anomaly (3 yr)	Minimum temperature anomaly (2 yr)	-0.08
Topographic wetness index	Precipitation anomaly (2 yr)	0.08
Basal area	Minimum temperature anomaly (4 yr)	0.08
Precipitation anomaly (3 yr)	Maximum temperature anomaly (4 yr)	0.08
Elevation	Precipitation anomaly (4 yr)	0.08
Canopy height	Climatic water balance anomaly (5 yr)	-0.08
Precipitation anomaly (5 yr)	Climatic water balance anomaly (1 yr)	0.08
Topographic wetness index	Climatic water balance anomaly (4 yr)	-0.08
Minimum temperature anomaly (1 yr)	Climatic water balance anomaly (5 yr)	-0.08
Canopy height	Minimum temperature anomaly (0 yr)	0.08
Elevation	Minimum temperature anomaly (5 yr)	0.08
Basal area	Maximum temperature anomaly (4 yr)	-0.08
Maximum temperature anomaly (0 yr)	Minimum temperature anomaly (5 yr)	-0.08
Elevation	Minimum temperature anomaly (0 yr)	-0.07
Precipitation anomaly (1 yr)	Maximum temperature anomaly (4 yr)	0.07
Available water content	Minimum temperature anomaly (5 yr)	-0.07
Precipitation anomaly (5 yr)	Maximum temperature anomaly (3 yr)	0.07
Canopy height	Precipitation anomaly (2 yr)	-0.07
Probability of broadleaf	Precipitation anomaly (5 yr)	0.07
Organic carbon content	Minimum temperature anomaly (2 yr)	0.07
Maximum temperature anomaly (4 yr)	Climatic water balance anomaly (2 yr)	-0.07
Canopy height	Climatic water balance anomaly (4 yr)	-0.07
Minimum temperature anomaly (3 yr)	Climatic water balance anomaly (1 yr)	-0.07
Basal area	Minimum temperature anomaly (5 yr)	0.07
Probability of broadleaf	Minimum temperature anomaly (1 yr)	-0.06
Topographic wetness index	Minimum temperature anomaly (3 yr)	-0.06
Topographic wetness index	Minimum temperature anomaly (0 yr)	0.06
Climatic water balance anomaly (5 yr)	Climatic water balance anomaly (3 yr)	0.06
Organic carbon content	Minimum temperature anomaly (4 yr)	-0.06

First variable	Second variable	Correlation
Precipitation anomaly (4 yr)	Maximum temperature anomaly (0 yr)	0.06
Topographic wetness index	Climatic water balance anomaly (0 yr)	-0.06
Precipitation anomaly (2 yr)	Maximum temperature anomaly (1 yr)	0.06
Probability of broadleaf	Climatic water balance anomaly (4 yr)	-0.06
Precipitation anomaly (0 yr)	Maximum temperature anomaly (4 yr)	-0.06
Organic carbon content	Climatic water balance anomaly (3 yr)	-0.06
Topographic wetness index	Climatic water balance anomaly (1 yr)	0.06
Topographic wetness index	Maximum temperature anomaly (5 yr)	0.06
Probability of broadleaf	Climatic water balance anomaly (1 yr)	-0.06
Maximum temperature anomaly (5 yr)	Climatic water balance anomaly (0 yr)	0.06
Topographic wetness index	Precipitation anomaly (4 yr)	-0.06
Climatic water balance anomaly (5 yr)	Climatic water balance anomaly (1 yr)	0.06
Precipitation anomaly (1 yr)	Minimum temperature anomaly (3 yr)	-0.06
Available water content	Climatic water balance anomaly (3 yr)	-0.06
Basal area	Precipitation anomaly (4 yr)	-0.06
Maximum temperature anomaly (3 yr)	Minimum temperature anomaly (1 yr)	-0.06
Precipitation anomaly (1 yr)	Climatic water balance anomaly (5 yr)	0.06
Maximum temperature anomaly (3 yr)	Climatic water balance anomaly (5 yr)	-0.05
Topographic wetness index	Maximum temperature anomaly (3 yr)	0.05
Canopy height	Minimum temperature anomaly (4 yr)	0.05
Available water content	Precipitation anomaly (5 yr)	0.05
Topographic wetness index	Climatic water balance anomaly (2 yr)	0.05
Clay content	Available water content	-0.05
Maximum temperature anomaly (3 yr)	Minimum temperature anomaly (0 yr)	0.05
Precipitation anomaly (5 yr)	Precipitation anomaly (3 yr)	0.05
Minimum temperature anomaly (5 yr)	Minimum temperature anomaly (2 yr)	-0.05
Minimum temperature anomaly (5 yr)	Minimum temperature anomaly (4 yr)	-0.05
Precipitation anomaly (0 yr)	Minimum temperature anomaly (3 yr)	-0.05
Minimum temperature anomaly (5 yr)	Minimum temperature anomaly (0 yr)	-0.05
Topographic wetness index	Minimum temperature anomaly (2 yr)	-0.05
Maximum temperature anomaly (0 yr)	Minimum temperature anomaly (3 yr)	0.05
Topographic wetness index	Precipitation anomaly (3 yr)	0.05
Topographic wetness index	Clay content	-0.05
Topographic wetness index	Minimum temperature anomaly (1 yr)	-0.05
Elevation	Climatic water balance anomaly (1 yr)	0.04
Precipitation anomaly (0 yr)	Climatic water balance anomaly (4 yr)	-0.04
Available water content	Maximum temperature anomaly (1 yr)	-0.04
Maximum temperature anomaly (4 yr)	Climatic water balance anomaly (3 yr)	-0.04
Topographic wetness index	Sand content	0.04
Topographic wetness index	Maximum temperature anomaly (1 yr)	0.04
Precipitation anomaly (2 yr)	Maximum temperature anomaly (0 yr)	0.04
Canopy height	Precipitation anomaly (4 yr)	-0.04
Topographic wetness index	Maximum temperature anomaly (2 yr)	0.04
Precipitation anomaly (5 yr)	Climatic water balance anomaly (3 yr)	0.04
Canopy height	Precipitation anomaly (5 yr)	-0.04
Available water content	Maximum temperature anomaly (5 yr)	0.04
Canopy height	Minimum temperature anomaly (5 yr)	-0.04

First variable	Second variable	Correlation
Organic carbon content	Climatic water balance anomaly (2 yr)	-0.04
Available water content	Minimum temperature anomaly (3 yr)	0.04
Probability of broadleaf	Topographic wetness index	0.04
Topographic wetness index	Canopy height	0.04
Minimum temperature anomaly (3 yr)	Climatic water balance anomaly (0 yr)	-0.04
Precipitation anomaly (1 yr)	Climatic water balance anomaly (3 yr)	0.03
Maximum temperature anomaly (5 yr)	Minimum temperature anomaly (0 yr)	0.03
Precipitation anomaly (5 yr)	Minimum temperature anomaly (1 yr)	-0.03
Topographic wetness index	Minimum temperature anomaly (4 yr)	0.03
Probability of broadleaf	Minimum temperature anomaly (4 yr)	-0.03
Basal area	Maximum temperature anomaly (5 yr)	-0.03
Basal area	Organic carbon content	0.03
Basal area	Minimum temperature anomaly (0 yr)	0.03
Basal area	Minimum temperature anomaly (3 yr)	-0.03
Canopy height	Minimum temperature anomaly (1 yr)	-0.03
Basal area	Minimum temperature anomaly (2 yr)	-0.03
Canopy height	Climatic water balance anomaly (1 yr)	-0.03
Precipitation anomaly (3 yr)	Climatic water balance anomaly (5 yr)	0.03
Organic carbon content	Climatic water balance anomaly (5 yr)	0.03
Basal area	Climatic water balance anomaly (4 yr)	-0.03
Basal area	Available water content	-0.03
Basal area	Climatic water balance anomaly (0 yr)	0.03
Minimum temperature anomaly (5 yr)	Climatic water balance anomaly (2 yr)	0.03
Sand content	Available water content	-0.03
Probability of broadleaf	Precipitation anomaly (1 yr)	0.03
Organic carbon content	Maximum temperature anomaly (3 yr)	0.02
Organic carbon content	Precipitation anomaly (0 yr)	0.02
Probability of broadleaf	Climatic water balance anomaly (5 yr)	-0.02
Topographic wetness index	Precipitation anomaly (0 yr)	-0.02
Climatic water balance anomaly (4 yr)	Climatic water balance anomaly (0 yr)	-0.02
Maximum temperature anomaly (4 yr)	Minimum temperature anomaly (2 yr)	0.02
Precipitation anomaly (4 yr)	Precipitation anomaly (0 yr)	-0.02
Topographic wetness index	Precipitation anomaly (5 yr)	0.02
Sand content	Minimum temperature anomaly (5 yr)	-0.02
Topographic wetness index	Minimum temperature anomaly (5 yr)	0.02
Maximum temperature anomaly (4 yr)	Climatic water balance anomaly (5 yr)	-0.02
Clay content	Organic carbon content	-0.01
Elevation	Precipitation anomaly (5 yr)	-0.01
Precipitation anomaly (2 yr)	Maximum temperature anomaly (4 yr)	0.01
Precipitation anomaly (4 yr)	Climatic water balance anomaly (0 yr)	-0.01
Precipitation anomaly (4 yr)	Maximum temperature anomaly (1 yr)	-0.01
Maximum temperature anomaly (0 yr)	Climatic water balance anomaly (4 yr)	0.01
Topographic wetness index	Climatic water balance anomaly (3 yr)	0.01
Basal area	Precipitation anomaly (0 yr)	-0.01
Organic carbon content	Maximum temperature anomaly (1 yr)	0.01
Organic carbon content	Precipitation anomaly (5 yr)	-0.01
Topographic wetness index	Climatic water balance anomaly (5 yr)	-0.01

First variable	Second variable	Correlation
Maximum temperature anomaly (0 yr)	Climatic water balance anomaly (2 yr)	-0.01
Maximum temperature anomaly (1 yr)	Climatic water balance anomaly (2 yr)	-0.01
Minimum temperature anomaly (4 yr)	Climatic water balance anomaly (4 yr)	0.01
Maximum temperature anomaly (4 yr)	Climatic water balance anomaly (1 yr)	-0.01
Organic carbon content	Minimum temperature anomaly (0 yr)	0.00
Precipitation anomaly (5 yr)	Maximum temperature anomaly (1 yr)	0.00
Available water content	Precipitation anomaly (3 yr)	0.00
Probability of broadleaf	Minimum temperature anomaly (0 yr)	0.00
Available water content	Climatic water balance anomaly (5 yr)	0.00
Precipitation anomaly (4 yr)	Minimum temperature anomaly (4 yr)	0.00
Maximum temperature anomaly (3 yr)	Climatic water balance anomaly (1 yr)	0.00
Canopy height	Precipitation anomaly (1 yr)	0.00
Probability of broadleaf	Precipitation anomaly (4 yr)	0.00
Clay content	Minimum temperature anomaly (5 yr)	0.00
Elevation	Minimum temperature anomaly (4 yr)	0.00

5.8. Variogram analysis of the standing deadwood in the Swiss forest reserves aggregated at 10 m

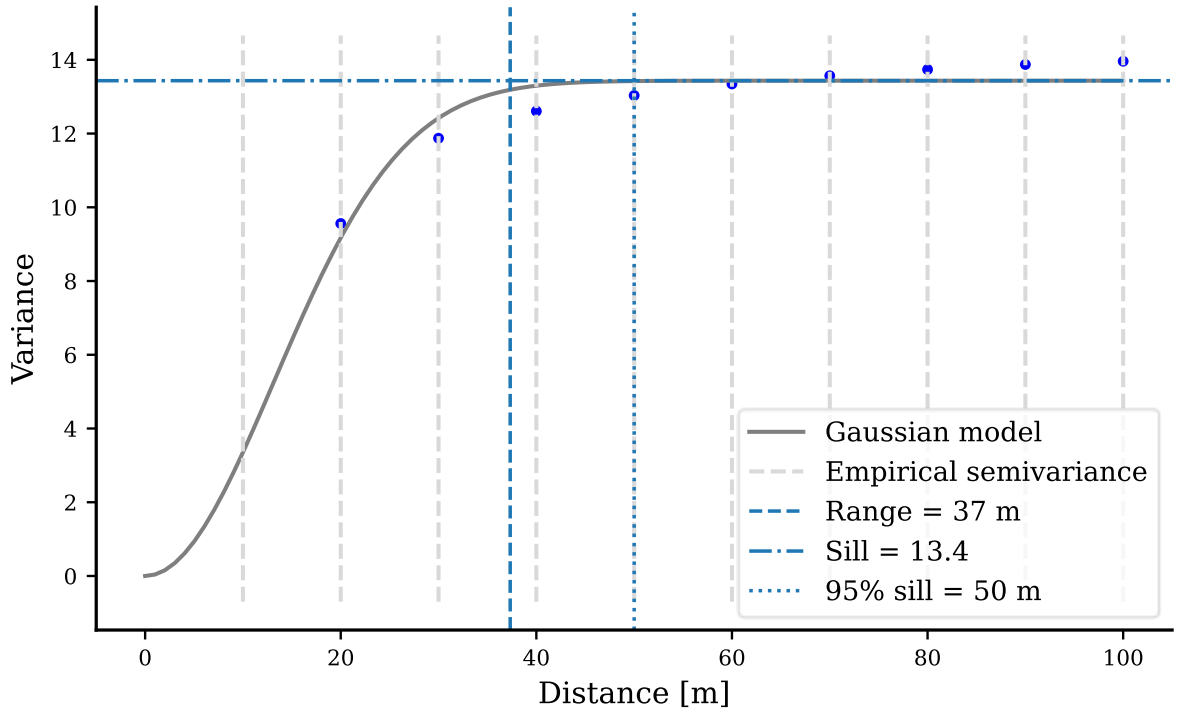

Figure S7: Variogram of standing deadwood aggregated at 10 m with the fitted gaussian model (solid line). Dots represent the empirical variance estimate; the sill, range, and 95% sill threshold (50 m) are marked.

5.9. Distribution of sampled standing deadwood pixels and corresponding environmental predictor values in the Swiss forest reserves used for the random forest models, aggregated at 10 m resolution.

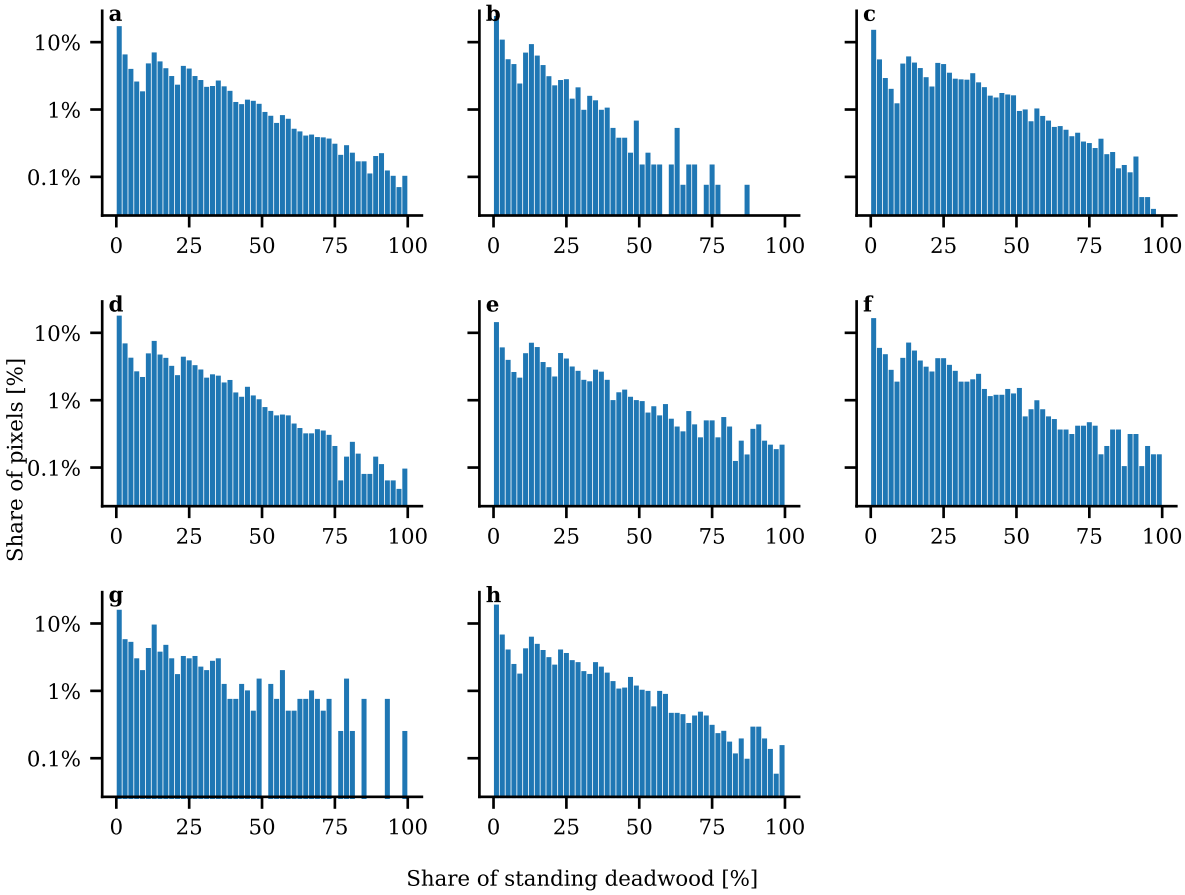

Figure S8: Distribution of standing deadwood pixels sampled from the forest reserves and used as response variable in the random forest models. Data are aggregated at 10 m spatial resolution. **a** Full dataset (2018–2023); **b–h** Individual ecoregions: **b** Continental Alps, **c** Jura, **d** Northern Pre-Alps, **e** Northern Intermediate Alps, **f** Southern Pre-Alps, **g** Southern Intermediate Alps, and **h** Swiss Central Plateau.

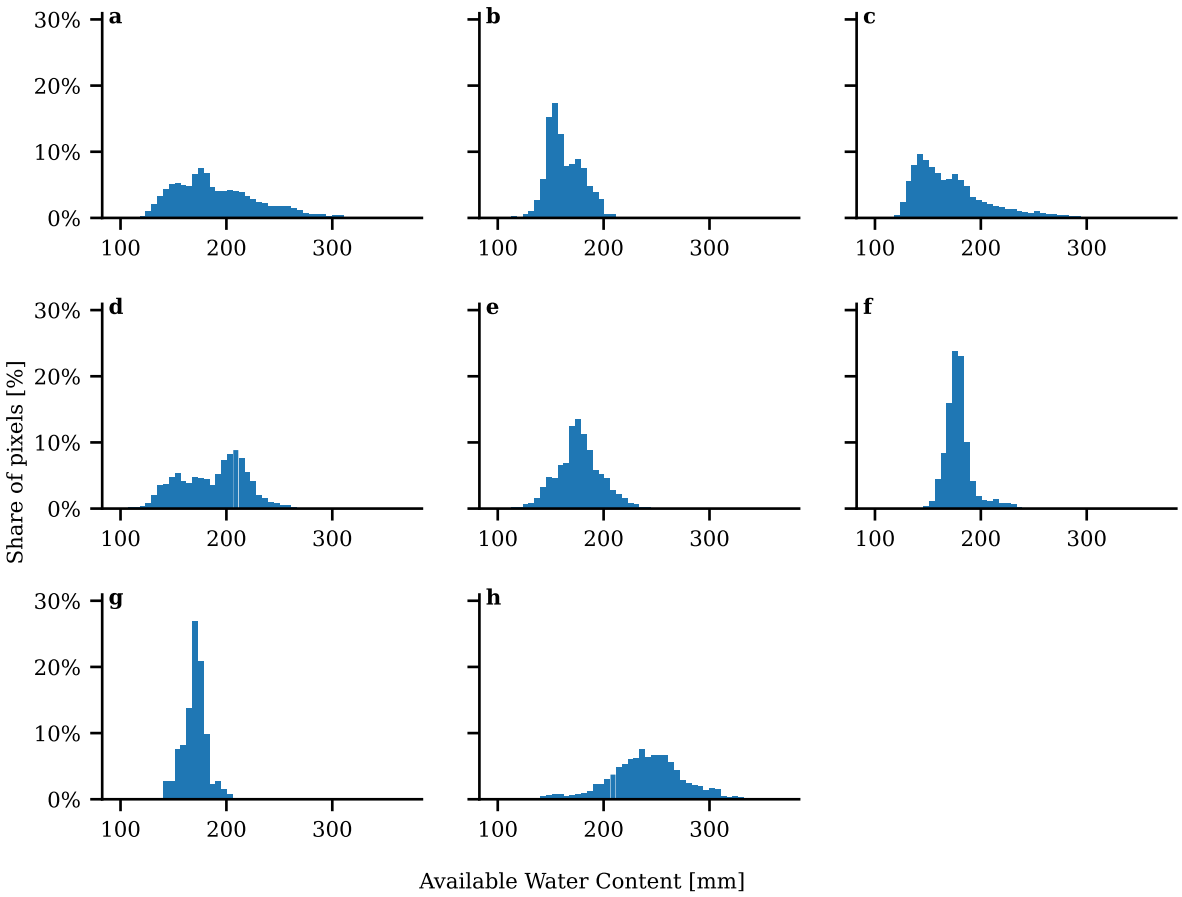

Figure S9: Distribution of Available Water Content pixels sampled from the forest reserves and used as predictor variable in the random forest models. Data are aggregated at 10 m spatial resolution. **a** Full dataset (2018–2023); **b–h** Individual ecoregions: **b** Continental Alps, **c** Jura, **d** Northern Pre-Alps, **e** Northern Intermediate Alps, **f** Southern Pre-Alps, **g** Southern Intermediate Alps, and **h** Swiss Central Plateau.

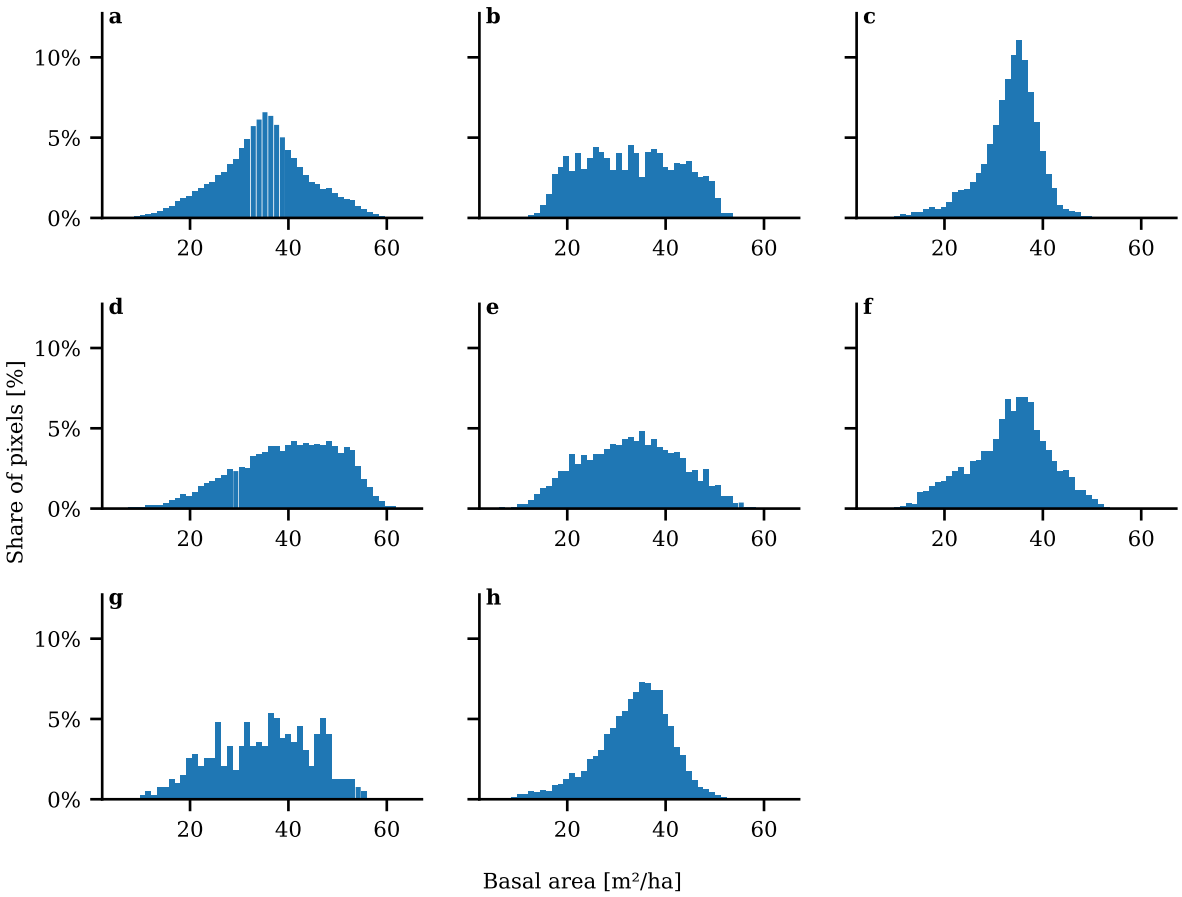

Figure S10: Distribution of basal area pixels sampled from the forest reserves and used as predictor variable in the random forest models. Data are aggregated at 10 m spatial resolution. **a** Full dataset (2018–2023); **b–h** Individual ecoregions: **b** Continental Alps, **c** Jura, **d** Northern Pre-Alps, **e** Northern Intermediate Alps, **f** Southern Pre-Alps, **g** Southern Intermediate Alps, and **h** Swiss Central Plateau.

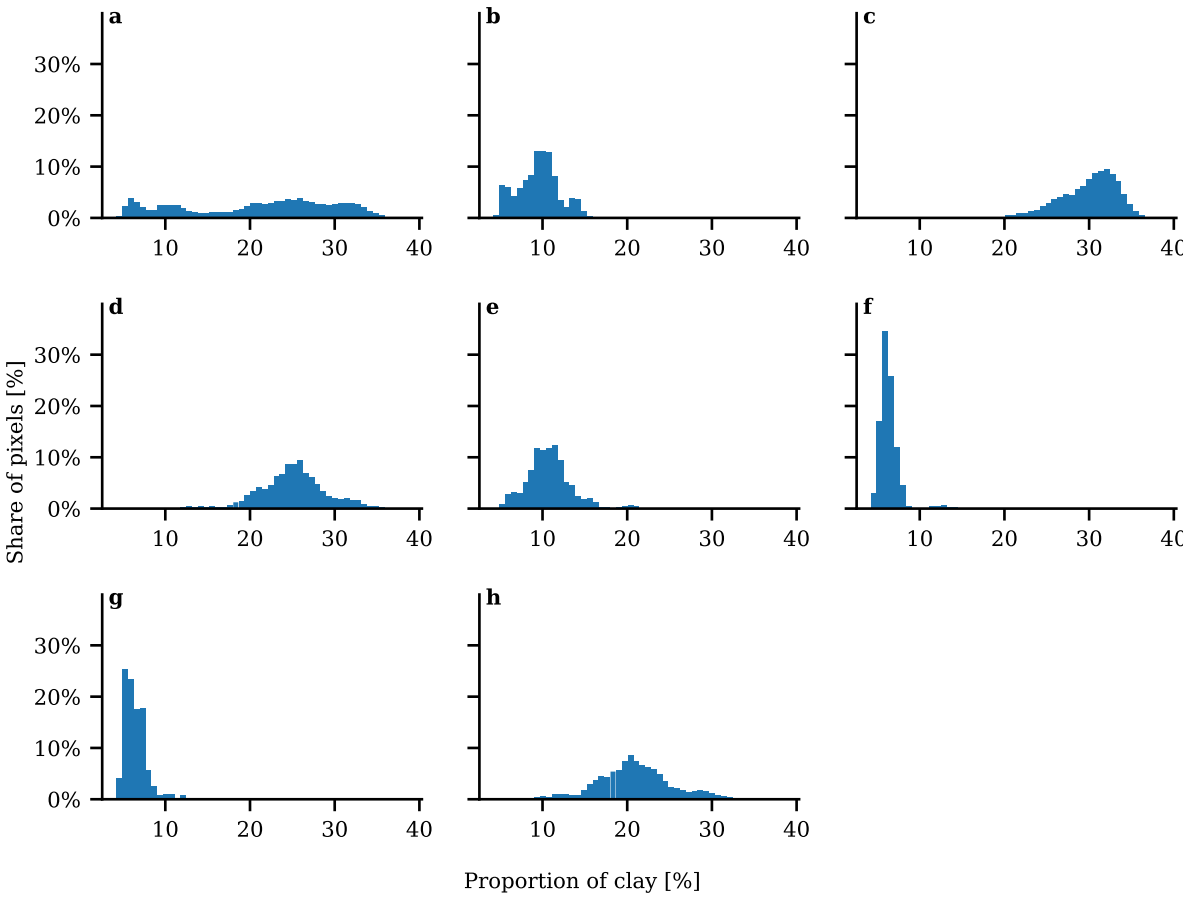

Figure S11: Distribution of clay content pixels sampled from the forest reserves and used as predictor variable in the random forest models. Data are aggregated at 10 m spatial resolution. **a** Full dataset (2018–2023); **b–h** Individual ecoregions: **b** Continental Alps, **c** Jura, **d** Northern Pre-Alps, **e** Northern Intermediate Alps, **f** Southern Pre-Alps, **g** Southern Intermediate Alps, and **h** Swiss Central Plateau.

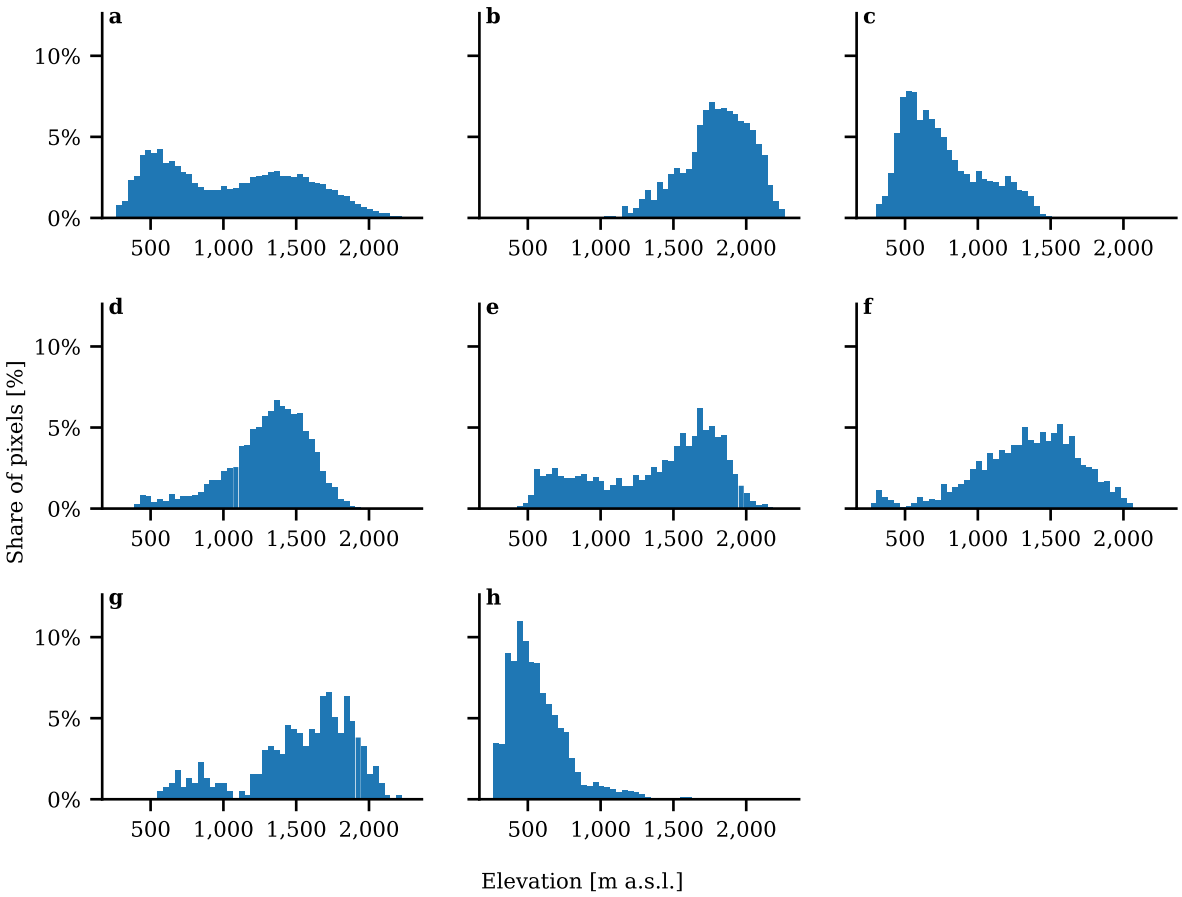

Figure S12: Distribution of elevation pixels sampled from the forest reserves and used as predictor variable in the random forest models. Data are aggregated at 10 m spatial resolution. **a** Full dataset (2018–2023); **b–h** Individual ecoregions: **b** Continental Alps, **c** Jura, **d** Northern Pre-Alps, **e** Northern Intermediate Alps, **f** Southern Pre-Alps, **g** Southern Intermediate Alps, and **h** Swiss Central Plateau.

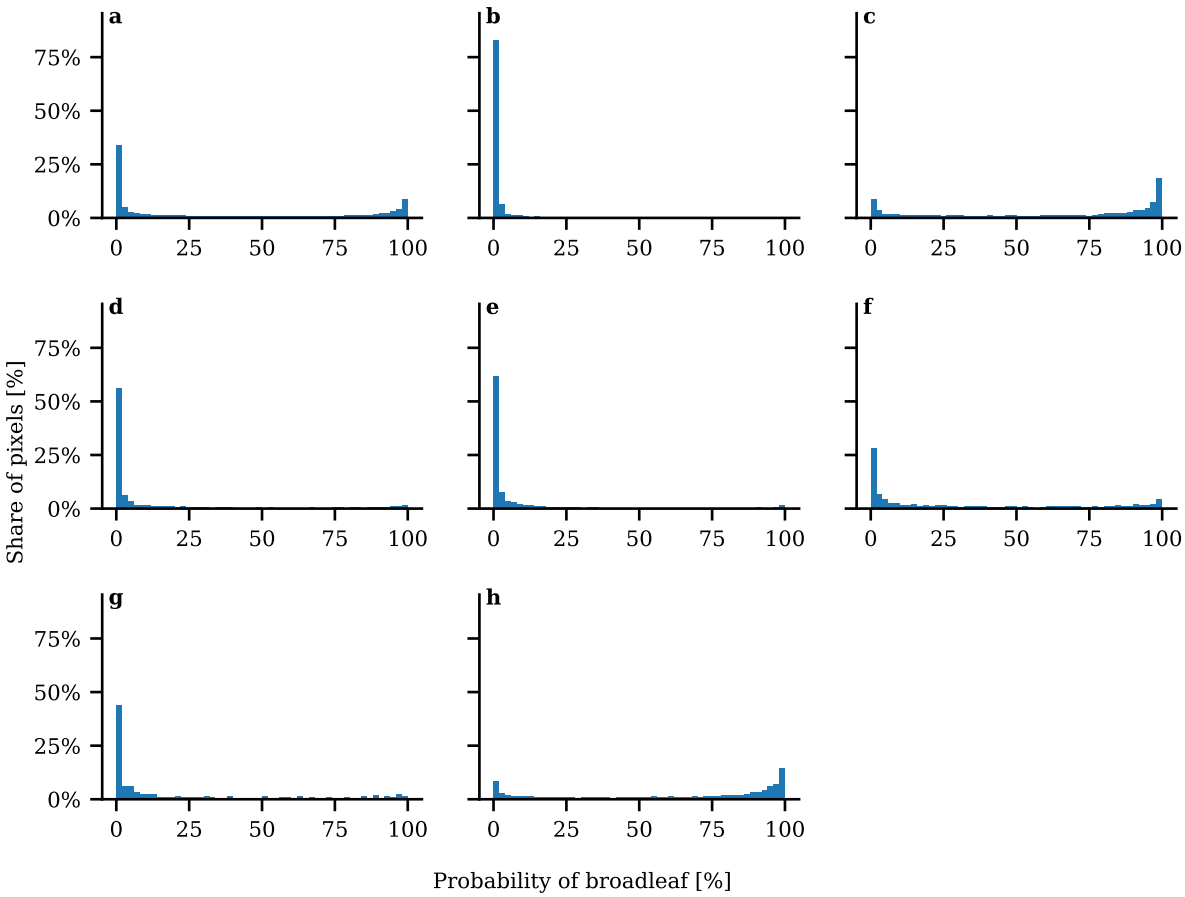

Figure S13: Distribution of Probability of broadleaf pixels sampled from the forest reserves and used as predictor variable in the random forest models. The value represents the probability of broadleaf forest, expressed as a percentage. Data are aggregated at 10 m spatial resolution. **a** Full dataset (2018–2023); **b–h** Individual ecoregions: **b** Continental Alps, **c** Jura, **d** Northern Pre-Alps, **e** Northern Intermediate Alps, **f** Southern Pre-Alps, **g** Southern Intermediate Alps, and **h** Swiss Central Plateau.

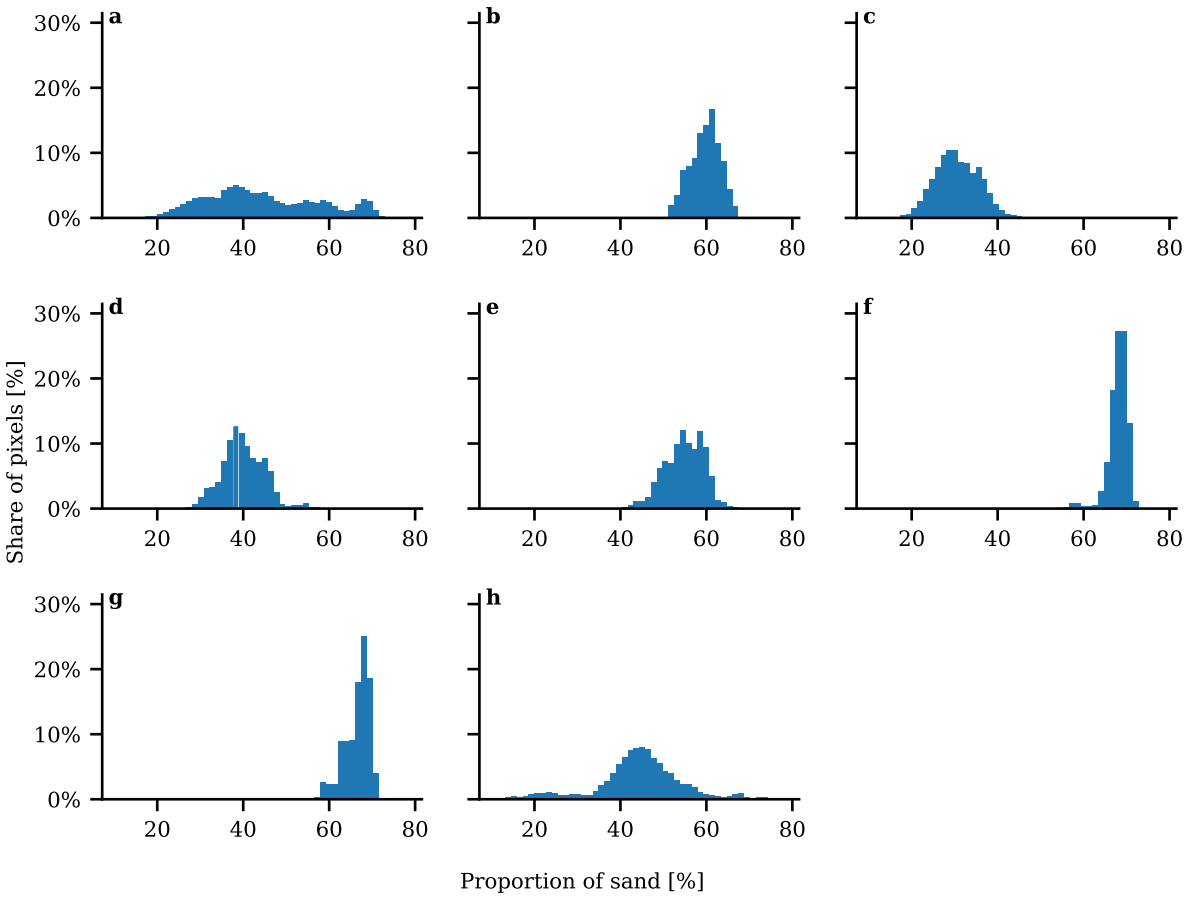

Figure S14: Distribution of sand content pixels sampled from the forest reserves and used as predictor variable in the random forest models. Data are aggregated at 10 m spatial resolution. **a** Full dataset (2018–2023); **b–h** Individual ecoregions: **b** Continental Alps, **c** Jura, **d** Northern Pre-Alps, **e** Northern Intermediate Alps, **f** Southern Pre-Alps, **g** Southern Intermediate Alps, and **h** Swiss Central Plateau.

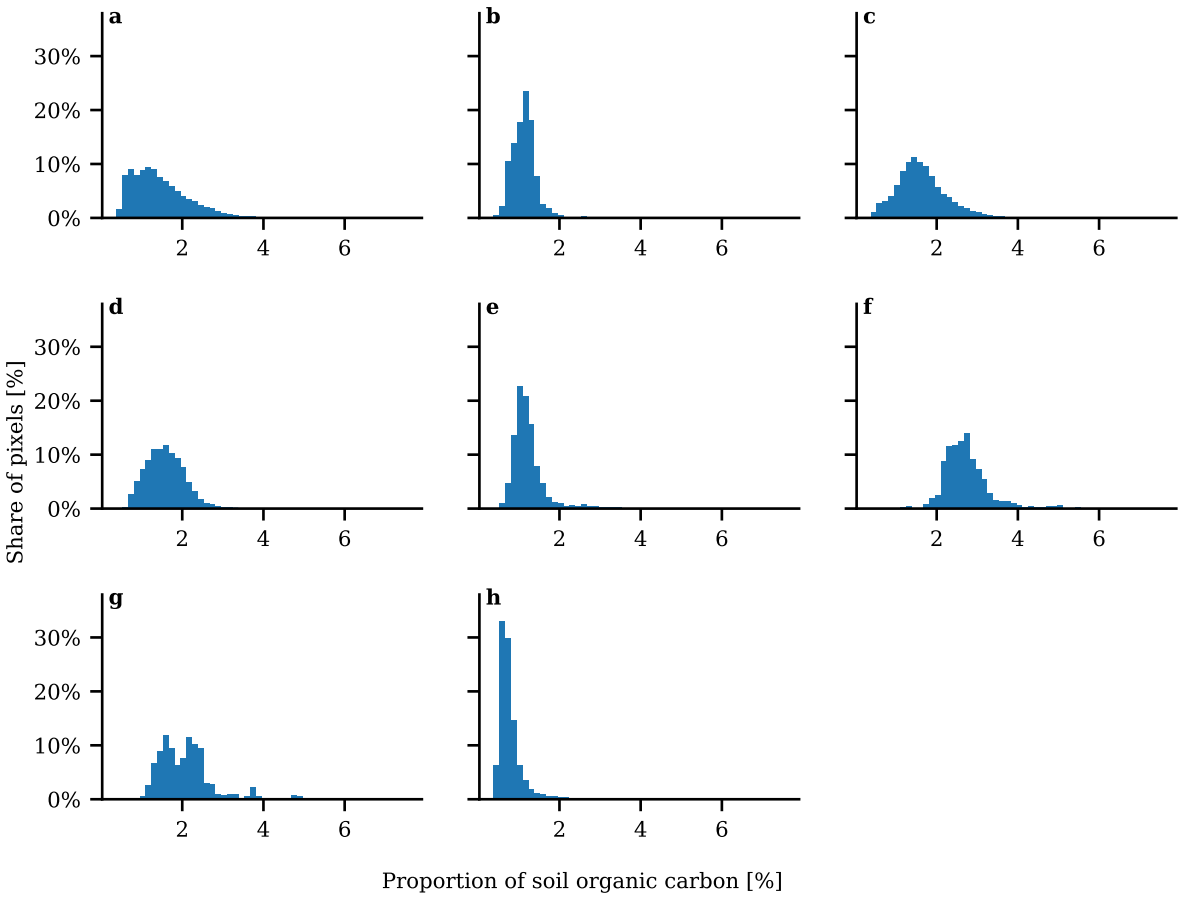

Figure S15: Distribution of soil organic carbon content pixels sampled from the forest reserves and used as predictor variable in the random forest models. Data are aggregated at 10 m spatial resolution. **a** Full dataset (2018–2023); **b–h** Individual ecoregions: **b** Continental Alps, **c** Jura, **d** Northern Pre-Alps, **e** Northern Intermediate Alps, **f** Southern Pre-Alps, **g** Southern Intermediate Alps, and **h** Swiss Central Plateau.

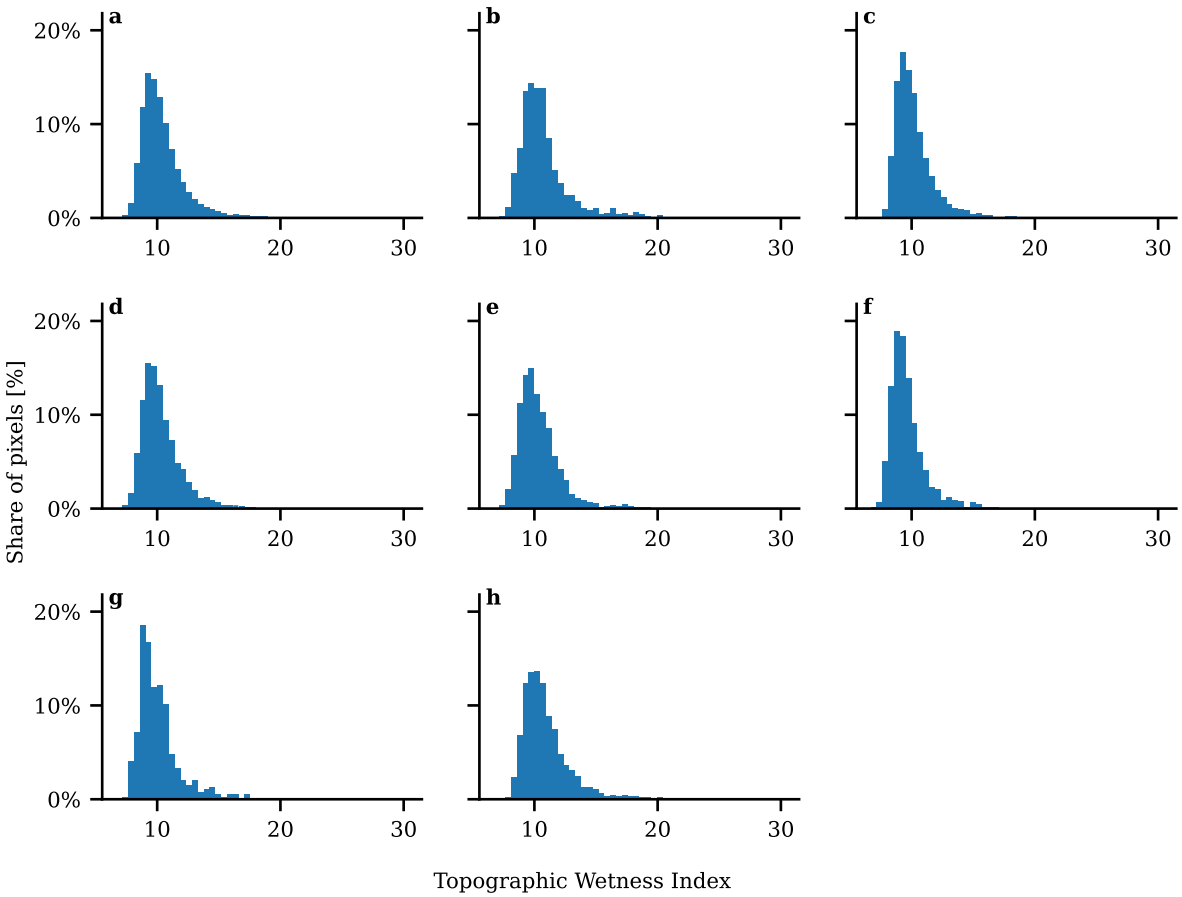

Figure S16: Distribution of Topographic Wetness Index pixels sampled from the forest reserves and used as predictor variable in the random forest models. Data are aggregated at 10 m spatial resolution. **a** Full dataset (2018–2023); **b–h** Individual ecoregions: **b** Continental Alps, **c** Jura, **d** Northern Pre-Alps, **e** Northern Intermediate Alps, **f** Southern Pre-Alps, **g** Southern Intermediate Alps, and **h** Swiss Central Plateau.

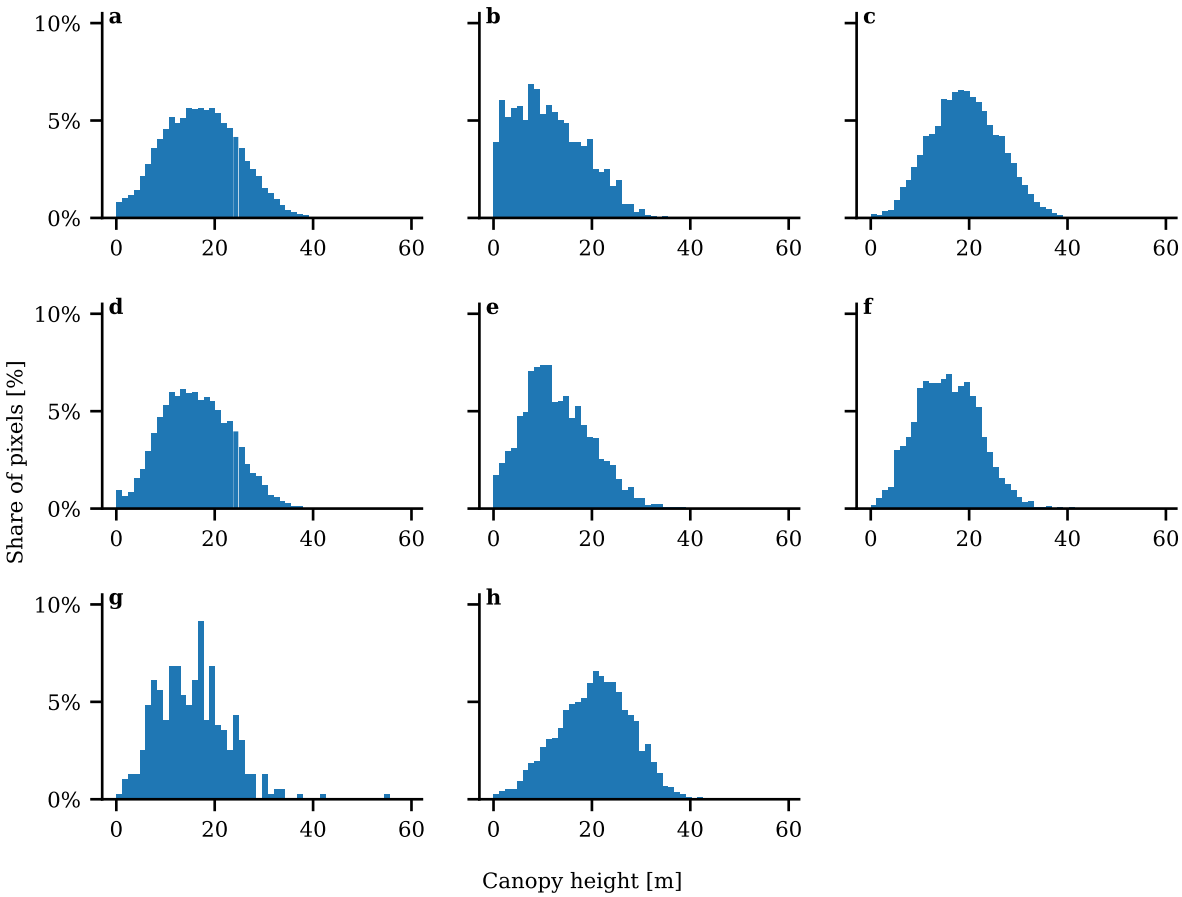

Figure S17: Distribution of canopy height pixels sampled from the forest reserves and used as predictor variable in the random forest models. Data are aggregated at 10 m spatial resolution. **a** Full dataset (2018–2023); **b–h** Individual ecoregions: **b** Continental Alps, **c** Jura, **d** Northern Pre-Alps, **e** Northern Intermediate Alps, **f** Southern Pre-Alps, **g** Southern Intermediate Alps, and **h** Swiss Central Plateau.

5.10. Aerial imagery, standing deadwood extent and share of standing deadwood

Table S6: Deadwood and forest extent per ecoregion. Deadwood corresponds to the cumulative mapped extent, as each ecoregion is represented by the most recent year of available imagery as in Figure 2 in the main manuscript.

Ecoregion	Deadwood extent [ha]	Leaf-on forest area [ha]	Share of deadwood [%]
Continental Alps	107.08	54,458.54	0.20%
Jura	1,388.90	167,583.36	0.83%
Northern Intermediate Alps	591.76	109,394.81	0.54%
Northern Pre-Alps	1,047.76	242,527.95	0.43%
Southern Intermediate Alps	162.22	37,844.83	0.43%
Southern Pre-Alps	303.06	96,854.80	0.31%
Swiss Central Plateau	833.16	231,466.66	0.36%
Total	4433.94	940130.95	0.47%

Table S7: Yearly forest area per ecoregion, forest area included in the leaf on aerial orthophotos at 10 cm, standing deadwood extent and share of standing deadwood.

Ecoregion	Total forest area [ha]	Leaf on forest area [ha]	Share of leaf on forest area[%]	Deadwood extent [ha]	Share of deadwood [%]
		2018			
Continental Alps	54458.5	108.9	0.2	0.26	0.24
Jura	173230.6	25274.6	14.6	54.41	0.22
Northern Intermediate Alps	109466.9	2324.3	2.1	4.54	0.2
Northern Pre-Alps	247377.9	111464.8	45.1	264.19	0.24
Southern Intermediate Alps	37844.8	23012.2	60.8	99.79	0.43
Southern Pre-Alps	96854.8	84682.5	87.4	237.04	0.28
Swiss Central Plateau	267539.7	57593.0	21.5	91.32	0.16
		2019			
Continental Alps	54458.5	31544.4	57.9	50.25	0.16
Northern Intermediate Alps	109466.9	58412.5	53.4	235.63	0.4
Northern Pre-Alps	247377.9	76572.9	31.0	311.55	0.41
Southern Intermediate Alps	37844.8	14832.7	39.2	47.53	0.32
Southern Pre-Alps	96854.8	11729.8	12.1	41.13	0.35
Swiss Central Plateau	267539.7	20251.4	7.6	116.57	0.58
		2020			
Continental Alps	54458.5	22805.2	41.9	50.51	0.22
Jura	173230.6	34648.8	20.0	391.13	1.13
Northern Intermediate Alps	109466.9	48658.1	44.5	331.92	0.68
Northern Pre-Alps	247377.9	34774.8	14.1	143.34	0.41
Southern Pre-Alps	96854.8	442.5	0.5	0.75	0.17
Swiss Central Plateau	267539.7	1650.7	0.6	18.2	1.1
		2021			
Continental Alps	54458.5	108.9	0.2	0.26	0.24
Jura	173230.6	63798.4	36.8	445.45	0.7
Northern Intermediate Alps	109466.9	2323.7	2.1	7.46	0.32

Ecoregion	Total forest area [ha]	Leaf on forest area [ha]	Share of leaf on forest area[%]	Deadwood extent [ha]	Share of deadwood [%]
Northern Pre-Alps	247377.9	105299.0	42.6	395.73	0.38
Southern Intermediate Alps	37844.8	23012.2	60.8	105.06	0.46
Southern Pre-Alps	96854.8	51037.5	52.7	128.47	0.25
Swiss Central Plateau	267539.7	65226.6	24.4	215.46	0.33
		2022			
Continental Alps	54458.5	31544.4	57.9	45.15	0.14
Jura	173230.6	8024.5	4.6	35.01	0.44
Northern Intermediate Alps	109466.9	53279.5	48.7	199.32	0.37
Northern Pre-Alps	247377.9	57361.9	23.2	269.95	0.47
Southern Intermediate Alps	37844.8	14832.7	39.2	57.16	0.39
Southern Pre-Alps	96854.8	11729.8	12.1	46.85	0.4
Swiss Central Plateau	267539.7	54854.9	20.5	281.63	0.51
		2023			
Continental Alps	54458.5	22745.0	41.8	61.59	0.27
Jura	173230.6	53873.9	31.1	554.51	1.03
Northern Intermediate Alps	109466.9	26230.6	24.0	133.89	0.51
Northern Pre-Alps	247377.9	49372.6	20.0	279.06	0.57
Southern Pre-Alps	96854.8	442.5	0.5	1.32	0.3
Swiss Central Plateau	267539.7	50781.7	19.0	282.79	0.56

Table S8: Yearly forest area per Swiss Canton, forest area included in the leaf on aerial orthophotos at 10 cm, standing deadwood extent and share of standing deadwood.

Cantons	Total forest area [ha]	Leaf on forest area [ha]	Leaf on [%]	Deadwood extent [ha]	Share of deadwood [%]
		2018			
Ticino	108424.7	107761.9	99.4	336.84	0.31
Aargau	45647.2	43261.3	94.8	74.7	0.17
Obwalden	14049.5	14049.5	100.0	42.56	0.3
Basel-Landschaft	19140.0	222.0	1.2	0.68	0.3
Valais	82038.4	1.2	0.0	0	0.08
Luzern	37030.0	35857.8	96.8	69.97	0.2
Nidwalden	7142.8	7132.7	99.9	11.97	0.17
Uri	12986.9	12630.1	97.3	26.02	0.21
Solothurn	30558.9	556.3	1.8	1.14	0.21
Bern	144407.7	82944.4	57.4	187.42	0.23
		2019			
Ticino	108424.7	662.8	0.6	2.62	0.4
Zürich	48076.2	1952.6	4.1	18.23	0.93
Zug	5894.3	4549.0	77.2	20.47	0.45
Aargau	45647.2	31.1	0.1	0.13	0.4
Glarus	14521.0	14521.0	100.0	44.03	0.3
Appenzell Ausserrhoden	6868.2	4687.1	68.2	22.55	0.48
Schwyz	22006.3	21243.6	96.5	98.57	0.46
Luzern	37030.0	665.1	1.8	2.68	0.4
Nidwalden	7142.8	10.1	0.1	0.01	0.14
Thurgau	19732.5	343.8	1.7	1.74	0.51
Graubünden	120965.8	120224.3	99.4	385.39	0.32

Cantons	Total forest area [ha]	Leaf on forest area [ha]	Leaf on [%]	Deadwood extent [ha]	Share of deadwood [%]
Uri	12986.9	356.7	2.7	0.7	0.2
St Gallen	48917.1	38919.2	79.6	185.7	0.48
Appenzell Innerrhoden	4169.2	3611.1	86.6	15.95	0.44
		2020			
Fribourg	35610.6	9265.0	26.0	39.69	0.43
Basel-Landschaft	19140.0	13.0	0.1	0.12	0.92
Valais	82038.4	81822.9	99.7	430.01	0.53
Jura	31774.2	29407.9	92.6	353.74	1.2
Vaud	80870.9	20852.5	25.8	100.26	0.48
Neuchâtel	25930.8	331.8	1.3	5.46	1.65
Bern	144407.7	1287.0	0.9	6.53	0.51
		2021			
Ticino	108424.7	73578.0	67.9	231.5	0.31
Basel-Stadt	515.9	515.9	100.0	2.85	0.55
Aargau	45647.2	125.6	0.3	0.85	0.67
Fribourg	35610.6	724.7	2.0	3.33	0.46
Obwalden	14049.5	12353.3	87.9	51.21	0.41
Basel-Landschaft	19140.0	17195.8	89.8	115.64	0.67
Schwyz	22006.3	218.5	1.0	0.57	0.26
Valais	82038.4	1.2	0.0	0	0.11
Luzern	37030.0	16608.1	44.9	136.81	0.82
Jura	31774.2	3305.8	10.4	38.81	1.17
Nidwalden	7142.8	5563.3	77.9	19.23	0.35
Vaud	80870.9	321.2	0.4	1.09	0.34
Graubünden	120965.8	588.1	0.5	2.3	0.39
Uri	12986.9	9370.2	72.2	30.42	0.32
Solothurn	30558.9	27439.2	89.8	152.23	0.55
Neuchâtel	25930.8	31.5	0.1	0.25	0.78

Cantons	Total forest area [ha]	Leaf on forest area [ha]	Leaf on [%]	Deadwood extent [ha]	Share of deadwood [%]
Bern	144407.7	142872.9	98.9	510.83	0.36
		2022			
Ticino	108424.7	662.8	0.6	2.85	0.43
Zürich	48076.2	44152.8	91.8	197.9	0.45
Zug	5894.3	5846.1	99.2	17.37	0.3
Aargau	45647.2	174.0	0.4	0.62	0.36
Fribourg	35610.6	49.7	0.1	0.34	0.69
Glarus	14521.0	14442.0	99.5	52.22	0.36
Schaffhausen	12012.3	11980.5	99.7	94.34	0.79
Schwyz	22006.3	21851.5	99.3	89.38	0.41
Luzern	37030.0	306.8	0.8	1.77	0.58
Nidwalden	7142.8	10.1	0.1	0.04	0.41
Graubünden	120965.8	114883.0	95.0	373.76	0.33
Uri	12986.9	552.8	4.3	2.52	0.46
St Gallen	48917.1	14353.3	29.3	91.35	0.64
Appenzell Innerrhoden	4169.2	476.9	11.4	2.79	0.59
Bern	144407.7	749.4	0.5	2.89	0.39
		2023			
Genève	3315.4	3315.4	100.0	17.03	0.51
Fribourg	35610.6	35610.6	100.0	180.25	0.51
Valais	82038.4	55448.5	67.6	231.28	0.42
Vaud	80870.9	79962.9	98.9	692.76	0.87
Neuchâtel	25930.8	25904.8	99.9	178.23	0.69
Bern	144407.7	3206.5	2.2	13.58	0.42

Table S9: Yearly standing deadwood across Switzerland based on the extent of aerial images from the Figure S1. * Share of deadwood [%] = deadwood extent / leaf-on forest area × 100.

Year	Total forest area [ha]	Leaf-on forest area [ha]	Share of leaf-on forest [%]	Deadwood extent [ha]	Share of deadwood [%]*	Deadwood per 1000 ha leaf-on forest
2018	986,773.27	304,460.14	30.85%	751.55	0.25	17.59
2019	813,542.62	213,343.61	26.22%	802.66	0.38	22.16
2020	948,928.44	142,980.02	15.07%	935.85	0.65	37.17
2021	986,773.27	310,806.23	31.50%	1297.89	0.42	26.72
2022	986,773.27	231,627.63	23.47%	935.07	0.40	27.22
2023	948,928.44	203,446.31	21.44%	1313.16	0.65	32.31

Table S10: Standing deadwood and forest areas mapped in paired survey years for the 2018–2021, 2019–2022, and 2020–2023 acquisition cycles for the overlapping forest areas and for forest reserves.

Survey	**Surveyed years**	**Total deadwood area [ha]**	**Total forest area [ha]**	**Total share of deadwood [%]**	**Deadwood area, forest reserves [ha]**	**Forest area, forest reserved**	**Share of deadwood, forest reserves [%]**
1st survey	2018-2021	513.96	199639.64	0.26%	43.58	12147.23	0.36%
2nd survey	2018-2021	733.19	199639.64	0.37%	61.12	12147.23	0.50%
1st survey	2019-2022	590.44	172677.15	0.34%	70.06	17798.17	0.39%
2nd survey	2019-2022	628.91	172677.15	0.36%	87.18	17798.17	0.49%
1st survey	2020-2023	346.88	86500.12	0.40%	20.88	3340.37	0.63%
2nd survey	2020-2023	452.48	86500.12	0.52%	21.25	3340.37	0.64%

5.11. Elevation dependence of standing deadwood and forest area

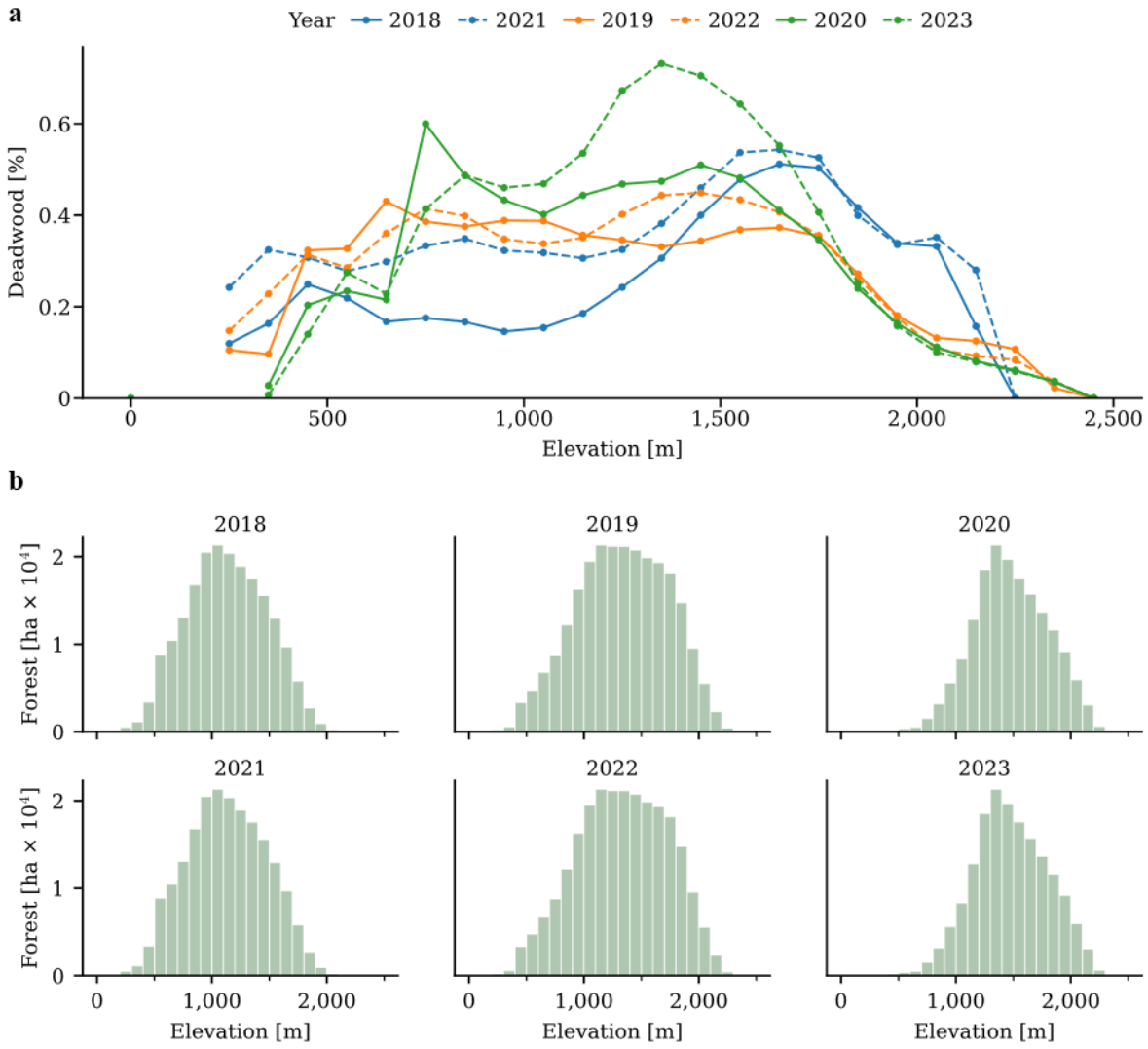

Figure S18: Elevation dependence of standing deadwood and forest area in the overlap regions across repeated surveys (2018 – 2021, 2019 – 2022, and 2020 – 2023) according to their distribution from **Error! Reference source not found.**e. **a** Yearly standing deadwood shares p er elevation class, and **b** yearly distribution of forest area across the elevation classes.

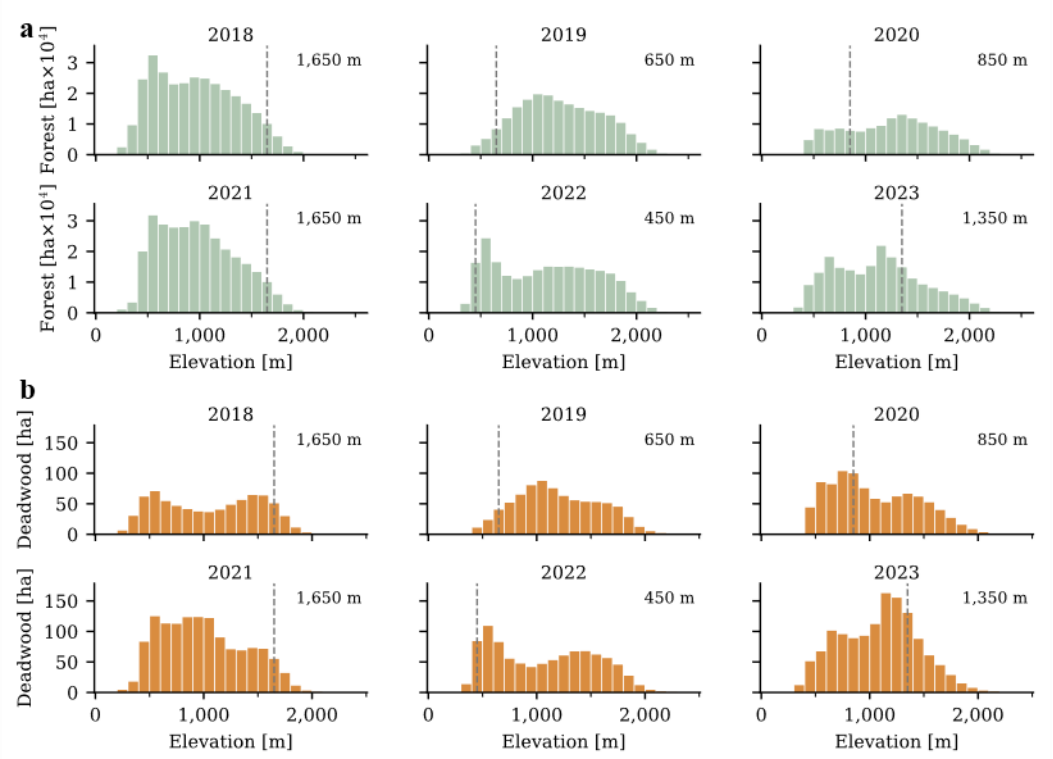

Figure S19: Deadwood and forest area distributions along the elevation gradient (2018–2023) according to their distribution given **Error! Reference source not found.**b,c. **a** Yearly d istribution of forest area across the elevation classes. **b** yearly distribution of deadwood area across the elevation classes. Peak elevations (maximum deadwood share) are highlighted by dashed vertical lines.

5.12. Random forest models performance and hyperparameters

Table S11: Performance metrics of the random forest regression models for standing deadwood predictions aggregated at 10 m. The number of trees and the minimum sample leaf parameters have been set through a 5-fold cross validated grid search.

Ecoregion	R^2 train	RMSE train	R^2 test	RMSE test	Test sample size	Trees	Min sample leaf
Full dataset	0.52	13.76	0.17	17.60	4,823	1,000	10
Northern intermediate Alps	0.52	14.65	0.21	18.81	640	300	10
Swiss Central Plateau	0.54	13.89	0.18	18.52	1,020	1,000	10
Southern Pre-Alps	0.50	14.71	0.17	19.01	382	1,000	10
Jura	0.53	13.38	0.16	17.89	1,198	300	10
Continental Alps	0.47	9.69	0.15	12.58	263	300	10
Northern Pre-Alps	0.46	13.38	0.08	18.67	1,242	1,000	10
Southern intermediate Alps	0.49	15.15	0.04	24.12	79	1,000	10

5.13. Standing deadwood drivers results: permutation importance and SHAP values

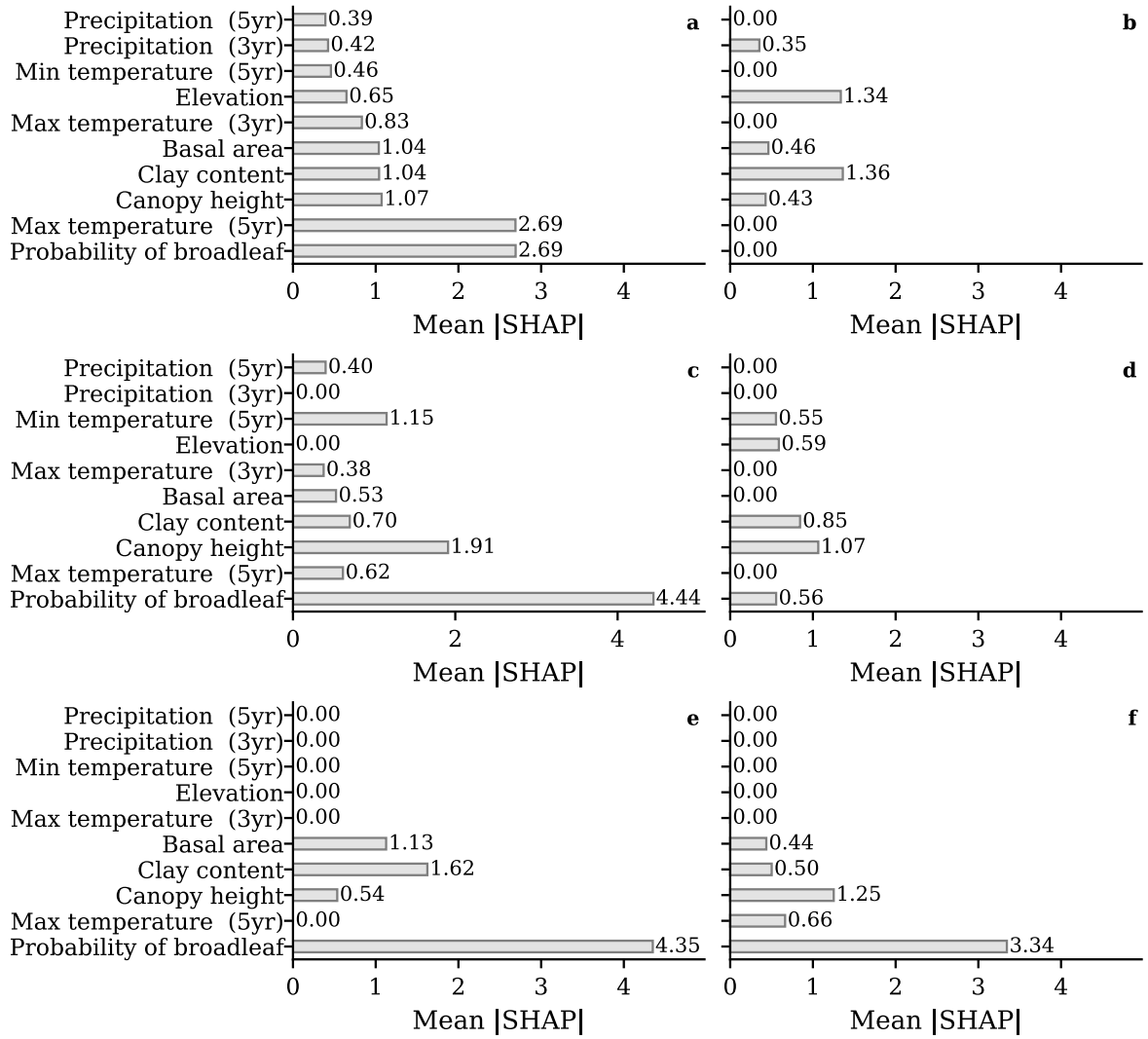

Figure S20: Absolute mean SHAP values of the ten most relevant variables from the random forest model fitted on the full dataset, and corresponding values in the ecoregion-specific models. **a** full dataset, **b** Continental Alps, **c** Jura, **d** Northern Intermediate Alps, **e** Southern Pre-Alps, **f** Swiss Central Plateau. Variables are in descending order according to the mean absolute SHAP value on the model fitted on the full dataset. SHAP values have been calculated on the entire test set of each model.

Table S12: Mean SHAP values from the fitted random forest models. Each value represents the variable's contribution to model predictions, where positive values indicate an increase and negative values a decrease in predicted standing deadwood.

Variable name	Full dataset	Continental Alps	Jura	Northern Intermediate Alps	Southern Pre-Alps	Swiss Central Plateau
Available water content	0.06	0.06	0.02	0.11	0.11	-0.02
Basal area	0.03	-0.06	0.06	-0.02	0.02	-0.02
Elevation	0.07	0.05	0.03	0.04	0.04	-0.03
Probability of broadleaf	0.03	0.00	-0.19	0.06	-0.17	-0.15
Topographic wetness index	-0.02	0.00	0.02	0.03	0.01	0.02
Canopy height	-0.11	0.00	-0.03	0.02	0.01	-0.01
Clay content	-0.24	0.01	-0.03	-0.19	0.13	0.05
Climatic water balance anomaly (1 yr)	0.06	0.01	0.03	0.02	0.03	-0.01
Precipitation anomaly (0 yr)	0.07	0.06	0.02	-0.13	0.01	0.05
Precipitation anomaly (2 yr)	-0.01	0.05	0.03	0.02	-0.11	-0.04
Precipitation anomaly (3 yr)	0.03	0.17	0.03	0.11	0.03	-0.01
Precipitation anomaly (4 yr)	0.07	-0.02	0.06	-0.26	-0.01	0.02
Precipitation anomaly (5 yr)	-0.05	-0.05	0.02	-0.08	0.01	0.01
Organic carbon content	0.01	0.02	0.03	0.12	-0.02	0.06
Maximum temperature anomaly (0 yr)	0.04	0.01	0.01	0.07	-0.11	0.16
Maximum temperature anomaly (1 yr)	0.00	0.01	0.02	0.01	0.12	0.01
Maximum temperature anomaly (2 yr)	0.07	-0.01	0.02	0.00	0.11	0.09
Maximum temperature anomaly (3 yr)	-0.04	0.00	0.01	-0.02	0.09	0.07
Maximum temperature anomaly (4 yr)	0.04	0.00	0.00	0.01	0.01	-0.02
Maximum temperature anomaly (5 yr)	-0.29	0.00	-0.01	-0.07	0.03	-0.10
Minimum temperature anomaly (0 yr)	0.05	0.04	0.04	-0.07	0.03	-0.03
Minimum temperature anomaly (1 yr)	0.04	-0.02	0.03	0.01	0.00	0.08
Minimum temperature anomaly (2 yr)	-0.04	-0.12	0.02	-0.10	0.01	0.00
Minimum temperature anomaly (3 yr)	0.02	0.03	0.03	0.01	0.05	-0.06
Minimum temperature anomaly (4 yr)	0.03	-0.01	0.00	0.02	0.05	0.06
Minimum temperature anomaly (5 yr)	0.22	0.04	-0.09	-0.05	0.05	0.02

Table S 13: Mean absolute SHAP values from the fitted random forest models. Each value represents the variable's contribution to model predictions.

Variable name	Full dataset	Continental Alps	Jura	Northern Intermediate Alps	Southern Pre-Alps	Swiss Central Plateau
Available water content	0.28	0.39	0.37	0.44	0.58	0.38
Basal area	1.04	0.46	0.53	0.44	1.13	0.44
Elevation	0.65	1.34	0.21	0.59	0.35	0.39
Probability of broadleaf	2.69	0.22	4.44	0.56	4.35	3.34
Topographic wetness index	0.31	0.32	0.21	0.69	0.50	0.19
Canopy height	1.07	0.43	1.91	1.07	0.54	1.25
Clay content	1.04	1.36	0.70	0.85	1.62	0.50
Climatic water balance anomaly (1 yr)	0.23	0.46	0.18	0.33	0.71	0.17
Precipitation anomaly (0 yr)	0.24	0.30	0.14	1.94	0.15	0.20
Precipitation anomaly (2 yr)	0.30	0.22	0.17	0.53	0.90	0.41
Precipitation anomaly (3 yr)	0.42	0.35	0.16	0.47	0.15	0.23
Precipitation anomaly (4 yr)	0.26	0.10	0.19	3.09	0.32	0.31
Precipitation anomaly (5 yr)	0.39	0.24	0.40	0.49	0.22	0.28
Organic carbon content	0.22	0.25	0.23	0.55	0.24	0.27
Maximum temperature anomaly (0 yr)	0.17	0.05	0.26	0.09	0.44	0.65
Maximum temperature anomaly (1 yr)	0.23	0.07	0.26	0.16	0.40	0.31
Maximum temperature anomaly (2 yr)	0.15	0.09	0.14	0.10	0.38	0.64

Variable name	Full dataset	Continental Alps	Jura	Northern Intermediate Alps	Southern Pre-Alps	Swiss Central Plateau
Maximum temperature anomaly (3 yr)	0.83	0.04	0.38	0.12	0.16	0.38
Maximum temperature anomaly (4 yr)	0.24	0.19	0.28	0.11	0.18	0.21
Maximum temperature anomaly (5 yr)	2.69	0.04	0.62	0.51	0.14	0.66
Minimum temperature anomaly (0 yr)	0.19	0.21	0.13	0.42	0.15	0.28
Minimum temperature anomaly (1 yr)	0.13	0.19	0.10	0.09	0.13	0.44
Minimum temperature anomaly (2 yr)	0.23	1.83	0.14	0.47	0.26	0.12
Minimum temperature anomaly (3 yr)	0.22	0.11	0.09	0.20	0.18	3.57
Minimum temperature anomaly (4 yr)	0.31	0.11	0.50	0.20	0.16	0.16
Minimum temperature anomaly (5 yr)	0.46	0.09	1.15	0.55	0.32	0.11

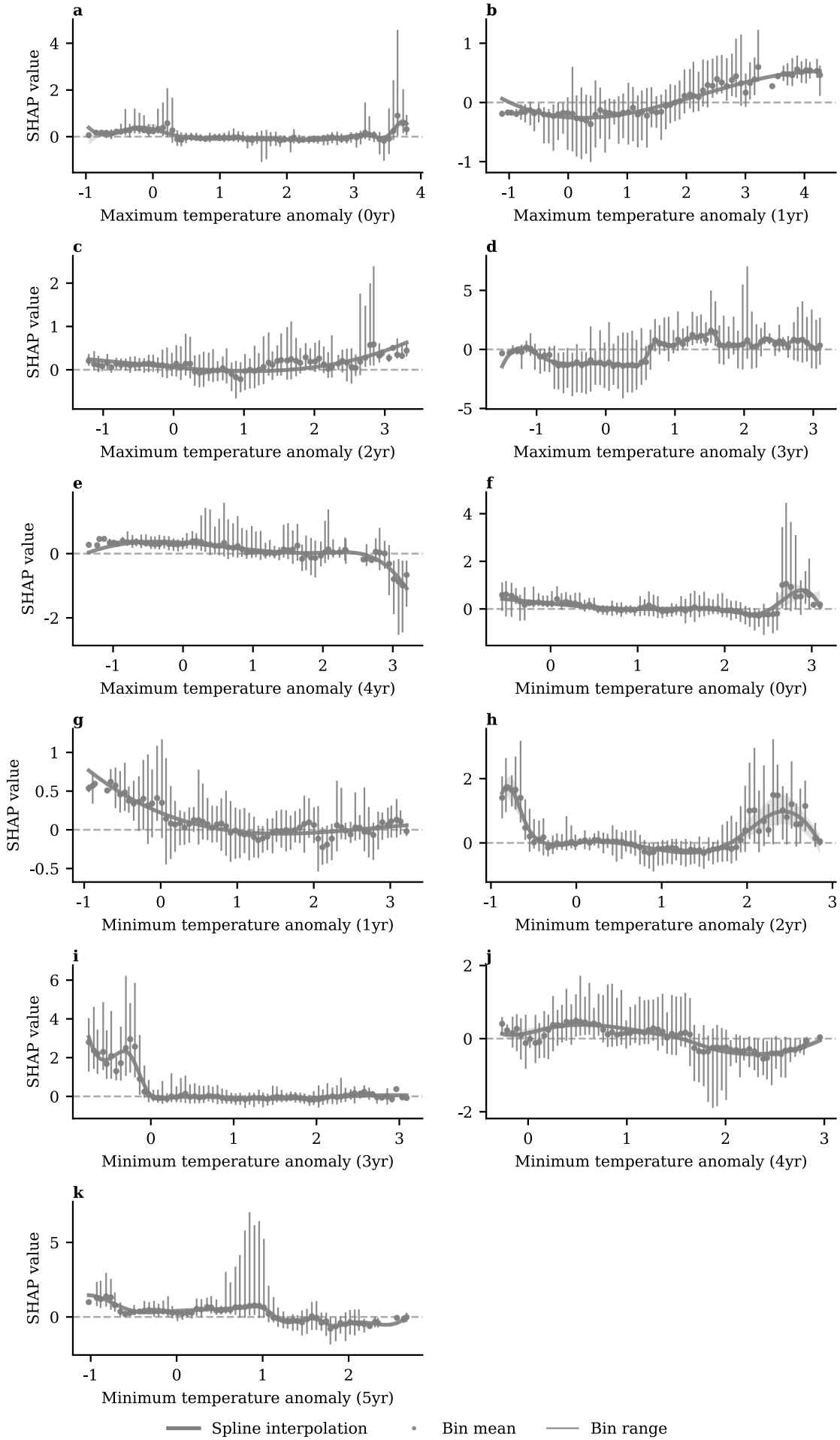
a
b
c
d
e
f
g
h
i
j
k
SHAP value
Maximum temperature anomaly (0yr)
Maximum temperature anomaly (1yr)
Maximum temperature anomaly (2yr)
Maximum temperature anomaly (3yr)
Maximum temperature anomaly (4yr)
Minimum temperature anomaly (0yr)
Minimum temperature anomaly (1yr)
Minimum temperature anomaly (2yr)
Minimum temperature anomaly (3yr)
Minimum temperature anomaly (4yr)
Minimum temperature anomaly (5yr)
Spline interpolation
Bin mean
Bin range

Figure S21: SHAP dependence plots for the full-dataset model showing the marginal effects on standing deadwood of temperature-related predictors that were not included in the five most relevant predictors. SHAP values for each predictor were binned in 70 bins, and a cubic spline was used to interpolate the average SHAP values for each bin. The solid grey lines represent the spline interpolation, the grey points each represent the average SHAP values for each bin, the vertical grey lines represent the range of SHAP values of each bin. The reported variables are: **a** 0-year lag maximum temperature anomaly**, b** 1-year lag maximum temperature anomaly, **c** 2-year lag maximum temperature anomaly, **d** 2-year lag maximum temperature anomaly, **e** 4-year lag maximum temperature anomaly, **f** 0-year lag minimum temperature anomaly **g** 1-year lag minimum temperature anomaly, **h** 2-year lag minimum temperature anomaly, **i** 3-year lag minimum temperature anomaly, **j** 4-year lag minimum temperature anomaly, **k** 5-year lag minimum temperature anomaly.

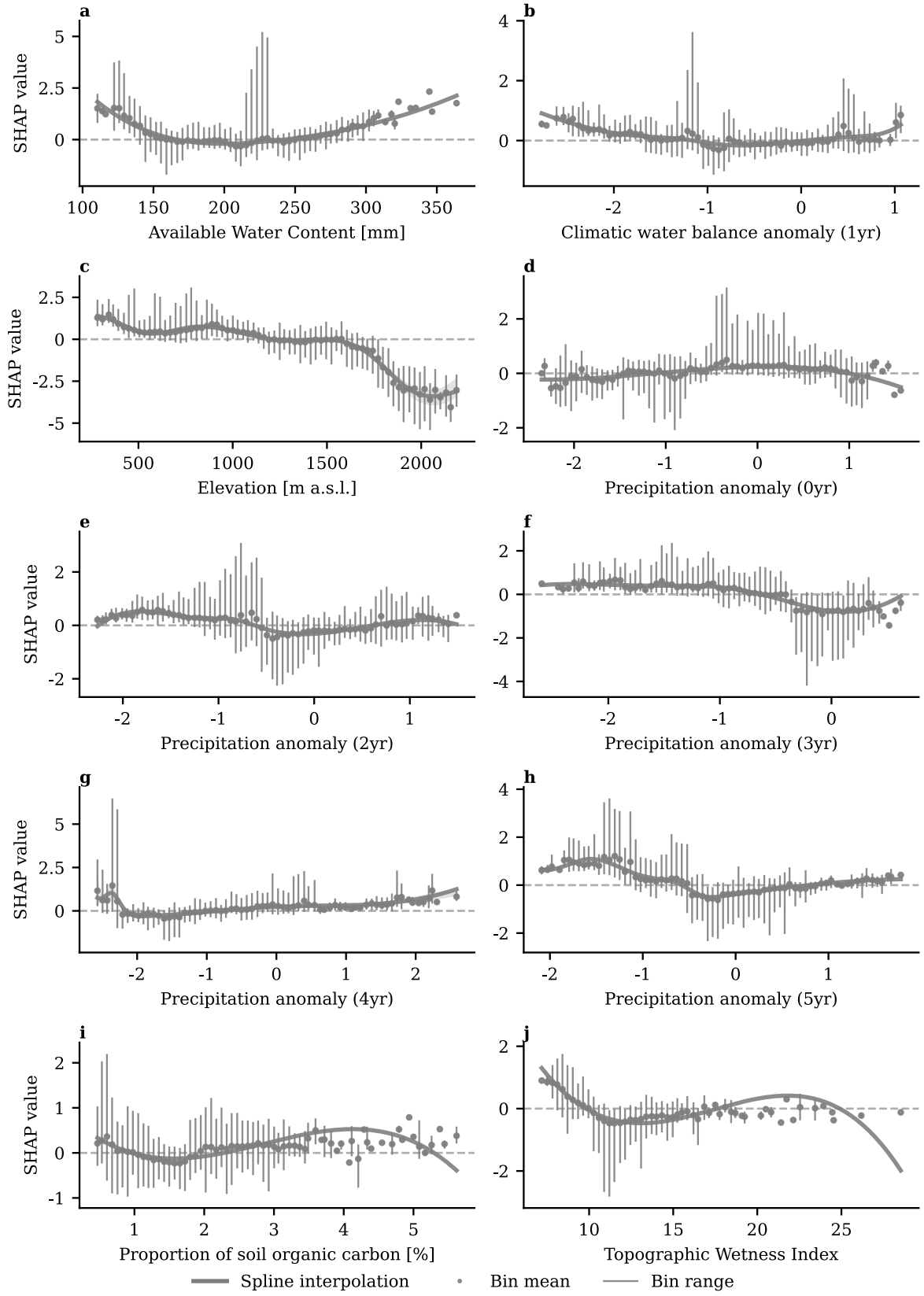

Figure S22: SHAP dependence plots for the full-dataset model showing the marginal effects on standing deadwood of precipitation anomalies, site, and edaphic conditions predictors that were not included in the ten most relevant predictors. SHAP values for each predictor were binned in 70 bins, and a cubic spline was used to interpolate the average SHAP values for each

bin. The solid grey lines represent the spline interpolation, the grey points each represent the average SHAP values for each bin, the vertical grey lines represent the range of SHAP values of each bin. The reported variables are **a** available water content, **b** 1-year lag climatic water balance anomaly, **c** elevation, **d** 0-year lag precipitation anomaly, **e** 2-year lag precipitation anomaly, **f** 3-year lag precipitation anomaly, **g** 4-year lag precipitation anomaly, **h** 5-year lag precipitation anomaly **i** proportion of soil organic carbon, **j** topographic wetness index.

Table S14: Variable permutation importance of the random forest models on the full and ecoregion-specific datasets, expressed as the change in RMSE (ΔRMSE) when that feature is randomly permuted. Positive values mean the model performs worse when the feature is shuffled, higher values indicate higher importance.

Variable name	Full dataset	Continental Alps	Jura	Northern Intermediate Alps	Southern Pre-Alps	Swiss Central Plateau	Ecoregion-specific model average
Available Water Content [mm]	0.07	0.02	0.00	0.00	0.13	-0.01	0.03
Basal area [mÂ²/ha]	0.12	0.03	0.07	0.06	0.20	0.04	0.08
Elevation [m a.s.l.]	0.17	0.28	0.00	0.06	0.10	0.06	0.10
Probability of broadleaf [%]	1.37	0.02	1.57	0.28	1.28	1.36	0.90
Topographic Wetness Index	0.03	-0.01	0.01	0.00	0.07	-0.01	0.01
Canopy Height [m]	0.28	0.07	0.26	0.60	0.06	0.12	0.22
Proportion of clay [%]	0.29	0.32	0.05	0.07	0.18	0.04	0.13
Climatic water balance anomaly (1 yr)	0.04	0.08	-0.01	0.08	0.23	0.01	0.08
Precipitation anomaly (0 yr)	0.04	0.09	0.02	0.74	0.02	-0.03	0.17
Precipitation anomaly (2 yr)	0.04	-0.03	-0.01	0.07	-0.03	0.00	0.00
Precipitation anomaly (3 yr)	0.07	0.11	0.00	0.06	0.00	0.03	0.04
Precipitation anomaly (4 yr)	0.04	-0.02	0.03	1.42	0.04	0.00	0.29
Precipitation anomaly (5 yr)	0.08	-0.01	0.06	0.04	0.01	-0.01	0.02
Proportion of soil organic carbon [%]	0.04	-0.01	-0.03	0.08	0.00	0.08	0.02
Maximum temperature anomaly (0 yr)	0.04	-0.01	0.04	-0.01	-0.01	0.21	0.05
Maximum temperature anomaly (1 yr)	0.01	0.00	0.02	-0.03	0.03	-0.03	0.00
Maximum temperature anomaly (2 yr)	0.00	-0.01	0.01	0.00	-0.09	0.13	0.01
Maximum temperature anomaly (3 yr)	0.25	-0.02	0.01	0.01	-0.03	0.00	-0.01
Maximum temperature anomaly (4 yr)	0.02	-0.01	0.02	0.01	-0.01	0.03	0.01

Variable name	Full dataset	Continental Alps	Jura	Northern Intermediate Alps	Southern Pre-Alps	Swiss Central Plateau	Ecoregion-specific model average
Maximum temperature anomaly (5 yr)	0.96	0.00	0.03	0.08	0.01	0.05	0.03
Minimum temperature anomaly (0 yr)	0.00	-0.04	0.01	0.18	-0.02	-0.02	0.02
Minimum temperature anomaly (1 yr)	0.01	0.00	-0.01	0.02	-0.01	0.01	0.00
Minimum temperature anomaly (2 yr)	0.01	0.49	-0.01	0.03	-0.01	-0.03	0.09
Minimum temperature anomaly (3 yr)	0.03	-0.01	0.00	0.00	0.01	1.34	0.27
Minimum temperature anomaly (4 yr)	0.04	-0.02	0.07	0.02	0.00	-0.02	0.01
Minimum temperature anomaly (5 yr)	0.14	0.00	0.13	0.23	0.03	-0.02	0.08